

Electronic Thesis and Dissertation Repository

4-4-2012 12:00 AM

Oxygen Delivery Strategies in Tissue-Engineering Constructs

Dawit Gezahegn Seifu
The University of Western Ontario

Supervisor
Dr. Kibret Mequanint
The University of Western Ontario

Graduate Program in Chemical and Biochemical Engineering
A thesis submitted in partial fulfillment of the requirements for the degree in Doctor of
Philosophy
© Dawit Gezahegn Seifu 2012

Follow this and additional works at: <https://ir.lib.uwo.ca/etd>

 Part of the [Other Chemical Engineering Commons](#)

Recommended Citation

Seifu, Dawit Gezahegn, "Oxygen Delivery Strategies in Tissue-Engineering Constructs" (2012). *Electronic Thesis and Dissertation Repository*. 416.
<https://ir.lib.uwo.ca/etd/416>

This Dissertation/Thesis is brought to you for free and open access by Scholarship@Western. It has been accepted for inclusion in Electronic Thesis and Dissertation Repository by an authorized administrator of Scholarship@Western. For more information, please contact wlsadmin@uwo.ca.

OXYGEN DELIVERY STRATEGIES IN TISSUE-ENGINEERED CONSTRUCTS

(Spine title: 3D Tissue Construct Oxygenation)

(Thesis format: Integrated-Article)

by

Dawit Gezahegn Seifu

Graduate Program

In

Chemical and Biochemical Engineering

A thesis submitted in partial fulfillment of the requirement for the degree of

Doctor of Philosophy

The School of Graduate and Postdoctoral Studies

The University of Western Ontario

London, Ontario, Canada

© Dawit Gezahegn Seifu 2012

THE UNIVERSITY OF WESTERN ONTARIO
SCHOOL OF GRADUATE AND POSTDOCTORAL STUDIES

CERTIFICATE OF EXAMINATION

<u>Supervisor</u> _____ Dr. Kibret Mequanint	<u>Examiners</u> _____ Dr. Diego Mantovani
<u>Co-Supervisor</u> _____	_____ Dr. Christopher G. Ellis
<u>Supervisory Committee</u> _____	_____ Dr. Ajay Ray
_____ Dr. Ajay Ray	_____ Dr. Amin Rizkalla
_____ Dr. Jingxu (Jesse) Zhu	

The thesis by

Dawit Gezahegn Seifu

entitled:

**OXYGEN DELIVERY STRATEGIES IN TISSUE-ENGINEERED
CONSTRUCTS**

is accepted in partial fulfillment of the
requirements for the degree of

Doctor of Philosophy

Date _____

Chair of the Thesis Examination Board

ABSTRACT

The supply of nutrients and the removal of waste products play a major role in tissue engineering. From all the nutrients necessary for cells seeded on scaffolds for tissue regeneration, oxygen is the limiting component due to its low solubility in culture media while cells consume five to six moles of oxygen for every mole of monosaccharide. The aim of the present work was to develop different strategies to improve the supply of oxygen to human coronary artery smooth muscle cells (HCASMC) seeded on three dimensional (3D) porous biostable polyurethane scaffolds. As a springboard for the study, the measured value of oxygen diffusivity through porous polyurethane scaffolds, fabricated by using pressure differential/particulate leaching technique, was used to screen the best polymer concentration. Scaffolds fabricated from 15 wt% polymer concentration not only had higher oxygen diffusivity but also have better pore interconnectivity as shown by SEM image analysis. Moreover a convective mass transfer approach showed an improvement in the infiltration of HCASMCs into the 3D scaffolds. An oxygen carrier molecule, perfluorodecalin (PFD), was found to improve dissolved oxygen concentration in culture media. PFD was shown to be not only non-toxic to HCASMC but also have no significant effect on the morphology of the HCASMCs. Therefore, higher cell density and infiltration depth into the polyurethane scaffolds were observed when HCASMCs were cultured in a media containing PFD. The final stage of this work was to introduce an oxygen vector into the skeleton of polyurethane scaffolds. For this reason, inert Zeolite Y particles were fluorinated and shown to enhance the amount of dissolved oxygen when suspended in culture media. Fluorinated Zeolite (FZ)

particles were then embedded into polyurethane scaffolds without modifying the porosity and morphology of the 3D structures. Subsequently, higher cell density and infiltration depths were observed when HCASMCs were cultured on FZ particles embedded polyurethane scaffolds in contrast to bare polyurethane scaffolds. Taken together, these data show three different but equally advantageous strategies of improving the supply of oxygen to HCASMC seeded into the interstices of 3D polyurethane scaffolds.

Keywords: Tissue engineering, polyurethane scaffolds, vascular grafts, oxygen diffusivity, vascular smooth muscle cells, oxygen carrier molecules, perfluorodecalin, fluorinated Zeolite particles, cell proliferation, cell infiltration,

CO-AUTHORSHIP

The work contained in this thesis is a joint effort between the student, Dawit G. Seifu and the supervisor, Dr Kibret Mequanint. Their specific contributions are summarized as follows:

Chapter 1: Dawit G. Seifu – wrote the Chapter; Dr. Kibret Mequanint – reviewed and edited the Chapter.

Chapter 2: Dawit G. Seifu – wrote the Chapter; Dr. Kibret Mequanint – reviewed and edited the Chapter.

Chapter 3: Dawit G. Seifu – designed experiments, synthesized and characterized materials, organized and analyzed data, wrote the Chapter; Dr. Kibret Mequanint – guided on designing the experiments and analyzing data, reviewed and edited the manuscript.

Chapter 4: Dawit G. Seifu – designed experiments, synthesized and characterized materials, organized and analyzed data, wrote the Chapter; Dr. Kibret Mequanint – guided on designing the experiments and analyzing data, reviewed and edited the manuscript.

Chapter 5: Dawit G. Seifu – designed experiments, synthesized and characterized materials, organized and analyzed data, wrote the Chapter; Tayirjan T. Isimjan – fluorinated the Zeolite Y particles, Dr. Kibret Mequanint – guided on designing the experiments and analyzing data, reviewed and edited the manuscript.

Chapter 6: Dawit G. Seifu – wrote the Chapter; Dr. Kibret Mequanint – reviewed and edited the Chapter.

"ቸርነትህና ምሕረትህ በሕይወቴ ዘመን ሁሉ ይከተሉኛል፤
በእግዚአብሔርም ቤት ለዘላለም እኖራለሁ"

መዝ 23፥6

*"Surely goodness and mercy shall follow me
All the days of my life;
And I will dwell in the house of the LORD
Forever."*

Psalms 23:6

I dedicate this thesis to the memory of my father Gezahegn Seifu, the yardstick of my life. His guiding hand on my shoulder will remain with me forever.

ACKNOWLEDGMENTS

I would like to sincerely thank my supervisor, Dr. Kibret Mequanint for giving me the opportunity to work under his guidance and for believing in my abilities to do the work documented in this thesis. I am also deeply thankful to him for the continuous assistance and input in this journey of my life. I am also thankful to my advisory committee members Dr. Ajay Ray and Dr. Jesse Zhu for their valuable suggestions and constructive criticism throughout my research.

I am thankful to Dr. Shigang Lin and Dr. Ying Xia for their help in cell culture studies, Dr. Alpesh Patel and Mr. Darryl Knight for their help around the lab, and for the many brainstorming discussions on my research.

I am also grateful to the staff of the Department of Chemical and Biochemical Engineering for providing me all necessary assistance during my studies. It would be improper not to mention Western Graduate Research Scholarships for offering financial assistance during my doctoral studies.

I would like to thank my parents for their unconditional support in every stage of my life. I owe a heart-felt thanks to my hero, my mother Enanu Shifferaw who single-handedly assisted and guided me to become the person I am now. A sincere thank you goes to all my family who played a big role in my life.

Last but not least, heartfelt thanks to the Almighty God for being my rock throughout this journey, being with me and blessing me on every stage of my life.

TABLE OF CONTENTS

CERTIFICATE OF EXAMINATION	ii
ABSTRACT.....	iii
CO-AUTHORSHIP	v
EPIGRAPH	vi
DEDICATION.....	vii
ACKNOWLEDGMENTS	viii
TABLE OF CONTENTS	ix
LIST OF TABLES	xiv
LIST OF FIGURES	xv
LIST OF ABBREVIATIONS	xix
1 INTRODUCTION.....	1
1.1 Overview	1
1.2 Thesis Outline.....	3
1.3 References	3
2 LITERATURE REVIEW	5
2.1 Anatomy and Physiology of Coronary Arteries.....	5
2.2 Coronary Artery Diseases	7
2.3 Surgical Intervention	8
2.4 Engineered Vascular Tissues as Functionally Competent Conduits.....	10
2.5 Engineered Vascular Tissues as Species-specific Predictive Organ Model.....	13
2.6 Engineered Vascular Tissues in Physiological Genomics Studies	14
2.7 Essential Elements of Tissue Engineering	16
2.7.1 Cell Sourcing	17

2.7.2 Scaffolds	19
2.7.3 Bioreactors.....	20
2.8 Oxygen Mass Transfer in Tissues.....	23
2.8.1 The Challenges of Oxygen Transfer in Engineered Tissues	23
2.8.2 In Vivo Oxygen Transfer.....	24
2.8.3 The Oxygen-hemoglobin Dissociation Curve	25
2.8.4 Alternative Oxygen Binding Chemicals.....	28
2.9 The Chemistry of Perfluorocarbon Compounds	29
2.9.1 Oxygen Solubility in PFCs	29
2.9.2 PFCs as Oxygen Delivery Systems	31
2.10 Diffusion in Porous Media and Its Relevance in Tissue Engineering	32
2.10.1 Squeeze Flow in Porous Scaffolds	34
2.10.2 Lattice Boltzmann’s Approach for Porous Fluid Flow	37
2.11 Summary.....	38
2.12 Hypothesis and Objectives of the Study.....	38
2.13 References	39
3 TISSUE ENGINEERING SCAFFOLD FABRICATION, EFFECTIVE DIFFUSION COEFFICIENT AND DYNAMIC CELL CULTURE	52
3.1 Introduction.....	53
3.2 Materials and Methods.....	54
3.2.1 Fabrication of PCU scaffolds	54
3.2.2 Measuring dissolved oxygen and diffusion coefficient	56
3.2.3 Cell culture in perfusion bioreactor	59
3.2.4 Fluorescence staining and laser scanning confocal microscopy	61
3.2.5 Histological analysis using haematoxylin and eosin staining	61
3.2.6 Protein extraction and Western blot analysis	62
3.2.7 Statistical analysis	62
3.3 Results	63

3.3.1 Scaffold fabrication.....	63
3.3.2 Effective oxygen diffusion coefficient in scaffolds.....	65
3.3.3 Fluorescence staining and confocal microscopy.....	67
3.3.4 Cross sectional histological staining.....	70
3.3.5 Western blot analysis.....	72
3.4 Discussion:	73
3.5 Conclusions.....	75
3.6 References.....	76
4 EXPERIMENTAL AND MODELING STUDIES OF OXYGEN TENSION IN VASCULAR TISSUE ENGINEERING WITH AND WITHOUT AN OXYGEN CARRIER.....	79
4.1 Introduction.....	80
4.2 Methods.....	83
4.2.1 Fabrication of 3D scaffolds.....	83
4.2.2 Dissolved oxygen measurements.....	85
4.2.3 Cell culture on 3D scaffolds	85
4.2.4 Cytotoxicity assay and cell number quantification.....	86
4.2.5 Fluorescence staining and laser scanning confocal microscopy	86
4.2.6 Mathematical model for lumen oxygen profile	87
4.2.7 Mathematical model for cell-seeded scaffold oxygen profile	88
4.2.8 Model parameters	89
4.2.9 Numerical solutions	90
4.2.10 Statistical analysis	90
4.3 Results and discussion	91
4.3.1 The effect of PFD on dissolved oxygen in HCASMCs culture medium, cell spreading and cell viability.	91
4.3.2 HCASMC proliferation when seeded to 3D scaffolds with 2% PFD- supplemented medium.....	94
4.3.3 Numerical solution for oxygen profiles in static 3D cultures.....	96

4.3.4 Numerical solution for oxygen profiles in 3D cultures with convection. .	100
4.4 Conclusions	106
4.5 References	107
5 TISSUE ENGINEERING SCAFFOLDS CONTAINING EMBEDDED FLUORINATED-ZEOLITE OXYGEN VECTORS	111
5.1 Introduction.....	112
5.2 Materials and Methods.....	114
5.2.1 Preparation of fluorinated-zeolite (FZ).....	114
5.2.2 Fabrication of PCU-FZ scaffolds.....	115
5.2.3 Dissolved oxygen measurement	115
5.2.4 Chemical composition and morphological studies of FZ and PCU-FZ scaffolds.....	116
5.2.5 Scaffold porosity measurements.....	117
5.2.6 Cell culture on PCU and PCU-FZ scaffolds	118
5.2.7 Cytotoxicity assay.....	118
5.2.8 Immunofluorescence staining and laser scanning confocal microscopy..	119
5.2.9 Statistical analysis.	120
5.3 Results and Discussion.....	120
5.3.1 Characterization of fluorinated zeolite (FZ)	120
5.3.2 Dissolved oxygen concentration in FZ particles.....	121
5.3.3 FZ modified scaffolds characterization	123
5.3.4 HCASMC growth on PCU and PCU-FZ scaffolds	128
5.3.5 HCASMC morphology and depth of infiltration on PCU-FZ scaffolds ..	130
5.4 Conclusions	135
5.5 References	136
6 GENERAL DISCUSSION AND CONCLUSIONS	140
6.1 Summary.....	140
6.2 Strengths and limitations	142

6.3 Future direction	144
6.4 Significance	144
6.5 References	145
APPENDIX	147
CURRICULUM VITAE.....	155

LIST OF TABLES

Table 2.1: Peak convection rates of blood in the vasculature. ¹³⁴	24
Table 4.1: Model parameters used to predict oxygen concentration profiles in a vascular tissue constructs oxygenated with PFD supplemented culture medium.	97
Table 5.1: Mercury porosimetry analysis data for PCU and PCU-FZ scaffolds.....	124
Table 5.2: XPS analysis of the fluorine content in FZ particles, PCU scaffolds and PCU-FZ scaffolds. The numbers in brackets indicate the corresponding binding energies.	128

LIST OF FIGURES

Figure 2. 1: Schematic representation and histology of coronary artery wall structure. ⁵ ...6	6
Figure 2. 2: Schematic representation of normal and diseased arteries.7	7
Figure 2. 3: Schematic drawing showing the compliance mismatch between the native tissue and a prosthetic graft leading to hemodynamic changes and thrombus formation.9	9
Figure 2. 4: Schematic processes in tissue engineering showing the essential stages in tissue fabrication11	11
Figure 2.5: Engineered tissue provides an opportunity for obtaining a wide variety of phenotypes previously restricted to whole animal studies, including mechanical measurements such as force of contraction, ⁵⁶15	15
Figure 2.6: Essential elements in tissue engineering. ⁷⁵17	17
Figure 2.7: Summary of different bioreactors used for tissue fabrication.22	22
Figure 2.8: Changes in the oxygen-hemoglobin dissociation curve. ¹³⁵26	26
Figure 2.9: Oxygen solubility in different hydrocarbons and fluorocarbons. ¹⁴³30	30
Figure 2. 10: Preparation of perfluorocarbon emulsion using surfactants and dispersion energy in order to overcome the PFC-water interfacial tension. ¹⁴³31	31
Figure 2.11: Squeeze flow model. The two boundaries are moving to each other at a velocity of V_h , and the space between them is $2h$ 35	35
Figure 3. 1: Schematic diagram of the assembled, solvent casting and particulate leaching. Scaffold fabrication method and fabricated from PCU.....56	56
Figure 3. 2: Schematic diagram of the diffusion cell apparatus.....57	57
Figure 3. 3: SEM photomicrographs of PCU scaffolds fabricated at different polymer concentration. 15 wt % (A and B), 20 % wt (C and D) 25 % wt (E and F), and 30 % wt (G and H) PCU concentration. Scale bars are 250 μ m for A, C, E G and 10 μ m for B, D, F and H.....64	64
Figure 3. 4: A) Oxygen concentration detected in the receiver chamber as a function of time. Data used to calculate the effective oxygen diffusivity, D_{eff} B) for 15%PCU, C) 20%PCU, D) 25%PCU and E) 30%PCU.....66	66

Figure 3. 5: Effective oxygen diffusivity (cm^2/s) in 3D scaffolds fabricated from different PCU concentrations.....	67
Figure 3. 6: Confocal microscopy images of HCASMCs cultured on disk shape PCU scaffold in static (A-D) and dynamic (E-H) culture conditions. The top of the scaffolds are shown in A and E whereas the bottom side are B and F, and the orthogonal projections are C and G. Scale for bar for all the images is 200nm.	68
Figure 3. 7: Confocal microscopy images of HCASMCs cultured on tubular PCU scaffolds in static (A, C, E and G) and dynamic (B, D, F and H) culture conditions for 4 days (A&B) 7days (C&D) 14 days (E& F) and 28 days (G&H). Scale bar for A,B,G and H is 200nm and for C.D.E and F is 100nm.	69
Figure 3. 8: H&E staining of cross sections of HCASMCs seeded tubular PCU scaffolds cultured under dynamic condition for 7 days (B and C), 14 days (E and F) and 28 days (G and H). Bare scaffold was stained and imaged as a control (A and B). Scale bar for A, C, E and G is 0.2mm and for B, D, F and H is 0.1mm.....	71
Figure 3. 9: Western blots of 14 days and 28 day cultures in static and dynamic conditions coomassie blue staining and antibody staining of elastin , SM- α -actin and GAPDH for 14 days culture.	72
Figure 4. 1: SEM and digital image of PCU scaffold (A), tubular construct of porous cell-seeded scaffold and mesh alignment of the model (B), perfusion bioreactor digital image and schematic flow diagram including the setup (C)	84
Figure 4. 2: Dissolved oxygen partial pressure in different fluids measured at 37 °C. Oxygen concentration was measured using fibre optic probe... ..	92
Figure 4. 3: Phase contrast images of HCASMC, cultured with PFD supplemented medium (A, C and E) and without PFD (B, D and F) for 1 days, 2 days and 7 days. Confocal microscopy images of HCASMs cultured on 3D scaffolds with PFD (H) and without PFD supplemented medium (G).....	93

Figure 4. 4: HCASMC viability using MMT assay on 3D PCU scaffold cultured with and without PFD supplemented medium.	94
Figure 4. 5: HCASMC proliferation on 3D scaffolds with and without PFD supplemented medium for 7 days (A) 14 days (B) and 21 Days (C).....	95
Figure 4. 6: Model prediction of oxygen profile in the lumen at static culture condition in 3D plot (A) and a plot of lumen-scaffold interface oxygen partial pressure for different cell densities (B).....	98
Figure 4. 7: Oxygen profile in the scaffold (tissue space) at static condition in 3D plot with and without PFD supplemented medium (B, C) and a plot of cross sectional oxygen partial pressure for different cell densities (C).....	99
Figure 4. 8: Oxygen profile in the lumen and in the scaffold at a flow condition. A 3D construct of the oxygen partial pressure in half of the lumen (A), a plot of lumen-scaffold interface oxygen partial pressure for different cell densities (B), a 3D construct of the oxygen partial pressure in scaffold (C) and a plot oxygen partial pressure across the cross section of the scaffold for different cell densities (D).	101
Figure 4. 9: A plot oxygen partial pressure across the cross section of the scaffold for 2.5×10^6 cell/mL density for zero order, Michaelis-Menten and first order kinetics. medium flow rate was 40 mL/min.....	105
Figure 5. 1: (A) Framework structure of zeolite Y, (B) chemical structure of PTES, and (C) XRD pattern of the synthesized fluorinated zeolite Y.	121
Figure 5. 2: Dissolved oxygen concentrations in deionized water at 37 °C, in the presence of non-fluorinated zeolite particles, and in the presence of different weight percentages of fluorinated zeolite particles.....	123
Figure 5. 3: Scaffold pore size distribution obtained by mercury porosimetry for PCU and PCU-FZ scaffolds plotted as a function of differential and cumulative intrusion volumes	125
Figure 5. 4: SEM and EDX analysis of fluorinated zeolite-modified PCU scaffolds. (A) Control PCU scaffolds; (B) FZ-modified PCU scaffolds; (C) high	

magnification images of the struts in FZ-modified PCU scaffolds (inset: high magnification image showing the FZ particles); (D) SEM image of the area where EDX mapping was undertaken; (E–J) EDX elemental mapping for (E) Al, (F) C, (G) F, (H) O, (I) Si and (J) a combination of all elements; (K) EDX spectrum for FZ-modified PCU scaffolds. Images were captured using a Zeiss LEO 1530 SEM microscope at working voltages of 1 keV for high magnifications and 5 keV for low magnifications.126

Figure 5. 5: HCASMC (A) viability and (B) growth on PCU, PCU-FZ, and PCU-non-FZ 3D scaffolds.130

Figure 5. 6: Confocal microscopy images of HCASM cultured on PCU and PCU-FZ scaffolds for 4 days(A, B, G, H), 7 days (C, D, I, J) and 14 days (E, F, K, L). HCASMC attached to both PCU and PCU-FZ scaffolds had similar morphologies but the cell density appeared to be higher on the PCU-FZ scaffolds. Scale bars: (A), (C), (E), (G), (I), (K), 200 μm ; (B), (D), (F), (H), (J), (L), 100 μm131

Figure 5. 7: The effect of FZ incorporation on HCASMC spreading and infiltration after 4, 7 and 14 days of culture. (A, B, E, F, K, L) PCU scaffolds; (C, D, G–J, M–P) PCU-FZ scaffolds. Orthogonal views of the confocal images are shown at the bottom. Scale bar: 200 μm133

LIST OF ABBREVIATIONS

2D	Two-dimensional
3D	Three-dimensional
ANOVA	Analysis of variance
BC	Boundary condition
BSA	Bovine serum albumin
C_a	Dissolved oxygen in aqueous phase
CABG	Coronary artery bypass grafts
CAD	Computer-aided design
CO ₂	Carbon dioxide
C_p	Dissolved oxygen in PFD
D_a	Aqueous phase oxygen diffusivity
DI	Deionized
DMF	Dimethylformamide
DNA	Deoxyribonucleic acid
D_p	Oxygen diffusivity in PFD
ECM	Extracellular matrix
EC	Endothelial cells
ePTFE	Expanded polytetrafluoroethylene
FZ	Fluorinated Zeolite
HBSS	Hank's balanced salt solution
HCASMC	Human coronary artery smooth muscle cells

HCl	Hydrochloric acid
hTERT	human telomerase reverse transcriptase
H&E	Hematoxylin and eosin
IC	Initial condition
ID	Internal diameter
IgG	Immunoglobulin G
MTT	3-(4,5-dimethylthiazol-2-yl)-2,5-diphenyltetrazolium bromide
MicroCT	Microcomputed tomography
NaCl	Sodium chloride
NaAlO ₂	Sodium aluminates
NH ₄ Cl	Ammonium chloride
PAGE	Polyacrylamide gel electrophoresis
PBS	Phosphate-buffered saline
PCU	Poly(carbonate urethane)
PCU-FZ	Fluorinated Zeolite containing PCU scaffold
PET	Polyethylene terephthalate
PFC	Perfluorocarbon
PFD	Perfluorodecalin
PTES	1H, 1H, 2H, 2H-perfluorodecyltriethoxysilane
SD	Standard deviation
SDS	Sodium dodecyl sulphate
SEM	Scanning electron microscopy
SIS	Small intestinal submucosa

SM- α -actin	Smooth muscle α -actin
SMC	Smooth muscle cells
SmGM-2	Smooth muscle growth medium-2 with bullet kit
SMMHC	Smooth muscle myosin heavy chain
SV	Saphenous vein
TEVA	Tissue-engineered vascular adventitia
TEVM	Tissue-engineered vascular media
TGF β	Transforming growth factor beta
OCT	Optimal cutting temperature
UIS	Urinary bladder submucosa
UV	Ultra-violet
V_{\max}	Maximum shear stress
V_m	Maximum oxygen consumption
VSMC	Vascular smooth muscle cells
τ_{wall}	Wall shear stress

CHAPTER

1

1 INTRODUCTION

1.1 Overview

Cardiovascular disease such as coronary artery occlusion is one of the leading causes of death in both Western and non-Western societies.¹ Conventional severe medically refractory coronary and peripheral artery diseases treatment options such as the use of autologous vessels and prosthetic grafts have suboptimal performances.^{2, 3} Over the past 15 years, the concept of vascular tissue engineering, representing an interdisciplinary effort with considerable potential to treat vascular disease, has emerged to be a viable treatment alternative.⁴ The strategies of in vitro tissue engineering are conceptually simple and clinically appealing yet these have proven to be a formidable engineering task. Despite rapid advances made in this field, success is still limited due to significant knowledge gaps in our ability to regulate tissue formation. Within the context of engineering, providing sufficient oxygen mass transport that is vital for cellular metabolism is perhaps one of the unmet challenges to fabricate tissues of clinical relevance.^{5, 6} It has long been known that the supply of oxygen and soluble nutrients becomes critically limiting for the in vitro culture of 3D tissues.⁷ The consequence of such a limitation is exemplified by early studies showing that cellular spheroids larger than 1 mm in diameter generally contain a hypoxic and necrotic center surrounded by a rim of viable cells.⁸ Similar observations beyond depths of 250 μm were reported for a

number of cells cultured on 3D scaffolds where a non-homogenous cell distribution is reported.⁹⁻¹¹ Because engineered blood vessels should be at least 500 μm in wall thickness, mass transfer limitations represent one of the challenges to be addressed for cell survival.

Unlike what is described above, *in vivo* mass transfer requirements are facilitated by convective transport of hemoglobin-bound oxygen to tissues to the proximity of capillaries. In most tissues, cells are no more than 100 μm from these capillaries allowing sufficient oxygen to be delivered. The small diameter of capillaries (between 6 and 8 μm) ensures a residence time long enough in tissues to permit the radial diffusion of chemical species¹². Thus *in vivo*, cells are constantly perfused with the flowing blood through the vasculature. At lower blood plasma concentrations of oxygen in tissues, oxygen dissociates from hemoglobin and diffuses into tissues and cells. As the blood vessels themselves are made up of cells, they too require sufficient oxygen and nutrients to survive. Since the wall of the larger blood vessels is too thick to allow diffusion between the blood stream and surrounding tissue of the wall, the adventitial layer of these vessels contains small arteries called vasa vasorum that supply the smooth muscle cells and fibroblasts within the media and adventitia their nutrient demand. Therefore mass transfer within the vascular wall is facilitated by the diffusion of oxygen both from the lumen and adventitial side.

1.2 Thesis Outline

In view of the above brief overview, the work presented in this thesis underscores the importance of addressing oxygen mass transfer to design and fabricate vascular tissues of clinical relevance. In Chapter 2, pertinent literature review is presented. Although the open literature documented far exceeded those cited in this thesis, an effort was made to focus on recent advances while equally acknowledging seminal works in the field. In Chapter 3, scaffold fabrication, diffusion measurements, and some cell culture data are presented. Chapters 4 and 5 describe two different approaches chosen to enhance oxygen mass transfer in 3D cell cultures each with specific objectives.^{13, 14} Finally, the significance, contributions, and limitations of the study are presented in Chapter 6.

1.3 References

1. Reddy, K. S., Cardiovascular disease in non-Western countries. *N Engl J Med* **2004**, 350, (24), 2438-40.
2. Agarwal, S. C.; Adams, P. C.; Ahmed, J. M., Aneurysm of saphenous vein graft causing anterior myocardial infarction by possibly compressing left internal mammary artery. *Int J Cardiol* **2006**, 109, (2), 284-5.
3. Zilla, P.; Bezuidenhout, D.; Human, P., Prosthetic vascular grafts: wrong models, wrong questions and no healing. *Biomaterials* **2007**, 28, (34), 5009-27.
4. L'Heureux, N.; Dusserre, N.; Marini, A.; Garrido, S.; de la Fuente, L.; McAllister, T., Technology insight: the evolution of tissue-engineered vascular grafts--from research to clinical practice. *Nat Clin Pract Cardiovasc Med* **2007**, 4, (7), 389-95.
5. Curcio, E.; Macchiarini, P.; De Bartolo, L., Oxygen mass transfer in a human tissue-engineered trachea. *Biomaterials* **2010**, 31, (19), 5131-6.
6. Lovett, M.; Lee, K.; Edwards, A.; Kaplan, D. L., Vascularization strategies for tissue engineering. *Tissue Eng Part B Rev* **2009**, 15, (3), 353-70.
7. Martin, I.; Wendt, D.; Heberer, M., The role of bioreactors in tissue engineering. *Trends Biotechnol* **2004**, 22, (2), 80-6.

8. Sutherland, R. M.; Sordat, B.; Bamat, J.; Gabbert, H.; Bourrat, B.; Mueller-Klieser, W., Oxygenation and differentiation in multicellular spheroids of human colon carcinoma. *Cancer Res* **1986**, 46, (10), 5320-9.
9. McClelland, R. E.; Coger, R. N., Use of micropathways to improve oxygen transport in a hepatic system. *J Biomech Eng* **2000**, 122, (3), 268-73.
10. Ishaug, S. L.; Crane, G. M.; Miller, M. J.; Yasko, A. W.; Yaszemski, M. J.; Mikos, A. G., Bone formation by three-dimensional stromal osteoblast culture in biodegradable polymer scaffolds. *J Biomed Mater Res* **1997**, 36, (1), 17-28.
11. Radisic, M.; Malda, J.; Epping, E.; Geng, W.; Langer, R.; Vunjak-Novakovic, G., Oxygen gradients correlate with cell density and cell viability in engineered cardiac tissue. *Biotechnol Bioeng* **2006**, 93, (2), 332-43.
12. Martin, Y.; Vermette, P., Bioreactors for tissue mass culture: design, characterization, and recent advances. *Biomaterials* **2005**, 26, (35), 7481-503.
13. Seifu, D.; Mequanint, K., Experimental and Modeling Studies of Oxygen Tension in Vascular Tissue Engineering With and Without an Oxygen Carrier. *J Biomater & Tissue Eng* **2011**, 1, (1), 49-59.
14. Seifu, D. G.; Isimjan, T. T.; Mequanint, K., Tissue engineering scaffolds containing embedded fluorinated-zeolite oxygen vectors. *Acta Biomater* **2011**, 7, (10), 3670-8.

CHAPTER

2

2 LITERATURE REVIEW

Overview: This chapter provides background information on the physiology and diseases of coronary arteries, surgical interventions and the need for and the challenges of tissue-engineered vascular substitutes. Elements of vascular tissue engineering are presented with a focus on the delivery of oxygen to engineered tissue constructs. It concludes with a statement of study rationale and an outline of specific hypotheses and objectives of this study.

2.1 Anatomy and Physiology of Coronary Arteries

Coronary arteries, which are the first to branch off from the ascending aorta, supply blood to the heart muscle. Both the right and left coronary arteries extend from the aorta to the heart walls supplying blood to the atria, ventricles, and septum of the heart. Coronary arteries are composed of three concentric tunics (Figure 2.1). The tunica intima forms the innermost lining composed of non-thrombogenic monolayer endothelial cells. By secreting specific molecules such as nitric oxide, endothelial cells inhibit platelet activation and prevent thrombus formation.^{1, 2} The tunica media is generally composed of a dense population of concentrically organized smooth muscle cells and is separated from the tunica intima by an internal elastic lamina.³ Under physiological conditions, smooth muscle cells possess a quiescent contractile phenotype and control the dilation and constriction of blood vessels thus regulating blood flow. Under pathological conditions, smooth muscle cells convert to a synthetic and non-contractile phenotype. This synthetic phenotype results in the proliferation and increased matrix production in the tunica media

resulting vessel stenosis.⁴ The tunica adventitia (externa) forms the external layer and contains a collagenous extracellular matrix and fibroblast cells. Ultimately, tissue-engineered blood vessels should contain all of these layers for proper functionality.

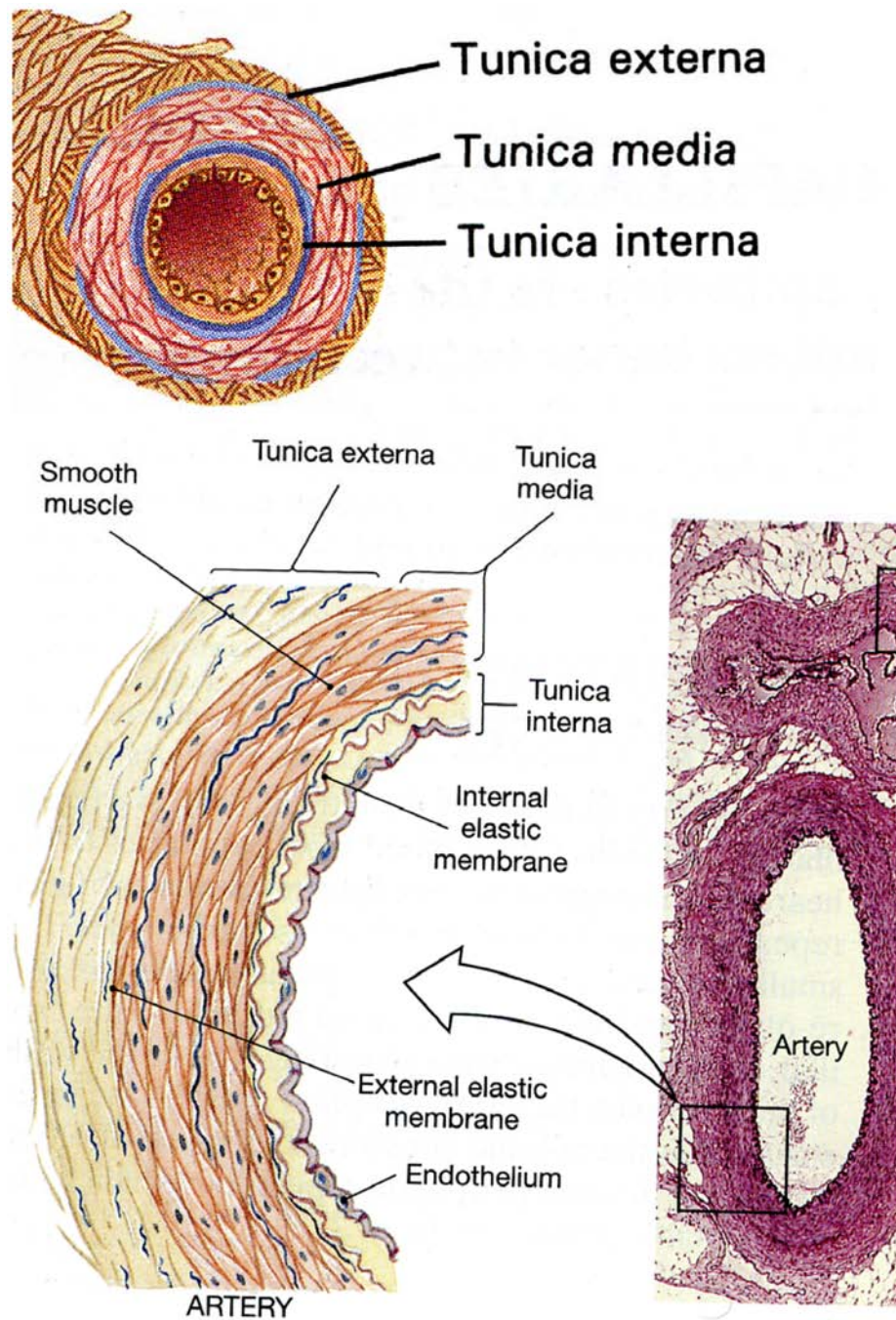


Figure 2.1: Schematic representation and histology of coronary artery wall structure.⁵

2.2 Coronary Artery Diseases

Coronary artery disease is the most common form of heart disease. Atherosclerosis, characterized by a progressive accumulation of lipids and fibrous elements in the lumen, is a widely recognized inflammatory disease affecting the vasculature (Figure 2.2). The early lesions of atherosclerosis consist of sub-endothelial accumulations of cholesterol-engorged macrophages, called 'foam cells' which acts as preferred sites for lesion formation.

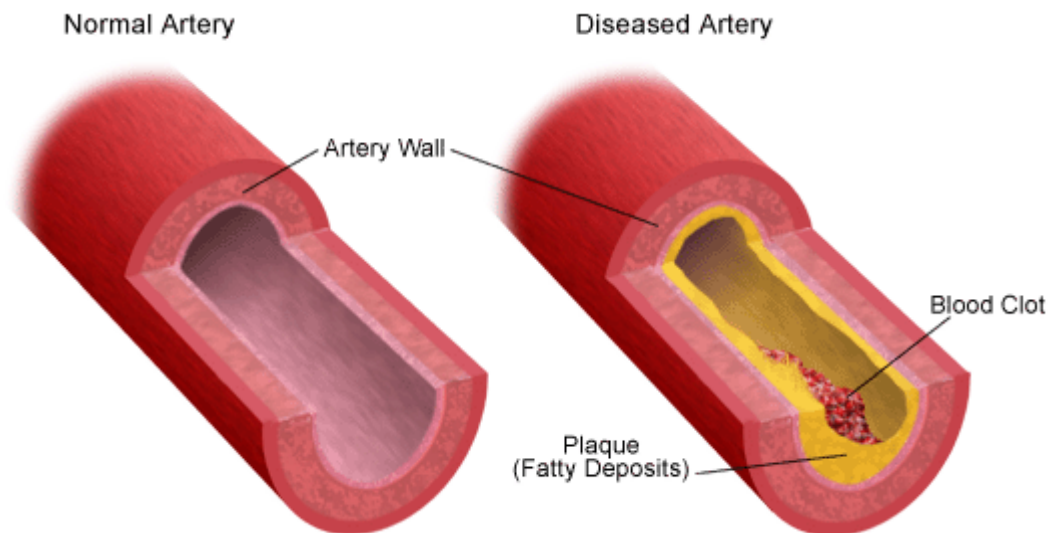


Figure 2.2: Schematic representation of normal and diseased arteries.

With time, the lesions grow and will reach a point where the artery is so narrow that blood flow becomes insufficient to supply the succeeding vessels leading to angina and ischemia. The deprivation of blood results in oxygen deficiency in the myocardium, and accumulation of carbon dioxide and lactic acid in the tissue.⁶ Unstable lesions with a thin fibrous cap are highly susceptible to plaque rupture and erosion, exposing the necrotic core and potentially leading to the formation of a thrombus. Thrombosis results in acute artery occlusion leading to potentially fatal heart attack.⁷ In addition to inflammatory

atherosclerotic lesions, congenital anomalies of the coronary artery are found in 1-2% of the population.⁸⁻¹⁰ While the majority of these anomalies do not result in signs, symptoms or complications, others such as coronary atresia, coronary hypoplasia, single coronary artery and ectopic coronary origin are associated with serious events such as myocardial infarction, cardiac arrhythmias, syncope, congestive heart failure and sudden death.¹¹⁻¹³

2.3 Surgical Intervention

In the early stages of the plaque build-up, a minimally invasive coronary balloon angioplasty intervention technique is a preferred method to surgery for reopening occluded atherosclerotic vessels. Following the intervention, stents are often deployed to prevent elastic recoil of the vessel wall.¹⁴ However, for advanced atherosclerotic lesions, coronary artery bypass grafting (CABG) is the only alternative. Autologous grafts remain the primary choice for CABG because of their compliance, immune acceptance, and non-thrombogenicity. The most commonly used autograft is the saphenous vein (SV)¹⁵ but the internal mammary artery and radial artery are also used.¹⁶ The extensive use of SV as CABG is, in part, because it is surgically easier to access and harvest.¹⁷ However, its performance is not sufficient in large due to the gradual deterioration when exposed to high-pressure arterial sites leading to excessive dilation and also due to a combination of intimal hyperplasia and accelerated atherosclerosis.¹⁸⁻²² Therefore, further surgical revascularization is often required in about 10 years after the initial bypass surgery but the availability of SV for second and third bypass surgery is a limitation.²³

Even though the preferred bypass vascular substitute is the patient's own arteries or veins, they are generally inadequate or unsuitable for approximately one-third of patients^{24, 25} suggesting the obvious need for alternative grafts.²⁶ Prosthetic grafts have been developed as an alternative to autografts and, the most commonly used materials are polyethylene terephthalate (PET, Dacron[®]) and expanded polytetrafluoroethylene (ePTFE, Teflon[®]). Dacron[®] and Teflon[®] have been used successfully in the replacing large arteries, however, when the vessel diameter is under 5 mm, the clinical outcome is disappointing.^{27, 28} The low patency of synthetic grafts in small diameter artery reconstruction is due to lower blood flow velocities resulting from intimal hyperplasia at the anastomotic site.¹³ The development of intimal hyperplasia is attributed to the compliance mismatch between the graft and the native vessel, and the thrombogenicity of the synthetic surface.^{29, 30} The difference in elasticity at the anastomotic site creates turbulence in the blood flow and damages the endothelial lining, resulting in thrombus formation and compliance mismatch as shown in Figure 2.3.^{31, 32} In order to avoid these complications, patients having prosthetic grafts often require extensive anticoagulant medications.

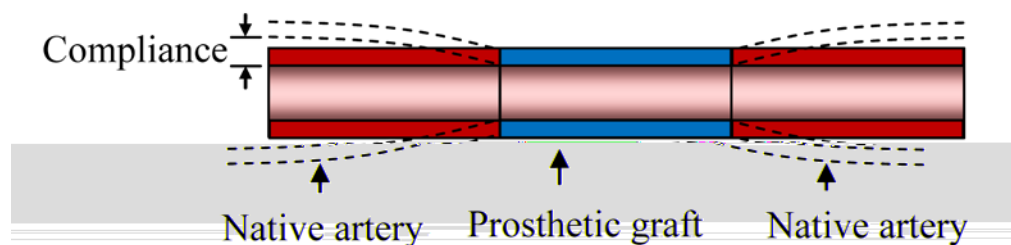


Figure 2.3: Schematic drawing showing the compliance mismatch between the native tissue and a prosthetic graft leading to hemodynamic changes and thrombus formation.

In addition to Dacron[®] and Teflon[®], polyurethanes have been tested as vascular graft materials due to improved compliance, thromboresistance, and reduced anastomotic hyperplasia.³³ Polyurethanes are also reported to promote the ingrowth of living tissues in and around the grafts potentially modifying the initial compliance of the graft.^{34, 35} However, their clinical use as prosthetic grafts was limited due to their poor biostability.^{36, 37} To overcome these issues, a newly developed polyurethane graft based on polycarbonate soft segment showed improved resistance to biodegradation for a 3 year period in a canine model.^{38, 39} The presence of the polycarbonate soft segment is responsible for the increased resistance to biodegradation in comparison to other soft segments.

2.4 Engineered Vascular Tissues as Functionally Competent Conduits

As stated above, the disappointing outcome of synthetic vascular grafts and the limited supply of autografts necessitate tissue engineering approaches for constructing autologous vessels. Vascular tissue engineering technology holds promise in the design of responsive living conduits with properties similar to those of the native tissue⁴⁰. In tissue engineering of blood vessels, synthetic biodegradable, non-degradable or ECM scaffolds are infiltrated with vascular cells and cultured under physiological conditions to mature before implantation into the patient⁴¹⁻⁴³ (Figure 2.4).

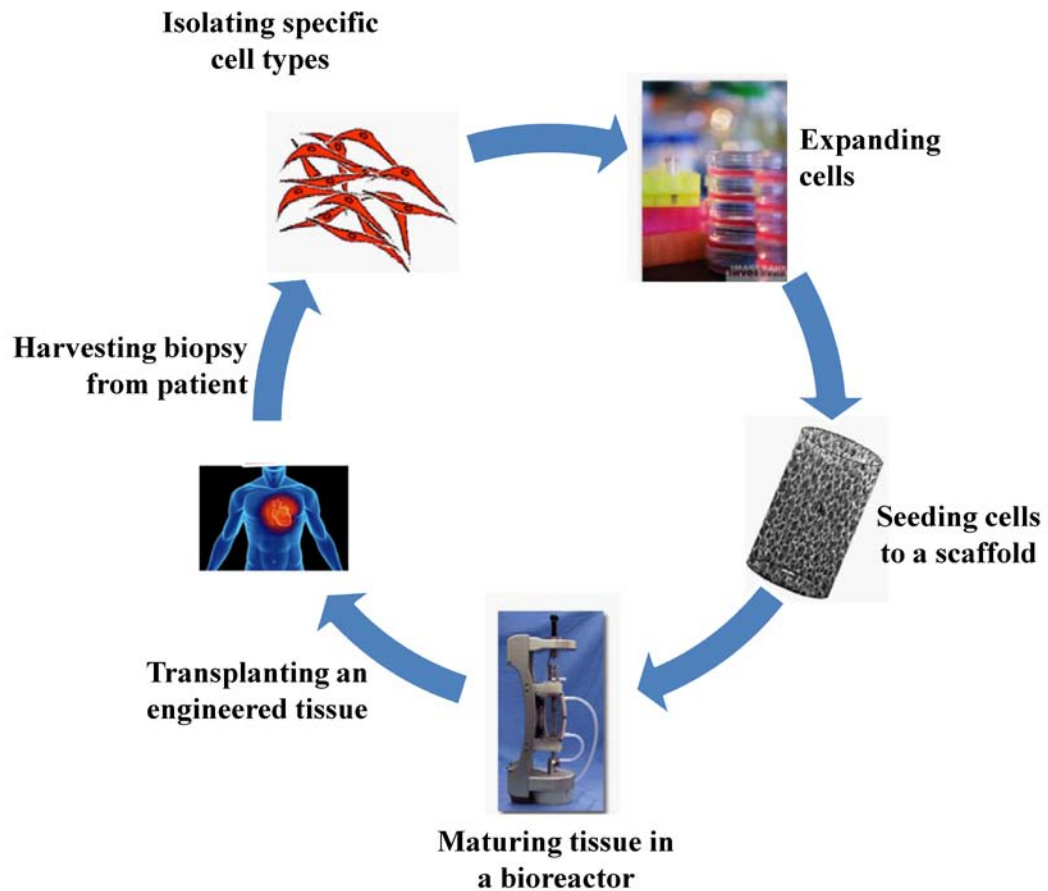


Figure 2. 4: Schematic processes in tissue engineering showing the essential stages in tissue fabrication

Tissue-engineered blood vessels thus have specific advantages since they are designed to be responsive both mechanically and biologically with respect to the load that changes with the hemodynamic environment. The first clinical application of a tissue-engineered vascular construct was reported in 2001 for a paediatric patient with congenital single ventricle cardiac anomaly.⁴¹ This was an exceptional case because no synthetic graft could be used with the capacity to grow, repair, and remodel as required with normal development. Since then, tissue-engineered conduits have been used for a total of 25 extracardiac cavopulmonary connections (median patient age 5.5 years) with only two late cardiac failure deaths reported.⁴⁴⁻⁴⁷ The success of this procedure can be partially

attributed to the relatively low-pressure environment (20 to 30 mmHg during systole) found in pulmonary circulation, which is less demanding than pressures found in coronary arteries (100 to 140 mmHg during systole). Despite the urgent need for an engineered vascular tissue substitute, success is still limited.⁴⁸ While engineering approaches for other tissue substitutes can rely on in vivo remodelling to approach functionality with time, tissue-engineered blood vessels must function immediately on implantation – a significant challenge that contributed to its limited success.⁴⁹ The long lead time associated with the fabrication of an autologous vascular substitute is commonly invoked as a major limitation to widespread clinical use. While this point may be valid for emergency coronary artery surgical procedures or critically ischemic limbs, in practice, most coronary and distal vascular bypass procedures can be predicted and delayed over extended periods, allowing sufficient time for tissue fabrication.⁴⁸

Clinical trials of engineered vascular substitutes for the adult population has been initiated to examine the use of these grafts as arteriovenous shunts, as well as coronary and lower limb bypass grafts.⁴⁸ The initial clinical trial was focused on the safety of the arteriovenous shunt model due to the lack of suitable vein for hemodialysis and the deplorable efficacy of synthetic vascular grafts. Although graft failure in this model is unlikely to be life or limb-threatening, the high flow rates encountered (ca. 800 ml/min) generate considerable hemodynamic loads.⁴⁸ Notwithstanding both technological and regulatory challenges that lie ahead, engineered vascular tissues continued to be the "holy grail" of future vascular intervention.⁵⁰

2.5 Engineered Vascular Tissues as Species-specific Predictive Organ Model

The use of vascular cells and whole sections of a harvested artery in combination with animal models to study vascular diseases (e.g. atherosclerosis, post angioplasty restenosis, and hypertension) in an attempt to develop therapeutics is not new but employing engineered human vascular tissues for this role is a novel concept.⁵¹ While conventional 2D cell cultures are indispensable to our understanding of tissue morphogenesis and function in physiological and pathological states, they do not accurately replicate the 3D microenvironment of human tissues.⁵² For example, 2D culturing of vascular cells for studying intimal hyperplasia without the arterial wall structure and extracellular matrix (ECM) cannot recapitulate the intricate vascular wall mechanics and morphogenesis.⁵³ Similarly, animal organ cultures and whole animal models do not completely mimic the human biology due to the inevitable inter-species difference.⁵⁴ Studies using closely related nonhuman primates are constrained by limited availability, legal restrictions, ethical concerns, and high cost making these animal models impractical.⁵⁵ When studying human vascular diseases and therapeutics, a realistic model is a human tissue but the inability to experiment directly on human subjects limits this progress. Thus the need for an engineered human vascular tissue model to close this gap is of vital importance. Engineered human vascular tissues are not likely to replace animal or human subjects; however, they have the potential to provide high throughput, substantive, and detailed information regarding very specific conditions under controlled environments to study disease models and therapeutic outcomes that are not possible with animal-based model. The impact of successfully engineered human tissues is, therefore, not only restricted to the clinic but also fills a critical gap in the pre-clinical model tool chest between

traditional cell culture and whole animal experiments and has the potential to accelerate the pace of basic biomedical research.⁵⁶ A number of important physiological characteristics of native tissues appear to be preserved in an engineered tissue; thus providing models for specific disease conditions such as elevated contractility of vascular smooth muscle cells in hypertension, elevated proliferation in atherosclerosis and post-angioplasty restenosis and, fibrosis and cardiovascular remodeling.⁵⁷⁻⁶¹ In this context, engineered vascular tissue technology may be used both to validate drug targets and to optimize loads. This allows for cardiovascular drug screening in a more controlled and efficient way than can be performed using a traditional whole animal approach, thereby minimizing the number of laboratory animals used and decreasing the overall cost of performing research.⁵⁶ In recent years, engineered 3D tissue models such as cardiac patch⁶², lung tissue⁶³, cornea⁶⁴ and solid tumor^{65, 66} have emerged as powerful tools for drug discovery. Although clinical applications of engineered 3D tissues attracted most media attention, it is evident that engineered tissue models can serve as platforms for tightly controlled, high-content screening of drugs and for pharmacodynamic analyses.

2.6 Engineered Vascular Tissues in Physiological Genomics Studies

Physiological genomics is an emerging field that brings together the disciplines of genomics and cell, organ and whole animal systems integrative physiology in an effort to link gene products and pathways to phenotypes and physiological systems.^{56, 67} Physiological genomics study has traditionally been costly, requiring significant time to breed and age animals before initiating expensive and time-consuming phenotyping protocols.⁵⁶ Towards this end, the use of in vitro fabricated 3D tissue systems to reduce

the cost and time required for physiological genomic research is a relatively unexplored concept (Figure 2.5).

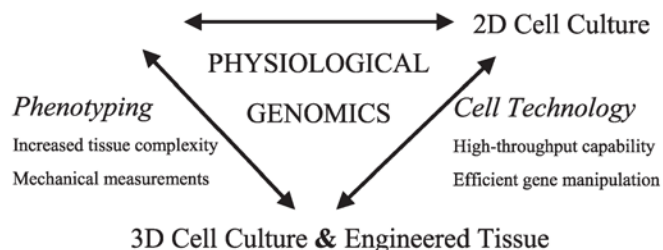


Figure 2.5: Engineered tissue provides an opportunity for obtaining a wide variety of phenotypes previously restricted to whole animal studies, including mechanical measurements such as force of contraction, in an environment that more closely replicates complex native tissue than 2D cell culture. This approach also captures practical advantages of 2D culture, including the ability to make high-throughput measurements and efficiently manipulate genomes. This unique model has the potential to provide a link between whole animal and traditional culture approaches to studying physiological genomics.⁵⁶

Recent progress in miniaturizing engineered tissues and associated physiological assay systems will accelerate our knowledge about interaction of the genome with both the phenome and the environment.⁵⁶ For example, using DNA microarrays with 9600 genes, Chien and coworkers⁶⁸ demonstrated that 77 vascular smooth muscle cells (VSMCs) genes were expressed more than twofold and 22 genes were expressed less than one-half in 3D matrix when compared with the 2D culture condition. Specifically, cells in 3D had less stress fibers and focal adhesions, and a lower level of tyrosine phosphorylation of focal adhesion kinase. The cyclin-dependent kinase inhibitor 1 (p21) was differentially upregulated in 3D leading to lower VSMC proliferation. Collagen I expression was also higher in 3D suggesting that VSMCs cultured on 3D matrix have increased ECM synthesis. In addition, Mequanint and coworkers⁶⁹ showed upregulation of the elastin gene and downregulation of VSMC differentiation marker genes when cultured on 3D

scaffolds compared with 2D surfaces. Differential gene expression is not limited to vascular cells. Several groups have reported preliminary evidence that gene expression of different cells cultured in 3D parallels more closely the in vivo situation.⁷⁰ Gene expression profiling experiments in various cell types clearly demonstrated close correlation between engineered and native tissues in tumor cells⁷¹, tendon⁷², bone⁷³, and skin⁷⁴. Collectively, these studies point to engineered tissue as a model system that could be used to test gene expression and study the effect of altered gene expression on function in vitro. In summary, successful application of these strategies may, in the near future, allow investigators to identify the gene or genes responsible for a phenotype or disease state in 3D culture rather than depending on the traditional positional cloning approach, which often requires years of painstaking breeding and phenotypic studies.⁵⁶

2.7 Essential Elements of Tissue Engineering

For tissue engineering to become a broadly accepted alternative for the treatment of diseased or otherwise compromised tissues and organs there are a number of critical elements that must still be addressed (Figure 2.6). These elements cover cell biology, materials design, bioprocess engineering, and clinical outcome. In the following sections each of the elements will be briefly discussed.

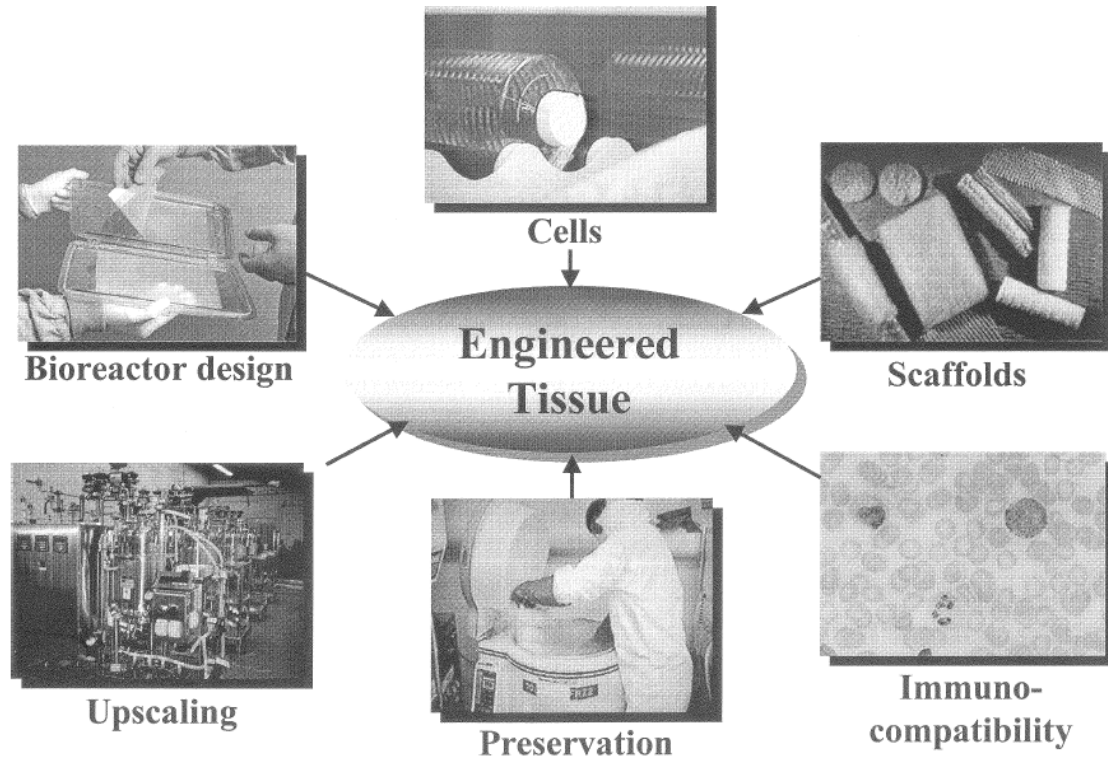


Figure 2.6: Essential elements in tissue engineering.⁷⁵ The fabrication of tissue-engineered products that meet the needs of clinical efficacy, quality, and regulatory requirements, manufacturing facility, and viable distribution mechanism requires expertise in each of several basic areas of research and development. These include cell sourcing and expansion, designing of biocompatible scaffolds that meet in vitro and in vivo tissue growth demands, designing bioreactors and large-scale manufacturing and preservation systems to enable cost-effective production and distribution. Finally, strategies for solving immunological issues must be developed.

2.7.1 Cell Sourcing

In order to engineer a tissue, cells are undoubtedly the starting point that needs to be considered. For vascular tissue engineering, the two main cell types needed are VSMCs and endothelial cells (ECs). VSMCs constitute the main cellular components of the tunica media of arterial vessels. In a mature artery, they display a contractile phenotype with a very low proliferative activity and produce only small amounts of ECM proteins⁷⁶ while expressing contractile cytoskeletal marker proteins such as smooth muscle α -actin

(SM- α -actin), smooth muscle myosin heavy chain (SMMHC), smoothelin-B, h-caldesmon and calponin; and contract in response to electrical, chemical and mechanical stimuli.^{77, 78} However, VSMCs may also acquire a synthetic phenotype and become predominantly proliferative if stimulated under certain biochemical and biomechanical conditions. In the synthetic phenotype, VSMCs suppress the expression of genes that define the contractile phenotype while rapidly upregulating genes required for proliferation including matrix metalloproteinases and l-caldesmon.^{4, 79-82} During vasculogenesis, VSMCs exist largely in the synthetic phenotype and synthesize ECM proteins such as elastin, collagens and glycosaminoglycans.⁸³ This phenotype modulation is useful to engineer vascular substitutes. VSMCs can be sourced from either the patient or a donor but the use of autologous cells is preferable since xenogenic and allogeneic cells introduce potential risks for immunorejection.^{84, 85} One limitation of patient-specific differentiated VSMCs is, however, their limited proliferative ability that results in extended time for cell expansion.⁸⁶⁻⁸⁸ In order to overcome senescence, ectopic expression of telomerase via human telomerase reverse transcriptase (hTERT) gene transfection of adult VSMC has been studied.^{89, 90} Despite robust cell growth that populated the scaffolds and resulted in a thick wall of the engineered artery, several issues related to the safety of telomerised cells need to be resolved before these cells are recommended for tissue engineering. For example, transfection with hTERT might lead to uncontrolled growth leading to intimal hyperplasia and possibly tumor development.⁹¹ Recent advances in sourcing VSMCs for fabricating vascular tissues have shifted towards stem cell niche with considerable success.⁹²⁻⁹⁶ Although VSMCs are the most studied in the context of engineered tissue fabrication, ECs play a significant role for the overall function of the engineered tissue. As such, a quiescent EC monolayer that regulates

contractile VSMCs phenotype is an important requirement for functional tissue-engineered vascular substitutes.⁹⁷ ECs have a dynamic nature and interact with the underlying VSMCs through direct cell-cell contact or through the synthesis and release of mediators into the surrounding medium.⁹⁸ In this thesis, human primary coronary artery smooth muscle cells are used.

2.7.2 Scaffolds

With the exception of some studies⁹⁹⁻¹⁰¹, porous scaffolds which mimic the extracellular matrix, are required for the 3D growth of cells to form engineered constructs.^{46, 102} Depending on the intended application, scaffolds may be designed to be biodegradable so that only the native tissue will remain after a given period of culture time or it may be biostable such that a composite tissue that provide long-term support could be fabricated.^{42, 46, 103-105} In the case of biodegradable scaffolds, cells will remodel the scaffold with their own ECM proteins creating the intended tissue without compromising tissue structural integrity. This, however, requires strict coordination of the scaffold biodegradation rate with the biosynthetic rate and is one of the major obstacles in the field today. In addition, a scaffold must have several required characteristics: biocompatibility, appropriate mechanical strength and compliance, optimal porosity for cell seeding, in vitro nutrient and oxygen transport, and the ability to bind to cells and release growth factors when needed. Although some of these criteria could be met with existing scaffolds, they do not provide biological cues for the cells imbedded in them and do not interact with the cells. In the body, cells reside within the ECM, which provides tissues with the appropriate architecture as well as signaling pathways that influence key cell function such as migration, proliferation, and differentiation. Regeneration of tissues in

in vitro thus requires that cells be given a more specific level of instruction so that tissue regeneration is successful. With the discovery of cell adhesion peptide domains in fibronectin, collagen and laminin, the design of synthetic extracellular matrices with biological activity has become an area of intense research activity.¹⁰⁶⁻¹⁰⁸ Scaffolds affect cellular functions such as adhesion, migration, proliferation, differentiation and secretion of ECM components.⁶⁹

2.7.3 Bioreactors

A bioreactor is a dynamic in vitro environment that uses both biochemical and mechanical signals to guide and regulate tissue developments.¹⁰⁹ The concept of bioreactors is neither new nor restricted to tissue engineering since cultivating proteins from microbial or mammalian cells for therapeutic or diagnostic applications is well-known.^{110, 111} They have been developed in response to static culture limitations and are used to distribute cells uniformly on 3D scaffolds, provide the desired concentrations of gases and nutrients in the culture medium, maintain efficient mass transfer to the growing tissue, and apply a physical stimuli to the developing tissue.^{112, 113} Several bioreactor designs such as rotating-wall, spinner flasks, and perfusion have been developed to engineer a variety of tissues (Figure 2.7). In order to properly simulate physiological conditions, vascular tissue engineering requires a system that mimics the hemodynamic forces experienced by vascular tissues. These mechanical forces include shear stress and stresses in the radial, circumferential and longitudinal directions. Shear stresses are tangential frictional forces that are directly perceived by endothelial cells and indirectly transmitted to smooth muscle cells as a result of interstitial flow and signalling.¹¹⁴⁻¹¹⁸ Initial attempts to create engineered blood vessels resulted in the manufacturing of grafts

with poor mechanical properties.¹¹⁹ The next generation of tissue engineered vascular substitutes had dramatically improved mechanical properties; however, it took several months to develop tissue engineered vascular grafts with desired optimal mechanical properties.¹⁰⁰ Because elastin and collagen are the main two components of ECM that determine the biomechanical properties of vascular tissues, dynamic mechanical conditioning of the construct accelerates the production of these two proteins. For example, the periodical radial distention resulted in accelerated maturation of engineered vascular tissues.^{120, 121} In an in vitro experiment with a rabbit pulmonary artery subjected to longitudinal stretch, the rate of elastin and collagen synthesis was related to the magnitude of the longitudinal stretch.¹²² It has been also reported that endothelial cell and smooth muscle cell proliferation rates in rabbit carotid arteries increased 50-fold and 15-fold respectively after three days of longitudinal stretch in vivo.¹²³ These data indicate that longitudinal stretch of arteries is an important mechanical force for accelerated cell proliferation, production of the ECM, and vascular remodeling.

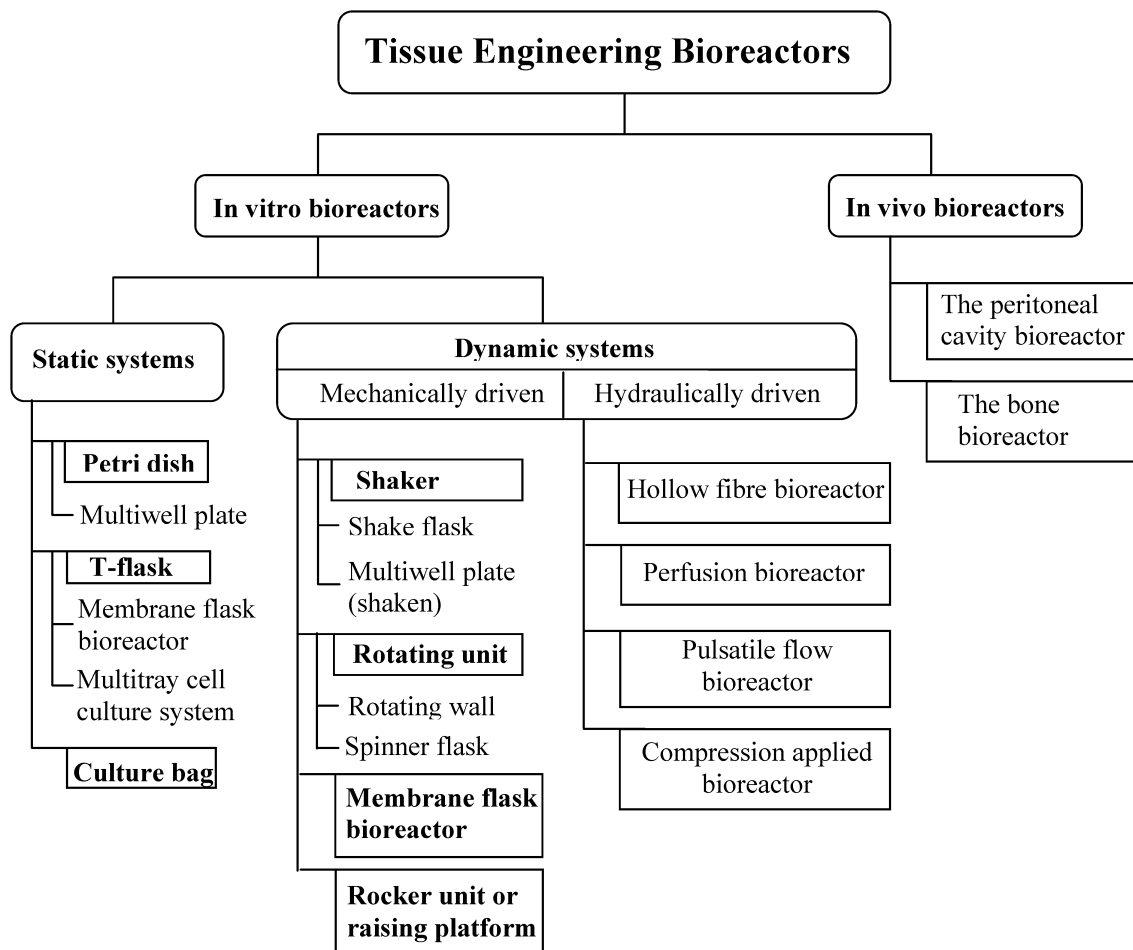


Figure 2.7: Summary of different bioreactors used for tissue fabrication.

The importance of mechanical forces on developing engineered vascular tissues is not fully understood. Most cells persist in the state of dynamic flux where gases and diffusible molecules may interact, either directly or indirectly as ligands by binding specific receptors on the cell surface, and thus modulating cellular phenotype.¹²⁴⁻¹²⁶ Shear forces act in a variety of different ways by acting on the endothelial cell membrane, thus indirectly affecting the cell, by acting on the cell as a whole, or by stressing specific molecules integrated into the cell membrane and transmit directly via transmembrane

proteins connecting to the cells interior organelles or indirectly through cell signalling cascades which lead to change in gene expression.^{21, 127, 128}

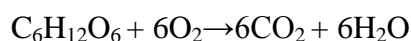
Blood vessels are permanently subjected to mechanical forces in the form of stretch, encompassing cyclic mechanical strain due to the pulsatile nature of blood flow and shear stress. Blood pressure is the major determinant of vessel stretching. It creates radial and tangential forces which counteract the effects of intraluminal pressure, and which affect all cell types in the vessel. In comparison, fluid shear stress results from the friction of blood against the vessel wall, and it acts in parallel to the vessel surface. Accordingly, shear is sensed principally by endothelial cells located at the interface between the blood and the vessel wall.¹²⁹ Alterations in stretch or shear stress invariably produce transformations in the vessel wall that will aim to accommodate the new conditions and to ultimately restore basal levels of tensile stress and shear stress. Hence, while acute changes in stretch or shear stress correlate with transient adjustments in vessel diameter, mediated through the release of vasoactive agonists or change in myogenic tone, chronically altered mechanical forces usually instigate important adaptive alterations of vessel wall shape and composition. The concept of vascular remodelling has therefore been used to describe these transformations that occur in vessels undergoing mechanical stresses.^{126, 130}

2.8 Oxygen Mass Transfer in Tissues

2.8.1 The Challenges of Oxygen Transfer in Engineered Tissues

As discussed above, bioreactors have been developed with the intent to mechanically stimulate the growing tissue constructs with physiologically relevant forces and to

improve mass transfer within the tissue. Although the former is largely successful, the later has shown to be a formidable engineering task. Therefore the delivery of nutrient and the removal of metabolic waste materials remained to be a fundamental consideration for fabricating engineered tissues. Oxygen delivery, in particular, is a limiting step for clinically-relevant size tissues because of its low solubility in culture media. This is further exacerbated by the fact that cells consume five to six moles of oxygen per mole of monosaccharide¹³¹⁻¹³³ according to the following mole balance.



Clearly, the delivery of this much oxygen to cells required the development of oxygen delivery system that is more efficient than molecular diffusion alone.

2.8.2 In Vivo Oxygen Transfer

In vivo, the above-mentioned limitation is mitigated by two specialized systems. First, the presence of the circulatory system carries the oxygen in blood by convection (Table 2.1) to the capillaries that are closer to the cells facilitating oxygen diffusion over shorter distances.

Table 2. 1: Peak convection rates of blood in the vasculature.¹³⁴

Compartment	cm/sec
Aorta	140±40
Common carotid	100±20
Vertebral	36±9
Femoral	90±13

However, at an arterial pO_2 (100 mmHg), only 0.3 ml oxygen dissolves in 100 ml plasma. Given that a human body needs 250 ml oxygen per minute,¹³⁴ plasma-dissolved oxygen contributes only to 15 ml/min at a cardiac output of 5 L/min. In the absence of an oxygen carrier, this translates to a cardiac output of 83 L/min which is impossible. This limitation is addressed by a second specialized system in which the oxygen carrier protein, hemoglobin, overcomes the very low solubility of oxygen in plasma.

2.8.3 The Oxygen-hemoglobin Dissociation Curve

The cooperative binding of oxygen to hemoglobin is described by the oxygen-hemoglobin dissociation curve. This is an equilibrium curve that expresses the fractional occupancy of the hemoglobin oxygen binding sites (Y) at a given oxygen partial pressure (pO_2) (Figure 2.7).

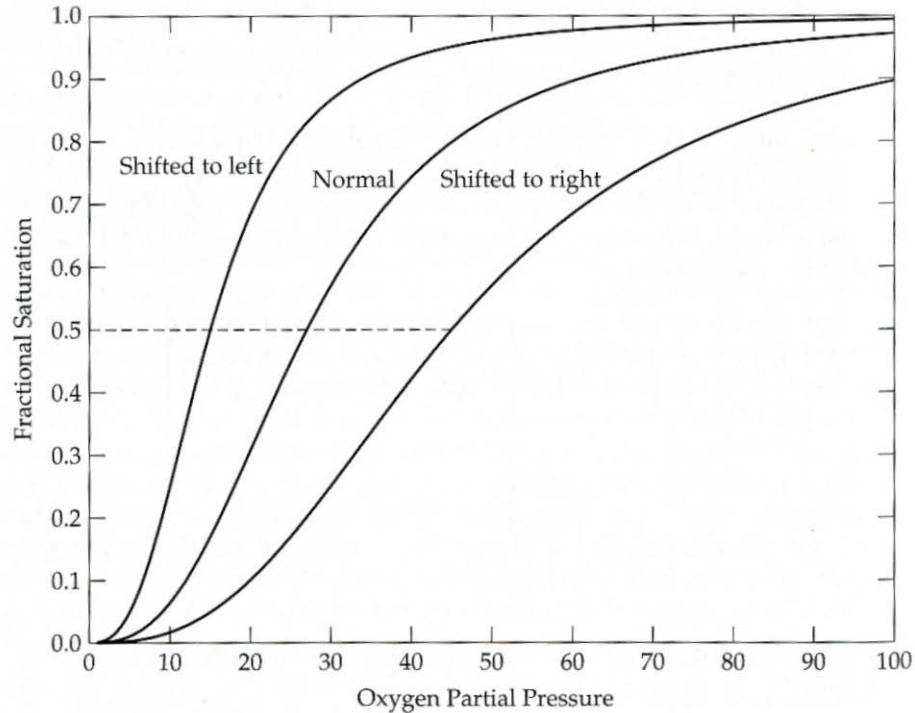


Figure 2.8: Changes in the oxygen-hemoglobin dissociation curve.¹³⁵ A shift to the right is often caused by increased CO_2 concentration or a decreased pH. The opposite is true for the shift to the left.

The equilibrium oxygen partial pressure above the solution of blood is related to the dissolved oxygen concentration by Henry's law.

$$yP \equiv pO_2 = HC \quad (1)$$

In the above equation, H is the Henry constant, which is $0.74 \left(\frac{\text{mmHg}}{\mu\text{M}} \right)$ for oxygen, C is

the dissolved oxygen concentration (μM) and y is the mole fraction of oxygen in the gas phase. It will be important to realize that the pO_2 is exerted only by the dissolved oxygen.

The oxygen bound to the hemoglobin does not affect pO_2 but serves only as a source for oxygen. With this in mind, hemoglobin bound oxygen is transported by the circulatory system to the capillaries where a change in the pO_2 levels along the length of the capillary causes oxygen to be released. This released oxygen then diffuses across the capillary wall

to reach the cells. The binding and releasing of oxygen to hemoglobin is represented by Hill's equation.



$$\frac{d[\text{Hb}]}{dt} = k_1 [\text{Hb}(\text{O}_2)_n] - k_{-1} [\text{Hb}][\text{O}_2]^n \quad (3)$$

Where k_1 and k_{-1} are the association and dissociation rate constants respectively.

The overall equation can also be written as:

$$[\text{Hb}(\text{O}_2)_n] = k [\text{Hb}][\text{O}_2]^n ; \text{ where } k = k_{-1} / k_1 \quad (4)$$

The oxygen demand of a tissue can be calculated through the basic material balances on a controlled volume. Let Γ represent the tissue metabolic volumetric oxygen consumption rate in $\left[\frac{\mu\text{M}}{\text{sec}} \right]$, V_t is volume of the tissue space (including the capillaries), q is the tissue blood perfusion rate (mL of blood /cm³ tissue/min), C is dissolved oxygen in plasma (μM), C' the concentration of oxygen in the blood that is bound to the hemoglobin (μM), C_t represents the concentration of oxygen dissolved in the interstitial space of the tissue (μM), P_c represents the permeability of oxygen through the capillary wall and S_c represents the total surface area of the capillaries (cm³). The mass balance in the blood will be:

$$0 = qV(C + C')_A - qV(C + C')_V - P_c S_c (C_v - C_t) \quad (5)$$

Whereas the mass balance in the tissue is:

$$0 = P_c S_c (C_v - C_t) - V_t \Gamma \quad (6)$$

Combining equations (5) and (6) the metabolic oxygen consumption is given by,

$$\Gamma = q[(C + C')_A - (C + C')_V] \quad (7)$$

At the normal tissue perfusion rate of 0.5 ml of blood /cm³ tissue/min, taking the partial pressure of oxygen in arterial and venous blood to be around 100 and 40 mmHg respectively, and assuming the density of the tissue ~1g/cm³, Γ will be 23 μM /sec. The experimentally measured average body oxygen consumption value reported in the literatures is in the order of 20 μM /sec which is in good agreement with the predicted value.¹³⁶

2.8.4 Alternative Oxygen Binding Chemicals

The search for alternative oxygen binding chemicals has been and still remained to be an active area of research.¹³⁷ From a clinical standpoint, this has been fuelled by increasing negative public perceptions about blood safety coupled with the potential risk of transmitting diseases due to transfusion.^{138, 139} The use of a blood substitute during surgery will reduce patient exposure to donor blood, thereby minimizing disease transmission and preventing other unwanted transfusion-related complications especially immunomodulatory reactions.¹³⁹ Alternative oxygen binding chemicals broadly fall in one of two categories: i) modified hemoglobin derived either from human and animal sources and crosslinked to improve intravascular persistence times or engineered genetically using recombinant technology.^{140, 141} ii) synthetic, inert, perfluorinated

compounds (PFC).¹⁴² Due to the relevance of PFCs to the work in this thesis, pertinent review is presented in the following section.

2.9 The Chemistry of Perfluorocarbon Compounds

PFCs are organic compounds whose hydrogen atoms in the carbon network are replaced by fluorine atoms. There is no surprise that replacing all the hydrogen atoms by fluorine in an organic molecule should bring significant changes in the properties of the resulting compound. Since all electrons in fluorine atom are packed in a proportionally less space, fluorine has a much denser electron cloud and higher ionization potential compared with hydrogen. The thermodynamic stability of PFCs is derived from the enhanced match between the carbon and fluorine orbitals as compared to that between carbon and hydrogen - leading to the strongest single bond (ca. 530 kJ/mol) found in PFC compounds.¹⁴³ Furthermore, the extreme electron attracting character of fluorine enhances the C-C bond energy in the skeleton by "shrinking" the orbitals of the carbons. These factors are responsible for the inertness of PFCs since there exists no low energy molecular orbitals accessible for reaction as the fluorine atoms shield the C-C skeleton sterically.¹⁴³ Given that PFCs are extremely stable and inert to many aggressive environments, they are also not metabolized as there are no enzymes able to break them down.

2.9.1 Oxygen Solubility in PFCs

PFCs have unique characteristics of low water and lipid solubility (i.e hydrophobic and lipophobic) but high dissolving power for oxygen and carbon dioxide making them attractive for both chemical and biological research.¹⁴⁴ Gas solubility is a result of

fluorine's low polarizability which translates to low van der Waals intermolecular interaction within the PFC molecule. Since van der Waals interactions are the only intermolecular forces that hold non-polar compounds together, these forces are feeble, in contrast with their intramolecular bonds. This low cohesive energy density in PFC compounds dissolves another low cohesive energy density compound such as oxygen (Figure 2.9).

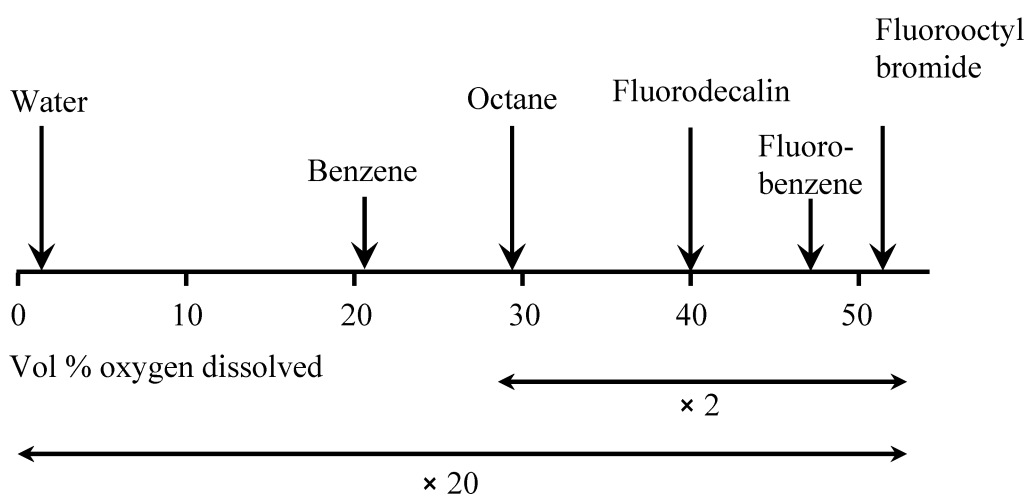


Figure 2.9: Oxygen solubility in different hydrocarbons and fluorocarbons.¹⁴³

Oxygen binds to hemoglobin by strong, localized chemical coordinate bond established between the oxygen molecule and the iron atom of a heme. In the case of PFC, however, there is a physical dissolution of oxygen characterized by loose non-directional van der Waals interaction among like materials¹⁴⁴. The difference in these interactions reflects the difference in oxygen uptake curves as a function of pO_2 which is sigmoid for hemoglobin and linear for PFC. The linearity is the result of Henry's law in which solubility is directly proportional to the gas's partial pressure, and not a localized chemical binding situation as

in hemoglobin. Consequent to this, oxygen can be rapidly and extensively extracted from PFCs when needed.

2.9.2 PFCs as Oxygen Delivery Systems

Their high oxygen dissolving power and outstanding chemical and biological inertness is the basis that made PFCs as candidates for in vivo O₂ delivery.¹⁴³ Although the ability of PFC in dissolving larger amounts of gases than any other solvent was already known, Clark and Gollan¹⁴⁵ were the first to demonstrate that mice could live while breathing an O₂-saturated liquid PFC without any harm to the animals. As indicated earlier, PFCs are both hydrophobic and lipophobic and thus are insoluble in water and lipids - two of the most abundant biological fluids. The PFC-water interfacial tension which opposes the dispersion of PFCs in water can reach as high as 60 mN/m. In order to effectively use them, they must be emulsified[~] demanding a stable, injectable, small-sized, narrowly distributed PFC emulsion (Figure 2.10). The non-ideal nature of the PFC-water solution suggests the difficulty to store the emulsion for an extended period of time.

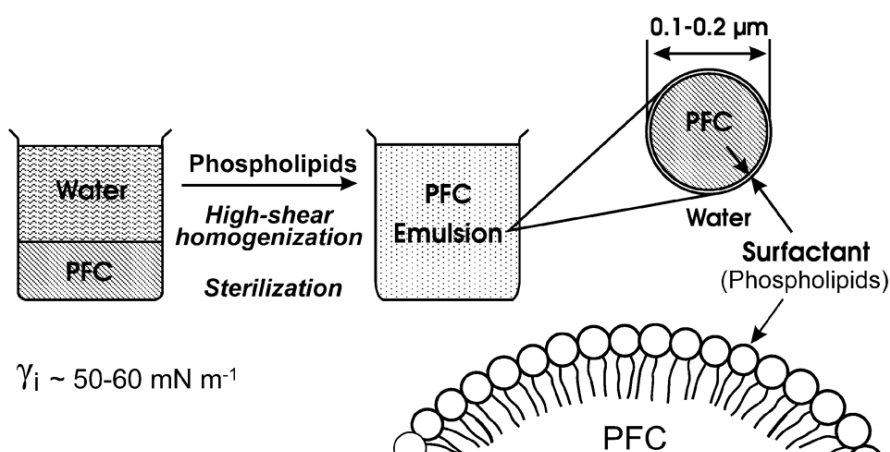


Figure 2.10: Preparation of perfluorocarbon emulsion using surfactants and dispersion energy in order to overcome the PFC-water interfacial tension. Terminal heat sterilization is achieved in a rotary sterilizer.¹⁴³

The first preparation of a physiologically adjusted PFC emulsion was reported by Sloviter and Kamimoto using bovine serum albumin as a surfactant.¹⁴⁶ Following this early report, a triblock copolymer of poly(ethylene oxide) and poly(propylene oxide), egg yolk phospholipids, potassium oleate and fluorinated surfactants or any combination thereof have been investigated as emulsifiers.¹³⁷ Although pure PFCs are not toxic at all, the toxicity of PFC emulsions to cultured cells is attributed to the emulsifiers used. Within the context of tissue engineering, PFCs have been shown to enhance oxygen delivery to the growing tissue construct, despite some limitation such as droplet settling due to density differences.^{147, 148}

2.10 Diffusion in Porous Media and Its Relevance in Tissue Engineering

It was stated earlier that one of the essential elements in tissue engineering is a porous 3D scaffold with interconnected pores. A porous 3D scaffold mimics the pores present within the extracellular fibrous matrix.¹³⁶ One important parameter in the study of porous materials is tortuosity¹⁴⁹ which is the ratio of the minimum inter-pore distance between two pores to the shortest distance between those pores. The movement of fluid molecule in a porous media follows tortuous pathways in the scaffold void space. Fluid flow governing equations in porous media can be numerically solved for the individual pores if the structures of the pore networks are known. Alternatively, the porous medium could be assumed to be a uniform material in a continuum approach and solved by using Darcy's law. In this later approach, there are three length scales namely: the average size (δ) of the pore, the distance (L) over which macroscopic change of physical quantities (e.g. fluid velocity and pressure) must be considered, and another length (l) between L and δ . This last length scale is introduced since L is chosen to be the characteristic linear dimension of

the porous medium (e.g. the size of the scaffold, or the size of the tissue) and is required to be at least two orders of magnitude larger than δ .¹³⁵ To define l , a volume of dimension l in the porous medium is considered. The volume fraction of the void space is then the volumetric porosity (ε) and, the volume fraction of the solid phase is equal to $1 - \varepsilon$. When l is closer to δ , ε is more sensitive to the value of l . Conversely, when l is selected to be large, the sensitivity decreases. There exists a value of l beyond which the sensitivity is minimal. In biological tissue $\delta < 0.1\mu m$, $l \approx 1\mu m$ and $L \approx 100\mu m$ allowing transport in biological tissues or scaffolds to be studied with the continuum approach.¹³⁵

Fluid transport in scaffolds must also satisfy the conservation of mass. Because both fluid production and fluid consumption are present when cells are seeded to scaffolds and cultured, the mass balance

$$\nabla v = \phi_B - \phi_L \quad (8)$$

$$\nabla \varepsilon v_f = \varphi_B - \varphi_L \quad (9)$$

Where, v is the fluid average velocity in representative volume, v_f is fluid average velocity in the volume, ϕ_B and ϕ_L are volumetric flow rates per unit volume of porous medium in sources and sinks respectively. The values of ϕ_B and ϕ_L are determined by Starling's Law.

$$\nabla v = \phi_B - \phi_L \quad (10)$$

Where J_v is flow rate, S is the surface area, L_p is the hydraulic conductivity, P is the hydrostatic pressure and π is the osmotic pressure.

It is also possible to express the velocity as follows:

$$v = -K\nabla P \quad (11)$$

∇P is the gradient of hydrostatic pressure and K is hydrostatic conductivity. In combination with equation (8)

$$\nabla(-K\nabla P) = \phi_B - \phi_L \quad (12)$$

Equations (11) and (12) are the governing equations for fluid flow in porous media. The scaffolds interstitial space can be considered a network of channels filled with porous media. Fluid flow in such channels may be correctly modeled by Darcy's law. When the specific permeability (k) of the porous media is low, equation (12) become the Brinkman equation.

$$\mu\nabla V - \frac{\mu}{K}V - \nabla P = 0 \quad (13)$$

These equations were used to model flow behavior in scaffolds and vascular tissue engineering bioreactors.¹⁵⁰⁻¹⁵²

2.10.1 Squeeze Flow in Porous Scaffolds

Squeeze flow refers to the fluid flow caused by the relative movement of solid boundaries towards each other. The boundaries can be either external or internal for fluid flow in a porous scaffold. Squeeze flow is applicable in the interstitial space of vascular tissue engineering scaffolds; because it mimics the compliance of the vasculature in response to the pulsatile force generated by the heart.¹⁵³⁻¹⁵⁵

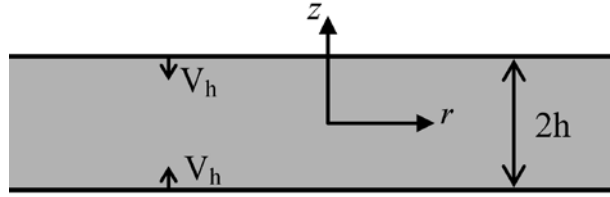


Figure 2.11: Squeeze flow model. The two boundaries are moving to each other at a velocity of V_h , and the space between them is $2h$.

Squeeze flow is best expressed by equation (13). In a cylindrical coordinate there is no

pressure gradient in z direction and hence $\frac{\partial P}{\partial z} = 0$. With this we have:

$$\mu \frac{\partial^2 V_r}{\partial z^2} - \frac{\mu}{k} V_r - \frac{\partial P}{\partial r} = 0 \quad (14)$$

Where k is the specific permeability of the scaffold. The equation is subject to the following boundary conditions:

$$V_r = 0 \Big|_{z=h}, \text{ and } \frac{\partial V_r}{\partial r} = 0 \Big|_{z=0}$$

The solution for (14) is then

$$V_r = C_1 \sinh\left(\frac{z}{\sqrt{k}}\right) + C_2 \cosh\left(\frac{z}{\sqrt{k}}\right) - \frac{k}{\mu} \frac{\partial P}{\partial r} \quad (15)$$

$$V_r = \frac{k}{\mu} \frac{\partial P}{\partial r} \left[\cosh\left(\frac{z}{\sqrt{k}}\right) \left(\cosh\left(\frac{h}{\sqrt{k}}\right) \right)^{-1} - 1 \right] \quad (16)$$

$$V_z = \frac{-k\sqrt{k}}{\mu} \left[\sinh\left(\frac{z}{\sqrt{k}}\right) \left(\cosh\left(\frac{h}{\sqrt{k}}\right) \right)^{-1} - \frac{z}{\sqrt{k}} \right] \left[\frac{\partial^2 P}{\partial r^2} + \frac{1}{r} \frac{\partial P}{\partial r} \right] \quad (17)$$

In a cylindrical coordinate system, the continuity equation is written as:

$$\frac{1}{r} \frac{\partial(rV_r)}{\partial r} + \frac{\partial V_z}{\partial z} = 0 \quad (18)$$

Subject to the boundary conditions $V_z = V_h|_{z=h}$, and $V_z = 0|_{z=0}$, the solution leads to:

$$\frac{V_h}{\frac{k\sqrt{k}}{\mu} \left[\tanh\left(\frac{h}{\sqrt{k}}\right) - \frac{h}{\sqrt{k}} \right]} = \left[\frac{\partial^2 P}{\partial r^2} + \frac{1}{r} \frac{\partial P}{\partial r} \right] \quad (19)$$

Thus solving (19) for the second order differential equation will give the pressure distribution as:

$$P = \frac{r^2}{4} A + B \ln r + C \quad (20)$$

Using the boundary conditions,

$$\frac{\partial P}{\partial r} = 0 \Big|_{r=0}, \text{ and } P = P_o \Big|_{r=R}$$

$$P = P_o + \frac{V_h}{\frac{4k\sqrt{k}}{\mu} \left[\tanh\left(\frac{h}{\sqrt{k}}\right) - \frac{h}{\sqrt{k}} \right]} (r^2 - R^2) \quad (21)$$

Therefore, equations (19-21) provide the fluid velocity and pressure profiles for a squeeze flow. The velocity profile will provide the shear stress distribution in the scaffold which is one of the parameters to be considered in dynamic cell culture experiments. The utility

of squeeze flow model has been demonstrated in cartilage, bone, and vascular tissue engineering strategies.¹⁵⁶⁻¹⁶⁰

2.10.2 Lattice Boltzmann's Approach for Porous Fluid Flow

The Lattice–Boltzmann method with computational fluid dynamics has been used to simulate the flow conditions within perfused cell-seeded cylindrical scaffolds.^{161, 162}

Microcomputed tomography imaging is used to define the scaffold micro-architecture for the simulations, which produces a 3D fluid velocity field throughout the scaffold porosity.

Shear stresses are then estimated at various media flow rates by multiplying the symmetric part of the gradient of the velocity field by the dynamic viscosity of the cell culture media. The shear stress algorithm was validated by modeling flow between infinite parallel plates and comparing the calculated shear stress distribution to the analytical solution. The simulation results relating to perfusion experiments gave an average surface shear stress to correspond to increased cell proliferation, while higher shear stresses were associated with upregulation of bone marker genes. Even though this model has been used for cartilage and bone tissue engineering, it is primarily used to compare results obtained for different perfusion bioreactor systems or different scaffold micro-architectures and may allow specific shear stresses to be determined that optimize the amount, type, or distribution of in vitro tissue growth transport. In particular, it is applicable and equally usable in vascular tissue engineering with load applied bioreactors.¹⁶³⁻¹⁶⁵

2.11 Summary

In the preceding sections, literature review pertinent to this thesis is presented. Due to rapid advances made in tissue engineering, it was not possible to include all aspects of the field. However, every effort is made to ensure that seminal works and significant research findings are included, with minimal bias, in this Chapter. Notwithstanding the different challenges and opportunities presented by tissue engineering strategies, this thesis will only attempt to address oxygen mass transfer limitations in engineered tissue constructs.

2.12 Hypothesis and Objectives of the Study

It is hypothesized that 3D polyurethane scaffolds with interconnected pores enhance oxygen diffusivity. It is further hypothesized that oxygen delivery strategies using PFC enhances mass transfer and human coronary artery smooth muscle cells (HCASMC) infiltration when seeded into 3D polyurethane. In order to test the above hypotheses, the following objectives were formulated:

- Fabricating 3D porous poly (carbonate urethane) (PCU) scaffolds using a pressure differential/particulate leaching technique at different PCU concentration.
- Measuring of effective diffusivity of oxygen through PCU 3D scaffolds
- Developing a mathematical model for oxygen profile on cell seeded 3D scaffold and in the lumen channel.
- Evaluating the supply of oxygen to HCASMC seeded on 3D PCU scaffolds using oxygen carrier particles embedded in the scaffold.

2.13 References

1. Bohl, K. S.; West, J. L., Nitric oxide-generating polymers reduce platelet adhesion and smooth muscle cell proliferation. *Biomaterials* **2000**, 21, (22), 2273-8.
2. Ross, R., The pathogenesis of atherosclerosis: a perspective for the 1990s. *Nature* **1993**, 362, (6423), 801-9.
3. D'Armiento, J., Decreased elastin in vessel walls puts the pressure on. *J Clin Invest* **2003**, 112, (9), 1308-10.
4. Owens, G. K.; Kumar, M. S.; Wamhoff, B. R., Molecular regulation of vascular smooth muscle cell differentiation in development and disease. *Physiol Rev* **2004**, 84, (3), 767-801.
5. Martini, F. H., *Fundamentals of Anatomy and physiology*. Prentice Hall: 1998; p 710 and 712.
6. Fawcett, D. W., *Bloom and Fawcett: A Textbook of Histology*. 12 ed.; A Hodder Arnold Publication: 1997; p 368-409.
7. Lulis, A. J., Atherosclerosis. *Nature* **2000**, 407, (6801), 233-41.
8. Yamanaka, O.; Hobbs, R. E., Coronary artery anomalies in 126,595 patients undergoing coronary arteriography. *Cathet Cardiovasc Diagn* **1990**, 21, (1), 28-40.
9. Engel, H. J.; Torres, C.; Page, H. L., Jr., Major variations in anatomical origin of the coronary arteries: angiographic observations in 4,250 patients without associated congenital heart disease. *Cathet Cardiovasc Diagn* **1975**, 1, (2), 157-69.
10. Fernandes, E. D.; Kadivar, H.; Hallman, G. L.; Reul, G. J.; Ott, D. A.; Cooley, D. A., Congenital malformations of the coronary arteries: the Texas Heart Institute experience. *Ann Thorac Surg* **1992**, 54, (4), 732-40.
11. Byrum, C. J.; Blackman, M. S.; Schneider, B.; Sondheimer, H. M.; Kavey, R. E., Congenital atresia of the left coronary ostium and hypoplasia of the left main coronary artery. *Am Heart J* **1980**, 99, (3), 354-8.
12. Musiani, A.; Cernigliaro, C.; Sansa, M.; Maselli, D.; De Gasperis, C., Left main coronary artery atresia: literature review and therapeutical considerations. *Eur J Cardiothorac Surg* **1997**, 11, (3), 505-14.
13. Desmet, W.; Vanhaecke, J.; Vrolix, M.; Van de Werf, F.; Piessens, J.; Willems, J.; de Geest, H., Isolated single coronary artery: a review of 50,000 consecutive coronary angiographies. *Eur Heart J* **1992**, 13, (12), 1637-40.

14. Grabow, N.; Martin, D. P.; Schmitz, K. P.; Sternberg, K., Absorbable polymer stent technologies for vascular regeneration. *J Chem Technol Biotechnol* **2010**, *85*, (6), 744-751.
15. Sabik, J. F., 3rd, Understanding saphenous vein graft patency. *Circulation* **2011**, *124*, (3), 273-5.
16. Verma, S.; Szmítko, P. E.; Weisel, R. D.; Bonneau, D.; Latter, D.; Errett, L.; LeClerc, Y.; Femes, S. E., Should radial arteries be used routinely for coronary artery bypass grafting? *Circulation* **2004**, *110*, (5), e40-6.
17. Desai, N. D.; Cohen, E. A.; Naylor, C. D.; Femes, S. E., A randomized comparison of radial-artery and saphenous-vein coronary bypass grafts. *N Eng J Med* **2004**, *351*, (22), 2302-2309.
18. Kobayashi, J., Current status of coronary artery bypass grafting. *Gen Thorac Cardiovasc Surg* **2008**, *56*, (6), 260-267.
19. Schmitto, J. D.; Rajab, T. K.; Cohn, L. H., Prevalence and variability of internal mammary graft use in contemporary multivessel coronary artery bypass graft. *Curr Opin Cardiol* **2010**, *25*, (6), 609-612.
20. Owens, C. D.; Wake, N.; Conte, M. S.; Gerhard-Herman, M.; Beckman, J. A., In vivo human lower extremity saphenous vein bypass grafts manifest flow mediated vasodilation. *J Vasc Surg* **2009**, *50*, (5), 1063-1070.
21. Akowuah, E. F.; Sheridan, P. J.; Cooper, G. J.; Newman, C., Preventing saphenous vein graft failure: Does gene therapy have a role? *Ann Thorac Surg* **2003**, *76*, (3), 959-966.
22. Tatoulis, J.; Buxton, B. F.; Fuller, J. A.; Meswani, M.; Theodore, S.; Powar, N.; Wynne, R., Long-Term Patency of 1108 Radial Arterial-Coronary Angiograms Over 10 Years. *Ann Thorac Surg* **2009**, *88*, (1), 23-30.
23. Weintraub, W. S.; Jones, E. L.; Craver, J. M.; Guyton, R. A., Frequency of Repeat Coronary-Bypass or Coronary Angioplasty after Coronary-Artery Bypass-Surgery Using Saphenous Venous Grafts. *Am J Cardiol* **1994**, *73*, (2), 103-112.
24. Kannan, R. Y.; Salacinski, H. J.; Butler, P. E.; Hamilton, G.; Seifalian, A. M., Current status of prosthetic bypass grafts: A review. *J Biomed Mater Res B* **2005**, *74B*, (1), 570-581.
25. Rashid, S. T.; Fuller, B.; Hamilton, G.; Seifalian, A. M., Tissue engineering of a hybrid bypass graft for coronary and lower limb bypass surgery. *FASEB J* **2008**, *22*, (6), 2084-2089.
26. Maisel, W. H., A device for proximal anastomosis of autologous coronary vein grafts - Report from the meeting of the circulatory system devices panel of the

- food and drug administration center for devices and radiologic health. *Circulation* **2005**, 112, (10), 1516-1518.
27. Abbott, W. M., Evaluation and Performance Standards for Arterial Prostheses - Reply. *J Vasc Surg* **1995**, 21, (3), 543-543.
 28. Bennion, R. S.; Williams, R. A.; Stabile, B. E.; Fox, M. A.; Owens, M. L.; Wilson, S. E., Patency of Autogenous Saphenous-Vein Versus Polytetrafluoroethylene Grafts in Femoropopliteal Bypass for Advanced Ischemia of the Extremity. *Surg Gynecol Obstet* **1985**, 160, (3), 239-242.
 29. Kannan, R. Y.; Salacinski, H. J.; Butler, P. E.; Hamilton, G.; Seifalian, A. M., Current status of prosthetic bypass grafts: a review. *J Biomed Mater Res B* **2005**, 74, (1), 570-81.
 30. Hoenig, M. R.; Campbell, G. R.; Rolfe, B. E.; Campbell, J. H., Tissue-engineered blood vessels: alternative to autologous grafts? *Arterioscler Thromb Vasc Biol* **2005**, 25, (6), 1128-34.
 31. Baguneid, M.; de Mel, A.; Yildirimer, L.; Fuller, B. J.; Hamilton, G.; Seifalian, A. M., In vivo study of a model tissue-engineered small-diameter vascular bypass graft. *Biotechnol App Bioc* **2011**, 58, (1), 14-24.
 32. Desai, M.; Seifalian, A. M.; Hamilton, G., Role of prosthetic conduits in coronary artery bypass grafting. *Eur J Cardio-Thorac* **2011**, 40, (2), 394-398.
 33. Zilla, P.; Bezuidenhout, D.; Human, P., Prosthetic vascular grafts: Wrong models, wrong questions and no healing. *Biomaterials* **2007**, 28, (34), 5009-5027.
 34. Annis, D., Polyether-Urethane Elastomers for Small-Diameter Arterial Prostheses. *Life Support Syst* **1987**, 5, (1), 47-52.
 35. Grasl, C.; Bergmeister, H.; Stoiber, M.; Schima, H.; Weigel, G., Electrospun polyurethane vascular grafts: In vitro mechanical behavior and endothelial adhesion molecule expression. *J Biomed Mater Res A* **2010**, 93A, (2), 716-723.
 36. Tiwari, A.; Salacinski, H.; Seifalian, A. M.; Hamilton, G., New prostheses for use in bypass grafts with special emphasis on polyurethanes. *Cardiovasc Surg* **2002**, 10, (3), 191-7.
 37. Brothers, T. E.; Stanley, J. C.; Burkel, W. E.; Graham, L. M., Small-caliber polyurethane and polytetrafluoroethylene grafts: a comparative study in a canine aortoiliac model. *J Biomed Mater Res* **1990**, 24, (6), 761-71.
 38. Rashid, S. T.; Salacinski, H. J.; Button, M. J. C.; Fuller, B.; Hamilton, G.; Seifalian, A. M., Cellular engineering of conduits for coronary and lower limb bypass surgery: Role of cell attachment peptides and pre-conditioning in optimising smooth muscle cells (SMC) adherence to compliant poly(carbonate-

- urea)urethane (MyoLink(TM)) scaffolds. *Eur J Vasc Endovasc* **2004**, 27, (6), 608-616.
39. Seifalian, A. M.; Salacinski, H. J.; Tiwari, A.; Edwards, A.; Bowald, S.; Hamilton, G., In vivo biostability of a poly(carbonate-urea)urethane graft. *Biomaterials* **2003**, 24, (14), 2549-2557.
 40. Stegemann, J. P.; Kaszuba, S. N.; Rowe, S. L., Review: advances in vascular tissue engineering using protein-based biomaterials. *Tissue Eng* **2007**, 13, (11), 2601-13.
 41. Shin'oka, T.; Imai, Y.; Ikada, Y., Transplantation of a tissue-engineered pulmonary artery. *N Engl J Med* **2001**, 344, (7), 532-3.
 42. Grenier, S.; Sandig, M.; Holdsworth, D. W.; Mequanint, K., Interactions of coronary artery smooth muscle cells with 3D porous polyurethane scaffolds. *J Biomed Mater Res A* **2009**, 89, (2), 293-303.
 43. Grenier, S.; Sandig, M.; Mequanint, K., Smooth Muscle alpha-actin and Calponin Expression and, Extracellular Matrix Production of Human Coronary Artery Smooth Muscle Cells in 3D Scaffolds. *Tissue Eng Part A* **2009**, 15, (10), 3001-3011.
 44. Shinoka, T.; Breuer, C., Tissue-engineered blood vessels in pediatric cardiac surgery. *Yale J Biol Med* **2008**, 81, (4), 161-6.
 45. Hibino, N.; McGillicuddy, E.; Matsumura, G.; Ichihara, Y.; Naito, Y.; Breuer, C.; Shinoka, T., Late-term results of tissue-engineered vascular grafts in humans. *J Thorac Cardiovasc Surg* **2010**, 139, (2), 431-6, 436 e1-2.
 46. Naito, Y.; Shinoka, T.; Duncan, D.; Hibino, N.; Solomon, D.; Cleary, M.; Rathore, A.; Fein, C.; Church, S.; Breuer, C., Vascular tissue engineering: towards the next generation vascular grafts. *Adv Drug Deliv Rev* **2011**, 63, (4-5), 312-23.
 47. Duncan, D. R.; Breuer, C. K., Challenges in translating vascular tissue engineering to the pediatric clinic. *Vasc Cell* **2011**, 3, (1), 23.
 48. L'Heureux, N.; Dusserre, N.; Marini, A.; Garrido, S.; de la Fuente, L.; McAllister, T., Technology insight: the evolution of tissue-engineered vascular grafts--from research to clinical practice. *Nat Clin Pract Cardiovasc Med* **2007**, 4, (7), 389-95.
 49. Patel, A.; Fine, B.; Sandig, M.; Mequanint, K., Elastin biosynthesis: The missing link in tissue-engineered blood vessels. *Cardiovasc Res* **2006**, 71, (1), 40-9.
 50. Dolgin, E., Taking tissue engineering to heart. *Nat Med* **2011**, 17, (9), 1032-5.
 51. Raimondi, M. T., Engineered tissue as a model to study cell and tissue function from a biophysical perspective. *Curr Drug Discov Technol* **2006**, 3, (4), 245-68.

52. Goodbye, flat biology? *Nature* **2003**, 424, (6951), 861.
53. Swanson, N.; Javed, Q.; Hogrefe, K.; Gershlick, A., Human internal mammary artery organ culture model of coronary stenting: a novel investigation of smooth muscle cell response to drug-eluting stents. *Clin Sci (Lond)* **2002**, 103, (4), 347-53.
54. Touchard, A. G.; Schwartz, R. S., Preclinical restenosis models: challenges and successes. *Toxicol Pathol* **2006**, 34, (1), 11-8.
55. Macchiarini, F.; Manz, M. G.; Palucka, A. K.; Shultz, L. D., Humanized mice: are we there yet? *J Exp Med* **2005**, 202, (10), 1307-11.
56. Petersen, M. C.; Lazar, J.; Jacob, H. J.; Wakatsuki, T., Tissue engineering: a new frontier in physiological genomics. *Physiol Genomics* **2007**, 32, (1), 28-32.
57. Auger, F. A.; D'Orleans-Juste, P.; Germain, L., Adventitia contribution to vascular contraction: hints provided by tissue-engineered substitutes. *Cardiovasc Res* **2007**, 75, (4), 669-78.
58. Laflamme, K.; Roberge, C. J.; Grenier, G.; Remy-Zolghadri, M.; Pouliot, S.; Baker, K.; Labbe, R.; D'Orleans-Juste, P.; Auger, F. A.; Germain, L., Adventitia contribution in vascular tone: insights from adventitia-derived cells in a tissue-engineered human blood vessel. *FASEB J* **2006**, 20, (8), 1245-7.
59. Laflamme, K.; Roberge, C. J.; Pouliot, S.; D'Orleans-Juste, P.; Auger, F. A.; Germain, L., Tissue-engineered human vascular media produced in vitro by the self-assembly approach present functional properties similar to those of their native blood vessels. *Tissue Eng* **2006**, 12, (8), 2275-81.
60. Elliott, N. T.; Yuan, F., A review of three-dimensional in vitro tissue models for drug discovery and transport studies. *J Pharm Sci* **2011**, 100, (1), 59-74.
61. L'Heureux, N.; Stoclet, J. C.; Auger, F. A.; Lagaud, G. J.; Germain, L.; Andriantsitohaina, R., A human tissue-engineered vascular media: a new model for pharmacological studies of contractile responses. *FASEB J* **2001**, 15, (2), 515-24.
62. Katare, R. G.; Ando, M.; Kakinuma, Y.; Sato, T., Engineered heart tissue: a novel tool to study the ischemic changes of the heart in vitro. *PLoS One* **2010**, 5, (2), e9275.
63. Huh, D.; Matthews, B. D.; Mammoto, A.; Montoya-Zavala, M.; Hsin, H. Y.; Ingber, D. E., Reconstituting organ-level lung functions on a chip. *Science* **2010**, 328, (5986), 1662-8.

64. Reichl, S.; Dohring, S.; Bednarz, J.; Muller-Goymann, C. C., Human cornea construct HCC-an alternative for in vitro permeation studies? A comparison with human donor corneas. *Eur J Pharm Biopharm* **2005**, 60, (2), 305-8.
65. Verbridge, S. S.; Choi, N. W.; Zheng, Y.; Brooks, D. J.; Stroock, A. D.; Fischbach, C., Oxygen-controlled three-dimensional cultures to analyze tumor angiogenesis. *Tissue Eng Part A* **2010**, 16, (7), 2133-41.
66. Hutmacher, D. W.; Horch, R. E.; Loessner, D.; Rizzi, S.; Sieh, S.; Reichert, J. C.; Clements, J. A.; Beier, J. P.; Arkudas, A.; Bleiziffer, O.; Kneser, U., Translating tissue engineering technology platforms into cancer research. *J Cell Mol Med* **2009**, 13, (8A), 1417-27.
67. Cowley, A. W., Physiological genomics: tools and concepts. *J Physiol* **2004**, 554, (Pt 1), 3.
68. Li, S.; Lao, J.; Chen, B. P.; Li, Y. S.; Zhao, Y.; Chu, J.; Chen, K. D.; Tsou, T. C.; Peck, K.; Chien, S., Genomic analysis of smooth muscle cells in 3-dimensional collagen matrix. *FASEB J* **2003**, 17, (1), 97-9.
69. Lin, S.; Sandig, M.; Mequanint, K., Three-dimensional topography of synthetic scaffolds induces elastin synthesis by human coronary artery smooth muscle cells. *Tissue Eng Part A* **2011**, 17, (11-12), 1561-71.
70. Birgersdotter, A.; Sandberg, R.; Ernberg, I., Gene expression perturbation in vitro-a growing case for three-dimensional (3D) culture systems. *Semin Cancer Biol* **2005**, 15, (5), 405-12.
71. Ghosh, S.; Spagnoli, G. C.; Martin, I.; Ploegert, S.; Demougin, P.; Heberer, M.; Reschner, A., Three-dimensional culture of melanoma cells profoundly affects gene expression profile: a high density oligonucleotide array study. *J Cell Physiol* **2005**, 204, (2), 522-31.
72. Sawaguchi, N.; Majima, T.; Iwasaki, N.; Funakoshi, T.; Shimode, K.; Onodera, T.; Minami, A., Extracellular matrix modulates expression of cell-surface proteoglycan genes in fibroblasts. *Connect Tissue Res* **2006**, 47, (3), 141-8.
73. Hamamura, K.; Jiang, C.; Yokota, H., ECM-dependent mRNA expression profiles and phosphorylation patterns of p130Cas, FAK, ERK and p38 MAPK of osteoblast-like cells. *Cell Biol Int* **2010**, 34, (10), 1005-12.
74. Smiley, A. K.; Klingenberg, J. M.; Aronow, B. J.; Boyce, S. T.; Kitzmiller, W. J.; Supp, D. M., Microarray analysis of gene expression in cultured skin substitutes compared with native human skin. *J Invest Dermatol* **2005**, 125, (6), 1286-301.
75. Naughton, G. K., From lab bench to market: critical issues in tissue engineering. *Ann N Y Acad Sci* **2002**, 961, 372-85.

76. Wamhoff, B. R.; Bowles, D. K.; Owens, G. K., Excitation-transcription coupling in arterial smooth muscle. *Circ Res* **2006**, 98, (7), 868-78.
77. Owens, G. K., Regulation of differentiation of vascular smooth muscle cells. *Physiol Rev* **1995**, 75, (3), 487-517.
78. Rensen, S. S.; Thijssen, V. L.; De Vries, C. J.; Doevendans, P. A.; Detera-Wadleigh, S. D.; Van Eys, G. J., Expression of the smoothelin gene is mediated by alternative promoters. *Cardiovasc Res* **2002**, 55, (4), 850-63.
79. Ueki, N.; Sobue, K.; Kanda, K.; Hada, T.; Higashino, K., Expression of high and low molecular weight caldesmons during phenotypic modulation of smooth muscle cells. *Proc Natl Acad Sci U S A* **1987**, 84, (24), 9049-53.
80. Sobue, K.; Hayashi, K.; Nishida, W., Expressional regulation of smooth muscle cell-specific genes in association with phenotypic modulation. *Mol Cell Biochem* **1999**, 190, (1-2), 105-118.
81. Menon, C.; Chacko, S., Expression of smooth muscle caldesmon in developing chicken gizzard. *Tissue Cell* **1998**, 30, (1), 118-26.
82. Kumar, M. S.; Owens, G. K., Combinatorial control of smooth muscle-specific gene expression. *Arterioscl Throm Vas* **2003**, 23, (5), 737-747.
83. Yoshida, T.; Owens, G. K., Molecular determinants of vascular smooth muscle cell diversity. *Circ Res* **2005**, 96, (3), 280-91.
84. Platt, J. L.; Nagayasu, T., Current status of xenotransplantation. *Clin Exp Pharmacol Physiol* **1999**, 26, (12), 1026-32.
85. Nerem, R. M.; Seliktar, D., Vascular tissue engineering. *Annu Rev Biomed Eng* **2001**, 3, 225-43.
86. Minamino, T.; Miyauchi, H.; Yoshida, T.; Tateno, K.; Komuro, I., The role of vascular cell senescence in atherosclerosis: antisenescence as a novel therapeutic strategy for vascular aging. *Curr Vasc Pharmacol* **2004**, 2, (2), 141-8.
87. Rabkin, E.; Schoen, F. J., Cardiovascular tissue engineering. *Cardiovasc Pathol* **2002**, 11, (6), 305-17.
88. Stegemann, J. P.; Kaszuba, S. N.; Rowe, S. L., Review: Advances in vascular tissue engineering using protein-based Biomaterials. *Tissue Eng* **2007**, 13, (11), 2601-2613.
89. McKee, J. A.; Banik, S. S.; Boyer, M. J.; Hamad, N. M.; Lawson, J. H.; Niklason, L. E.; Counter, C. M., Human arteries engineered in vitro. *EMBO Rep* **2003**, 4, (6), 633-8.

90. Poh, M.; Boyer, M.; Solan, A.; Dahl, S. L.; Pedrotty, D.; Banik, S. S.; McKee, J. A.; Klinger, R. Y.; Counter, C. M.; Niklason, L. E., Blood vessels engineered from human cells. *Lancet* **2005**, 365, (9477), 2122-4.
91. Kassem, M.; Abdallah, B. M.; Yu, Z.; Ditzel, N.; Burns, J. S., The use of hTERT-immortalized cells in tissue engineering. *Cytotechnology* **2004**, 45, (1-2), 39-46.
92. Kane, N. M.; Xiao, Q.; Baker, A. H.; Luo, Z.; Xu, Q.; Emanuelli, C., Pluripotent stem cell differentiation into vascular cells: a novel technology with promises for vascular re(generation). *Pharmacol Ther* **2011**, 129, (1), 29-49.
93. Liu, J. Y.; Peng, H. F.; Andreadis, S. T., Contractile smooth muscle cells derived from hair-follicle stem cells. *Cardiovasc Res* **2008**, 79, (1), 24-33.
94. Sundaram, S.; Niklason, L. E., Smooth Muscle and Other Cell Sources for Human Blood Vessel Engineering. *Cells Tissues Organs* **2012**, 195, (1-2), 15-25.
95. Wang, A.; Tang, Z.; Li, X.; Jiang, Y.; Tsou, D. A.; Li, S., Derivation of Smooth Muscle Cells with Neural Crest Origin from Human Induced Pluripotent Stem Cells. *Cells Tissues Organs* **2012**, 195, (1-2), 5-14.
96. Gong, Z.; Niklason, L. E., Small-diameter human vessel wall engineered from bone marrow-derived mesenchymal stem cells (hMSCs). *FASEB J* **2008**, 22, (6), 1635-48.
97. Chan-Park, M. B.; Shen, J. Y.; Cao, Y.; Xiong, Y.; Liu, Y.; Rayatpisheh, S.; Kang, G. C.; Greisler, H. P., Biomimetic control of vascular smooth muscle cell morphology and phenotype for functional tissue-engineered small-diameter blood vessels. *J Biomed Mater Res A* **2009**, 88, (4), 1104-21.
98. Heydarkhan-Hagvall, S.; Chien, S.; Nelander, S.; Li, Y. C.; Yuan, S.; Lao, J.; Haga, J. H.; Lian, I.; Nguyen, P.; Risberg, B.; Li, Y. S., DNA microarray study on gene expression profiles in co-cultured endothelial and smooth muscle cells in response to 4- and 24-h shear stress. *Mol Cell Biochem* **2006**, 281, (1-2), 1-15.
99. Gauvin, R.; Ahsan, T.; Larouche, D.; Levesque, P.; Dube, J.; Auger, F. A.; Nerem, R. M.; Germain, L., A novel single-step self-assembly approach for the fabrication of tissue-engineered vascular constructs. *Tissue Eng Part A* **2010**, 16, (5), 1737-47.
100. L'Heureux, N.; Paquet, S.; Labbe, R.; Germain, L.; Auger, F. A., A completely biological tissue-engineered human blood vessel. *FASEB J* **1998**, 12, (1), 47-56.
101. Norotte, C.; Marga, F. S.; Niklason, L. E.; Forgacs, G., Scaffold-free vascular tissue engineering using bioprinting. *Biomaterials* **2009**, 30, (30), 5910-7.
102. Sengupta, D.; Heilshorn, S. C., Protein-engineered biomaterials: highly tunable tissue engineering scaffolds. *Tissue Eng Part B Rev* **2010**, 16, (3), 285-93.

103. Ratcliffe, A., Tissue engineering of vascular grafts. *Matrix Biol* **2000**, 19, (4), 353-7.
104. Grenier, S.; Sandig, M.; Mequanint, K., Smooth muscle alpha-actin and calponin expression and extracellular matrix production of human coronary artery smooth muscle cells in 3D scaffolds. *Tissue Eng Part A* **2009**, 15, (10), 3001-11.
105. Grenier, S.; Sandig, M.; Mequanint, K., Polyurethane biomaterials for fabricating 3D porous scaffolds and supporting vascular cells. *J Biomed Mater Res A* **2007**, 82, (4), 802-9.
106. Li, J.; Ding, M.; Fu, Q.; Tan, H.; Xie, X.; Zhong, Y., A novel strategy to graft RGD peptide on biomaterials surfaces for endothelization of small-diameter vascular grafts and tissue engineering blood vessel. *J Mater Sci Mater Med* **2008**, 19, (7), 2595-603.
107. Dubey, G.; Mequanint, K., Conjugation of fibronectin onto three-dimensional porous scaffolds for vascular tissue engineering applications. *Acta Biomater* **2011**, 7, (3), 1114-25.
108. Ma, P. X., Biomimetic materials for tissue engineering. *Adv Drug Deliv Rev* **2008**, 60, (2), 184-98.
109. Martin, I.; Wendt, D.; Heberer, M., The role of bioreactors in tissue engineering. *Trends Biotechnol* **2004**, 22, (2), 80-6.
110. Nilsang, S.; Nehru, V.; Plieva, F. M.; Nandakumar, K. S.; Rakshit, S. K.; Holmdahl, R.; Mattiasson, B.; Kumar, A., Three-dimensional culture for monoclonal antibody production by hybridoma cells immobilized in macroporous gel particles. *Biotechnol Prog* **2008**, 24, (5), 1122-31.
111. Nilsang, S.; Nandakumar, K. S.; Galaev, I. Y.; Rakshit, S. K.; Holmdahl, R.; Mattiasson, B.; Kumar, A., Monoclonal antibody production using a new supermacroporous cryogel bioreactor. *Biotechnol Prog* **2007**, 23, (4), 932-9.
112. Isenberg, B. C.; Williams, C.; Tranquillo, R. T., Small-diameter artificial arteries engineered in vitro. *Circ Res* **2006**, 98, (1), 25-35.
113. Bilodeau, K.; Mantovani, D., Bioreactors for tissue engineering: focus on mechanical constraints. A comparative review. *Tissue Eng* **2006**, 12, (8), 2367-83.
114. Riha, G. M.; Lin, P. H.; Lumsden, A. B.; Yao, Q.; Chen, C., Roles of hemodynamic forces in vascular cell differentiation. *Ann Biomed Eng* **2005**, 33, (6), 772-9.
115. Bilodeau, K.; Couet, F.; Boccafoschi, F.; Mantovani, D., Design of a perfusion bioreactor specific to the regeneration of vascular tissues under mechanical stresses. *Artif Organs* **2005**, 29, (11), 906-12.

116. Lee, A. A.; Graham, D. A.; Dela Cruz, S.; Ratcliffe, A.; Karlon, W. J., Fluid shear stress-induced alignment of cultured vascular smooth muscle cells. *J Biomech Eng* **2002**, 124, (1), 37-43.
117. Zhao, S.; Suciu, A.; Ziegler, T.; Moore, J. E., Jr.; Burki, E.; Meister, J. J.; Brunner, H. R., Synergistic effects of fluid shear stress and cyclic circumferential stretch on vascular endothelial cell morphology and cytoskeleton. *Arterioscler Thromb Vasc Biol* **1995**, 15, (10), 1781-6.
118. Davies, P. F., Flow-mediated endothelial mechanotransduction. *Physiol Rev* **1995**, 75, (3), 519-60.
119. Weinberg, C. B.; Bell, E., A blood vessel model constructed from collagen and cultured vascular cells. *Science* **1986**, 231, (4736), 397-400.
120. Niklason, L. E.; Gao, J.; Abbott, W. M.; Hirschi, K. K.; Houser, S.; Marini, R.; Langer, R., Functional arteries grown in vitro. *Science* **1999**, 284, (5413), 489-493.
121. Niklason, L. E., Medical technology - Replacement arteries made to order. *Science* **1999**, 286, (5444), 1493-1494.
122. Kolpakov, V.; Rekhter, M. D.; Gordon, D.; Wang, W. H.; Kulik, T. J., Effect of Mechanical Forces on Growth and Matrix Protein-Synthesis in the in-Vitro Pulmonary-Artery - Analysis of the Role of Individual Cell-Types. *Circ Res* **1995**, 77, (4), 823-831.
123. Jackson, Z. S.; Gotlieb, A. I.; Langille, B. L., Wall tissue remodeling regulates longitudinal tension in arteries. *Circ Res* **2002**, 90, (8), 918-25.
124. Bissell, M. J.; Barcelloshoff, M. H., The Influence of Extracellular-Matrix on Gene-Expression - Is Structure the Message. *J Cell Sci* **1987**, 327-343.
125. Lehoux, S.; Tedgui, A., Signal transduction of mechanical stresses in the vascular wall. *Hypertension* **1998**, 32, (2), 338-345.
126. Lehoux, S.; Tedgui, A., Cellular mechanics and gene expression in blood vessels. *J Biomech* **2003**, 36, (5), 631-643.
127. Streuli, C., Extracellular matrix remodelling and cellular differentiation. *Curr Opin Cell Biol* **1999**, 11, (5), 634-640.
128. Humphries, M. J.; Travis, M. A.; Clark, K.; Mould, A. P., Mechanisms of integration of cells and extracellular matrices by integrins. *Biochem Soc T* **2004**, 32, 822-825.
129. Glagov, S., Intimal hyperplasia, vascular modeling, and the restenosis problem. *Circulation* **1994**, 89, (6), 2888-2891.

130. Tronc, F. o.; Mallat, Z.; Lehoux, S. p.; Wassef, M.; Esposito, B.; Tedgui, A., Role of Matrix Metalloproteinases in Blood Flow-Induced Arterial Enlargement : Interaction With NO. *Arterioscl Throm Vas* **2000**, 20, (12), e120-e126.
131. Malda, J.; Rouwkema, J.; Martens, D. E.; le Comte, E. P.; Kooy, F. K.; Tramper, J.; van Blitterswijk, C. A.; Riesle, J., Oxygen gradients in tissue-engineered PEGT/PBT cartilaginous constructs: Measurement and modeling. *Biotechnol Bioeng* **2004**, 86, (1), 9-18.
132. Radisic, M.; Deen, W.; Langer, R.; Vunjak-Novakovic, G., Mathematical model of oxygen distribution in engineered cardiac tissue with parallel channel array perfused with culture medium containing oxygen carriers. *Am J Physiol-Heart C* **2005**, 288, (3), H1278-H1289.
133. Radisic, M.; Malda, J.; Epping, E.; Geng, W. L.; Langer, R.; Vunjak-Novakovic, G., Oxygen gradients correlate with cell density and cell viability in engineered cardiac tissue. *Biotechnol Bioeng* **2006**, 93, (2), 332-343.
134. Schauf, C. L.; Moffett, D. F.; Moffett, S. B., *Human Phisology*, p.433. Mosby College Publishing: 1990.
135. Gerorge A. Truskey, F. Y., David F, Katz, *Transport Phenomena in Biological Systems*. Prarson Prentice Hall: 2004; p 398-411.
136. L.Fournier, R., *Basic Transport Phenomena In Biomedical Engineering*. Second Edition ed.; Taylor & Francis: 2007; p 203-207.
137. Riess, J. G., Oxygen carriers ("blood substitutes")--raison d'etre, chemistry, and some physiology. *Chem Rev* **2001**, 101, (9), 2797-920.
138. Finucane, M. L.; Slovic, P.; Mertz, C. K., Public perception of the risk of blood transfusion. *Transfusion* **2000**, 40, (8), 1017-22.
139. Lowe, K. C., Engineering blood: synthetic substitutes from fluorinated compounds. *Tissue Eng* **2003**, 9, (3), 389-99.
140. Jahr, J. S.; Akha, A. S.; Holtby, R. J., Crosslinked, Polymerized, and PEG-conjugated Hemoglobin-based Oxygen Carriers: Clinical Safety and Efficacy of Recent and Current Products. *Curr Drug Discov Technol* **2011**.
141. Zuckerman, S. H.; Doyle, M. P.; Gorczynski, R.; Rosenthal, G. J., Preclinical biology of recombinant human hemoglobin, rHb1.1. *Artif Cells Blood Substit Immobil Biotechnol* **1998**, 26, (3), 231-57.
142. Spiess, B. D., Perfluorocarbon emulsions as a promising technology: a review of tissue and vascular gas dynamics. *J Appl Physiol* **2009**, 106, (4), 1444-52.

143. Riess, J. G., Understanding the fundamentals of perfluorocarbons and perfluorocarbon emulsions relevant to in vivo oxygen delivery. *Artif Cells Blood Substit Immobil Biotechnol* **2005**, 33, (1), 47-63.
144. Riess, J. G., Perfluorocarbon-based oxygen delivery. *Artif Cells Blood Substit Immobil Biotechnol* **2006**, 34, (6), 567-580.
145. Clark, L. C., Jr.; Gollan, F., Survival of mammals breathing organic liquids equilibrated with oxygen at atmospheric pressure. *Science* **1966**, 152, (3730), 1755-6.
146. Sloviter, H. A.; Kamimoto, T., Erythrocyte substitute for perfusion of brain. *Nature* **1967**, 216, (5114), 458-60.
147. Radisic, M.; Deen, W.; Langer, R.; Vunjak-Novakovic, G., Mathematical model of oxygen distribution in engineered cardiac tissue with parallel channel array perfused with culture medium containing oxygen carriers. *Am J Physiol* **2005**, 288, (3, Pt. 2), H1278-H1289.
148. Radisic, M.; Park, H.; Chen, F.; Salazar-Lazzaro, J. E.; Wang, Y. D.; Dennis, R.; Langer, R.; Freed, L. E.; Vunjak-Novakovic, G., Biomimetic approach to cardiac tissue engineering: Oxygen carriers and channeled scaffolds. *Tissue Eng* **2006**, 12, (8), 2077-2091.
149. Botchwey, E. A.; Dupree, M. A.; Pollack, S. R.; Levine, E. M.; Laurencin, C. T., Tissue engineered bone: measurement of nutrient transport in three-dimensional matrices. *J Biomed Mater Res A* **2003**, 67, (1), 357-67.
150. Hidalgo-Bastida, L. A.; Thirunavukkarasu, S.; Griffiths, S.; Cartmell, S. H.; Naire, S., Modeling and design of optimal flow perfusion bioreactors for tissue engineering applications. *Biotechnol Bioeng*, **2012**, 109, (4), 1095-1099
151. Lesman, A.; Blinder, Y.; Levenberg, S., Modeling of Flow-Induced Shear Stress Applied on 3D Cellular Scaffolds: Implications for Vascular Tissue Engineering. *Biotechnol Bioeng* **2010**, 105, (3), 645-654.
152. Wang, Y. W.; Tomlins, P. E.; Coombes, A. G. A.; Rides, M., On the Determination of Darcy Permeability Coefficients for a Microporous Tissue Scaffold. *Tissue Eng Part C-Methods* **2010**, 16, (2), 281-289.
153. Mak, A. F., The Apparent Viscoelastic Behavior of Articular-Cartilage - the Contributions from the Intrinsic Matrix Viscoelasticity and Interstitial Fluid-Flows. *J Biomech Eng-T Asme* **1986**, 108, (2), 123-130.
154. Buschmann, M. D.; Kim, Y. J.; Wong, M.; Frank, E.; Hunziker, E. B.; Grodzinsky, A. J., Stimulation of aggrecan synthesis in cartilage explants by cyclic loading is localized to regions of high interstitial fluid flow. *Arch Biochem Biophys* **1999**, 366, (1), 1-7.

155. Steck, R.; Niederer, P.; Tate, M. L. K., A finite element analysis for the prediction of load-induced fluid flow and mechanochemical transduction in bone. *J Theor Biol* **2003**, 220, (2), 249-259.
156. Fritton, S. P.; Weinbaum, S., Fluid and Solute Transport in Bone: Flow-Induced Mechanotransduction. *Annu Rev Fluid Mech* **2009**, 41, 347-374.
157. Dvir, T.; Levy, O.; Shachar, M.; Granot, Y.; Cohen, S., Activation of the ERK1/2 cascade via pulsatile interstitial fluid flow promotes cardiac tissue assembly. *Tissue Eng* **2007**, 13, (9), 2185-2193.
158. Jaalouk, D. E.; Lammerding, J., Mechanotransduction gone awry. *Nat Rev Mol Cell Biol* **2009**, 10, (1), 63-73.
159. Haemer, J. M.; Song, Y.; Carter, D. R.; Giori, N. J., Changes in articular cartilage mechanics with meniscectomy: A novel image-based modeling approach and comparison to patterns of OA. *J Biomech* **2011**, 44, (12), 2307-2312.
160. Price, C.; Zhou, X. Z.; Li, W.; Wang, L. Y., Real-Time Measurement of Solute Transport Within the Lacunar-Canalicular System of Mechanically Loaded Bone: Direct Evidence for Load-Induced Fluid Flow. *J Bone Miner Res* **2011**, 26, (2), 277-285.
161. Porter, B.; Zauel, R.; Stockman, H.; Guldberg, R.; Fyhrie, D., 3-D computational modeling of media flow through scaffolds in a perfusion bioreactor. *J Biomech* **2005**, 38, (3), 543-549.
162. Hutmacher, D. W.; Singh, H., Computational fluid dynamics for improved bioreactor design and 3D culture. *Trends Biotechnol* **2008**, 26, (4), 166-172.
163. Voronov, R.; VanGordon, S.; Sikavitsas, V. I.; Papavassiliou, D. V., Computational modeling of flow-induced shear stresses within 3D salt-leached porous scaffolds imaged via micro-CT. *J Biomech* **2010**, 43, (7), 1279-1286.
164. Moaty Sayed, A.; Hussein, M.; Becker, T., An innovative lattice Boltzmann model for simulating Michaelis–Menten-based diffusion–advection kinetics and its application within a cartilage cell bioreactor. *Biomech Model Mechanobiol* **2009**, (2), 141-151.
165. Rauh, J.; Milan, F.; Gunther, K. P.; Stiehler, M., Bioreactor Systems for Bone Tissue Engineering. *Tissue Eng Part B-Reviews* **2011**, 17, (4), 263-280.

CHAPTER

3

3 TISSUE ENGINEERING SCAFFOLD FABRICATION, EFFECTIVE DIFFUSION COEFFICIENT AND DYNAMIC CELL CULTURE*

Overview: This chapter discusses scaffolds fabrication procedures with different polymer concentrations, measuring oxygen diffusivity of scaffolds and screening them using their morphology and oxygen diffusivity, seeding cells on tubular and disk shaped scaffolds, culturing cell-seeded scaffolds in perfusion bioreactor, and analyzing the cultured cell seeded scaffold using confocal microscopy, hematoxylin and eosin staining, and Western blots.

Summary

Tubular and disk shaped poly (carbonate urethane) (PCU) scaffolds for in vitro tissue engineering of vascular grafts were fabricated by a solvent casting and particulate leaching method using NH_4Cl as porogen. A better pore interconnectivity and oxygen diffusion coefficient were resulted in scaffolds fabricated using 15% PCU in N,N-dimethylformamide (DMF). Human coronary artery smooth muscle cells (HCASMCs) were seeded in these scaffolds and cultured up to 28 days under static or under flow conditions in a perfusion bioreactor. For disk-shaped scaffolds, a better cell infiltration depth and distribution was observed in the flow condition than static culture controls whereas for cell seeded tubular scaffolds, higher number of cells were seeded and cells

* A version of this chapter is submitted for publication and is currently under review.

infiltrate into the tubular scaffolds and, a uniform distribution of cells throughout the scaffold thickness was observed as shown by hematoxylin and eosin staining. Finally, Western blot data suggested an upregulation of ECM proteins such as elastin. The results demonstrate that scaffolds with low diffusivity were able to successfully integrate HCASMCs as a step toward to the development of tissue engineered vascular grafts.

Keywords: Oxygen diffusivity, 3D scaffolds, perfusion bioreactor, tissue engineering

3.1 Introduction

Tissue engineering and regenerative medicine have emerged as promising methods for addressing the increasing demand of small-diameter replacements for diseased vasculature.^{1, 2} However, small-diameter arterial reconstructions (inner diameter <6 mm), are not available to date.³ Natural or synthetic polymeric scaffolds have been widely used in tissue engineering and regenerative medicine.⁴⁻⁶ The optimal scaffold structure is selected based upon a combination of mechanical and physical factors, one of which is the degree to which oxygen can diffuse through the scaffolds.^{7, 8} The ability of scaffold to support cell growth throughout its thickness is affected by the scaffold oxygen diffusivity. In vitro tissue maturation and immediately after surgical implantation until adequate vascularisation has occurred, cells seeded into the scaffold mostly depend on the process of diffusion for oxygenation.⁹⁻¹¹ Therefore, the measurement of oxygen diffusivity in scaffolds is a logical method for comparing the ability of scaffolds to support cell viability, migration and infiltration within the scaffold.^{12, 13}

Tissue-engineered small diameter vascular grafts have the ability to sense hemodynamic loading during dynamic culture, speciality when the culture media flows through the lumen, and respond through mechanical and biological responses.^{2, 14, 15} Mechanical stimulation of cells seeded in vascular tissue engineering scaffold promotes the circumferential orientation of cells as well as the deposition of extracellular matrix. Perfusion bioreactors also mimic the physiological conditions of coronary arteries and can impose mechanical stimulation to cells and the hemodynamic loading during cultures to engineer small diameter vascular grafts.^{16, 17}

In the present study, scaffolds with different morphology were fabricated by varying the PCU concentration, and were screened based on the measured effective oxygen diffusivity. Based on morphology and oxygen diffusion coefficient, the best polymer concentration for fabricating scaffolds was chosen. In view of developing small diameter vascular grafts in vitro, HCASMCs were seeded on PCU scaffolds with disk and tubular shapes. The cell seeded scaffolds were cultured in a perfusion bioreactor under physiological flow conditions for several days. The advantage of dynamic culture in regulating cell proliferation and distribution was evaluated by comparing the results with static culture controls.

3.2 Materials and Methods

3.2.1 Fabrication of PCU scaffolds

3D scaffolds were fabricated by a solvent casting and particulate leaching method as shown in Figure 3.1.¹⁸ Ground and sieved NH_4Cl porogens (180-220 μm) were packed into a tubular glass mold (6 mm outer diameter, 5 mm inner diameter and 8 cm height)

using a pressure differential created from an air supply line (550 kPa) from the top pushing and (0.014 kPa) suction applied from the bottom of the assembly. A medical grade poly(carbonate urethane) (PCU) (Bionate[®] 55D) was obtained from DSM Biomedical (Berkeley, CA). Different concentration of the PCU solution (15, 20, 25 and 30 wt%, dissolved in N,N-dimethylformamide) was subsequently poured over the porogen bed and pressurized to infiltrate the porogen bed. Following this, the scaffolds were removed from the assembly and the solvent was allowed to evaporate in a fume hood. Finally, NH₄Cl porogens were leached out using deionized water and, the scaffolds were sectioned into 1.5 mm height disks using a microtome. This height (or thickness) of the scaffolds was chosen to mimic the thicknesses of many soft tissues that are the subject of tissue engineering.

Tubular scaffolds were made in the same apparatus but with different assembly; a cylindrical stainless steel rod (4 mm diameter) was placed at the center of the tubular glass mold and the NH₄Cl porogens were packed in the space between the rod and the glass mold. A polymer solution (15 wt %) was poured and pressurised to infiltrate into the porogens bed; the mold is then removed from the assembly and placed in the fume hood for 3 days for the solvent to evaporate completely. Finally, the scaffolds were removed from the mold and the NH₄Cl porogens were leached using deionized water (DI) and the rod was removed from the center of the scaffold, the scaffolds were sectioned into 120 mm length using a microtome.

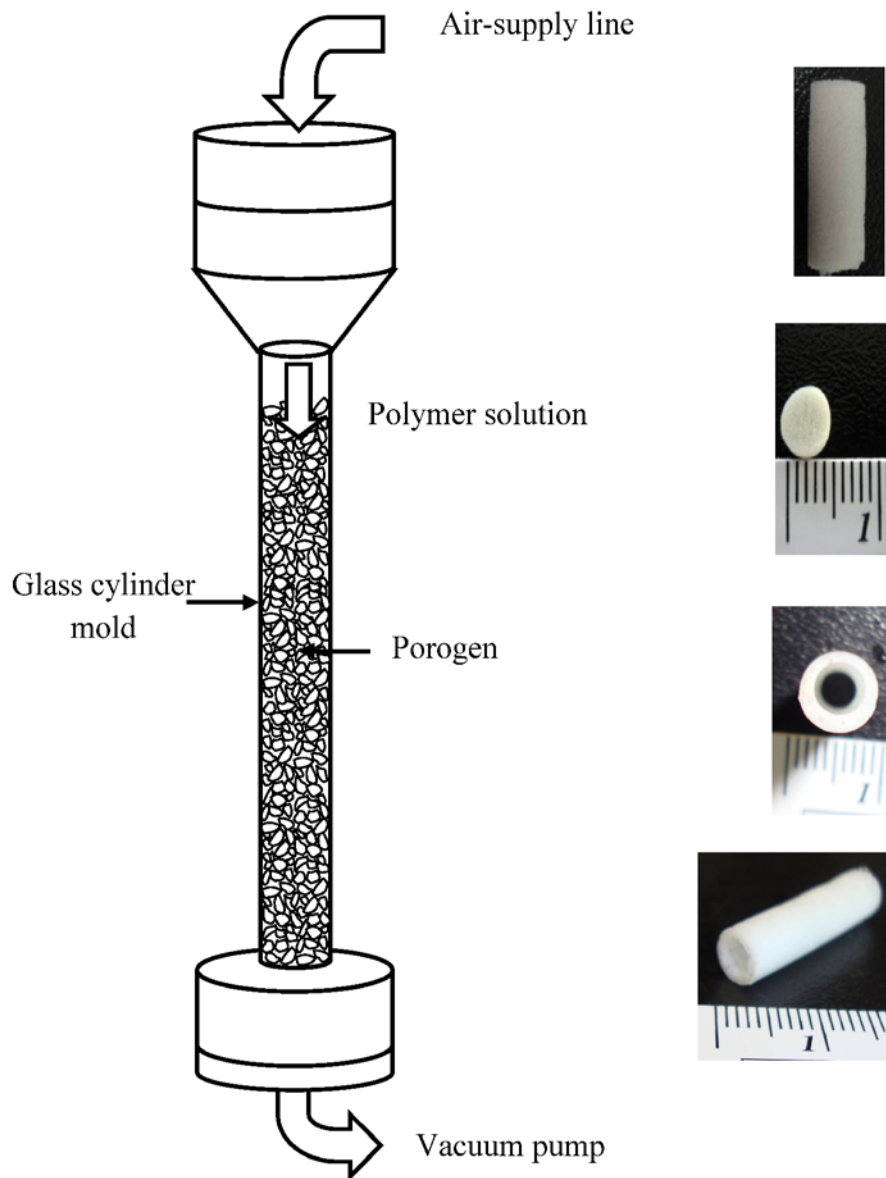


Figure 3.1: Schematic diagram of the assembled, solvent casting and particulate leaching, scaffold fabrication method and scaffolds fabricated from PCU.

3.2.2 Measuring dissolved oxygen and diffusion coefficient

The diffusion apparatus, built by the University Machine Shop, consisted of two 100 ml chambers separated by the test scaffold, which was secured between the glass chambers with stainless steel insert and rubber gasket o-rings (Figure 3.2). The opening between the

two chambers had an area of 19.625 cm^2 . Each chamber was filled with 100 ml DI water. The DI water in the donor chamber was saturated with ambient air; the DI water in the receiver chamber was purged of dissolved oxygen by saturating with 100% nitrogen. To approximate a well-mixed system, the solutions in each chamber were stirred throughout the experiments. The oxygen concentration in the donor chamber was kept constant by a continuous supply of ambient air. Both chambers were maintained at 37°C by an external water bath. Fibre optic oxygen sensor model NeoFox (Ocean Optics, Dunedin, FL) equipped with NeoFox software was used to measure dissolved oxygen. The oxygen sensor was placed in the receiving chamber and measured dissolved oxygen every 10 seconds.

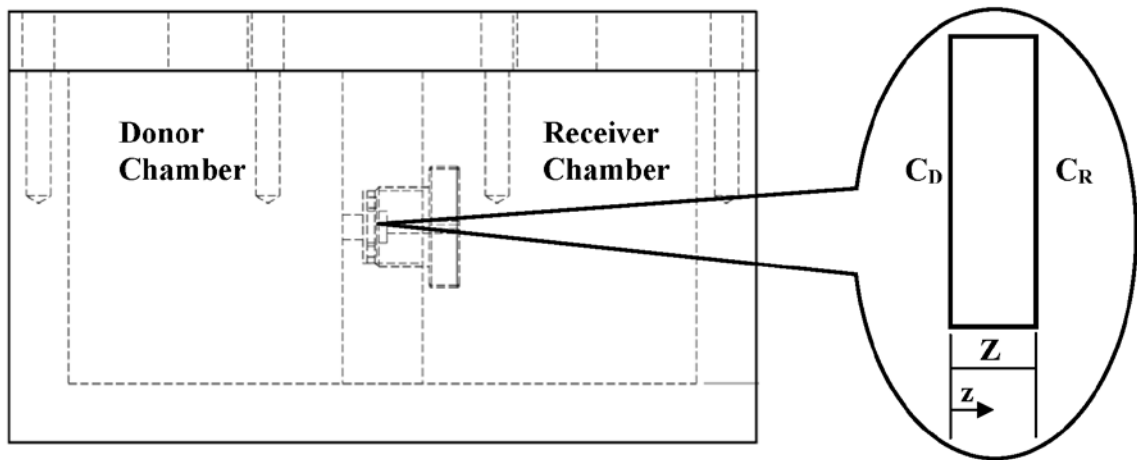


Figure 3.2: Schematic diagram of the diffusion cell apparatus

The flux of oxygen in the test scaffold can be calculated by performing a shell material balance on the scaffold in one dimension leading to,

$$\text{Accumulation} = \text{Input} - \text{Output} + \text{Production} - \text{Consumption}$$

$$V_s \frac{\partial C}{\partial t} = J_{\text{in}} \Big|_z A - J_{\text{out}} \Big|_{z+\Delta z} A + PV_s - GV_s \quad (1)$$

Where:

V_s is volume of the fraction of scaffolds where the mass balance was calculated

A is the cross sectional area of the scaffold

J_{in} is the inlet flux crossing the area

J_{out} is the outlet flux crossing the area

Z is the thickness of the scaffold, and

P and G are production and consumption of oxygen per volume of scaffold respectively.

At a steady state and with no consumption and production of oxygen in the scaffold, the above equation reduces to diffusion in the z direction.

$$D_{eff} \frac{d^2C}{dz^2} = 0 \quad (2)$$

Where D_{eff} is the effective diffusivity.

With both donor and receiver chambers well-mixed, the boundary conditions for (2) are the concentration of oxygen in the donor and receiver chambers. Thus,

$$BC1: C(0) = C_D \quad BC2: C(Z) = C_R(t)$$

Where C_D and C_R are the concentration of oxygen in the donor chamber and receiver chamber respectively.

The solution of the diffusion equation (2) will be,

$$C = \left(\frac{C_R(t) - C_D}{Z} \right) x + C_D \quad (3)$$

Therefore, the flux in the scaffold will be,

$$J = -D_{eff} \frac{\partial C}{\partial z} = -D_{eff} \left(\frac{C_R(t) - C_D}{Z} \right) \quad (4)$$

Since the mass balance in the receiving chamber will be unsteady state with no consumption and production, equation (1) reduces to.

$$V_R \frac{\partial C_R(t)}{\partial t} = JA \quad (5)$$

Where, V_R is the volume of the receiver chamber. Substituting the flux from (3) and solving for the receiver chamber oxygen concentration gives:

$$\varphi \ln \left(\frac{C_{R0} - C_D}{C_R(t) - C_D} \right) = D_{eff} t \quad (6)$$

where $\varphi = \frac{V_R Z}{A}$

Oxygen concentration was measured as a function of time for each scaffold and plotted as a function of time. Using equation (4), the linear slope of the best fit line (as calculated by the least-squares method using Sigma Plot Version 10) gives the effective diffusivity, D_{eff} , of the each scaffolds.

3.2.3 Cell culture in perfusion bioreactor

Primary human coronary artery smooth muscle cells (HCASMCs) and smooth muscle growth media (SmGM[®]-2 BulletKit) were purchased from Lonza Walkersville Inc. (Walkersville, MD, USA). Cells were cultured according to supplier's instructions in SmGM[®]-2, supplemented with 100 units/ml penicillin G sodium, and 100 µg/ml

streptomycin sulphate (Invitrogen, Burlington, ON, Canada). All cultures were maintained in a humidified incubator at 37°C containing 5% CO₂. HCASMCs were passaged every 7 days at a split ratio of 1:3 and used between passages 4 to 7. Disk-shaped scaffolds were affixed to glass coverslips using silicone grease, sterilized with 70% ethanol for 30 min and allowed to dry under germicidal UV light in tissue culture hood for 30 min. After soaking the scaffolds in Hank's Buffered Salt Solution (HBSS, Invitrogen, Burlington, ON, Canada), all scaffolds were coated with fibronectin (10 µg/cm²; Santa Cruz, CA, USA). Cells were seeded into the interstices of fibronectin-coated PCU scaffolds at an initial cell density of $\sim 3 \times 10^4$ cells/scaffold. After HCASMCs attached to the scaffold for two days in static culture, the cell seeded scaffolds were transferred to a perfusion bioreactor and cultured for 4 and 7 days. The culture medium was purged through the porous cell seeded scaffold at a flow rate of 40 ml/min. A parallel static HCASMCs cultures were carried out as controls for 4 days and 7 days where culture medium was changed every other day.

A similar sterilization and preconditioning steps were used for tubular scaffolds but cells were seeded into the lumen of fibronectin-coated PCU tubular scaffolds at an initial cell density of $\sim 1 \times 10^6$ cells/scaffold. HCASMCs were statically cultured in a slowly rotating glass tube for two days to achieve uniform seeding and attachment to the scaffold. The cell-seeded scaffolds were then transferred to a perfusion bioreactor and cultured for a further 4 days, 7 days and 14 days at a medium flow rate of 40 ml/min. The calculated wall shear stress was ($\tau_w = 1.74$ dyns/cm²) and it is below the physiological maximum shear stress in coronary arteries.¹⁰

3.2.4 Fluorescence staining and laser scanning confocal microscopy

HCASMCs were fixed at room temperature for 1h with 4% (w/v) paraformaldehyde (EMD Chemicals Inc.) and the tubular scaffolds then sectioned circumferentially using microtome and axially using surgical blades. The cells were permeabilized for 10 min in cation-free phosphate buffered saline (PBS) containing 0.1% (v/v) Triton X-100. Cells were incubated for 1h at room temperature in 1% BSA/PBS containing AlexaTM Fluor 488-conjugated phalloidin (1:50 dilution), followed by three washes with PBS. DAPI (300nM in PBS; Invitrogen, Burlington, ON, Canada) was used to label nuclei. Samples were mounted on slides in SHUR/MountTM (TBS[®], NC, USA) and analyzed with a Zeiss LSM 410 confocal microscope (Zeiss, Canada) equipped with an argon/neon as well as a UV laser.

3.2.5 Histological analysis using haematoxylin and eosin staining

HCASMCs cultured on PCU scaffolds were washed twice by ice cold PBS and embedded in optimum cutting temperature (OCT) media (Tissue-Tek, VWR, Canada) in dry ice bath and frozen to -80°C for 12h. The frozen blocks were transferred to cryotome crostat (-20°C) and allowed the temperature of the frozen blocks to equilibrate to that of the cryotome crostat. 50µm thickness samples were sectioned using cryotome and placed on glass slides and the slides were heated to 30°C allowing the Tissue-Tek to melt. The sectioned samples were carefully washed twice with PBS and fixed using 4% (w/v) paraformaldehyde for 5 min, followed by two washes with DI water and then stained first with hematoxylin and then with eosin (Sigma-Aldrich) with washes with DI water in the intermediate and final stages of staining.

3.2.6 Protein extraction and Western blot analysis

Following prescribed culture times, constructs were washed with ice cold PBS and proteins were extracted using lyses buffer. The lysate was collected and spun in a centrifuge and the supernatants were collected. The amount of total protein was quantified using BSA protein assay kit (Thermo Scientific, ON, Canada). 50 μ g protein samples were separated by 10% SDS-PAGE and subsequently transferred at 90 V for 1 hour at 4°C to nitrocellulose membrane in a Tris-glycine buffer. Coomassie blue was used to stain the total protein in gel. In addition the transfer efficiency and homogeneous loading was assessed by Ponceau red stain. Nitrocellulose membranes were blocked with 5% nonfat dry milk in PBS and incubated overnight at 4°C with primary antibodies (monoclonal mouse anti-elastin at 1:200; anti-SM- α -actin and anti-GAPDH at 1:2000). The blots were then labeled with Alexa 680- and IRDye 800-conjugated secondary antibody (Invitrogen, Burlington, ON, Canada), and labeled proteins were visualized by the Bio-Rad system (Bio-Rad Laboratories, Mississauga, Canada).

3.2.7 Statistical analysis

The results for the dissolved oxygen study and effective diffusion study were analyzed by Student's *t*-test. For all analyses, significance was assigned for $p < 0.05$.

3.3 Results

3.3.1 Scaffold fabrication

Tissue engineering scaffolds are required to have high porosity and pore interconnectivity, and high surface area to volume ratio for cellular infiltration, matrix remodelling, and nutrient transport to take place. In such scaffolds, cell seeding density and distribution increases with pore interconnectivity. We therefore sought to examine the effect of polymer concentration on porosity and interconnectivity of the scaffolds. Different polymer concentrations (15, 20, 25, and 30 wt %, PCU dissolved in N,N-dimethylformamide) were used to make PCU scaffold and the resulting scaffold were characterized using SEM. The strut thickness increased and pore interconnectivity decreased as the amount of polymer increased in the polymeric solution as shown in Figure 3.3. Scaffolds with lower polymer concentration were tried to fabricate but the structures were fragile and difficult to handle. Therefore, 15 wt% polymer concentration in DMF has been selected for further cell studies.

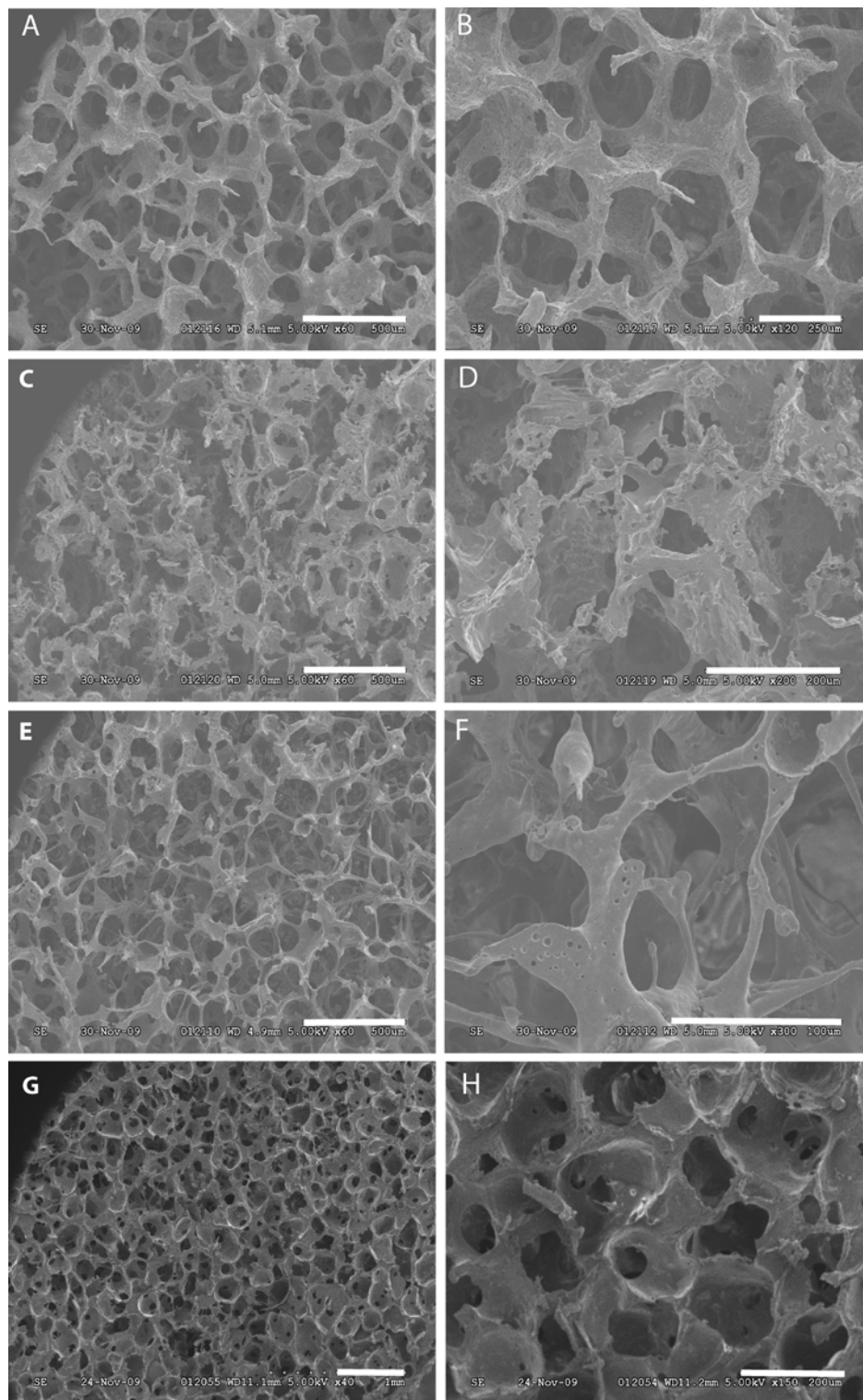


Figure 3.3: SEM photomicrographs of PCU scaffolds fabricated from different polymer concentrations. 15 wt % (A and B), 20 % wt (C and D) 25 % wt (E and F), and 30 % wt (G and H) PCU concentration. Scale bars are 250µm for A, C, E G and 10µm for B, D, F and H.

3.3.2 Effective oxygen diffusion coefficient in scaffolds

Fick's first law of diffusion on the passive transport of dissolved oxygen through the thickness of clinically relevant scaffolds within an enclosed, well-mixed system was applied to measure effective diffusion coefficient. Effective diffusivity measures the resistance or the ability of a material to allow the passage of oxygen through it and Figure 3.4 show how the effective diffusivity can be calculated using the measured values of dissolved oxygen in the receiver chamber by means of equation (6). Scaffolds fabricated from 15 wt% polymer concentrations showed lower effective diffusivity than the other concentrations (Figure 3.5). As the concentration of polymer used to making scaffold increases the effective diffusivity increases as shown in the Figure 3.5. The higher effective diffusivity in the scaffold will have higher cell retention and easier to supply oxygen to the cells seeded on the scaffold. Therefore, scaffolds fabricated from 15 wt % polymer concentration will have less resistance to oxygen supply to the seeded cells. This result in combination with the SEM result suggests that 15% PCU concentration to be suitable for cell culture and have been chosen for further cell culture studies.

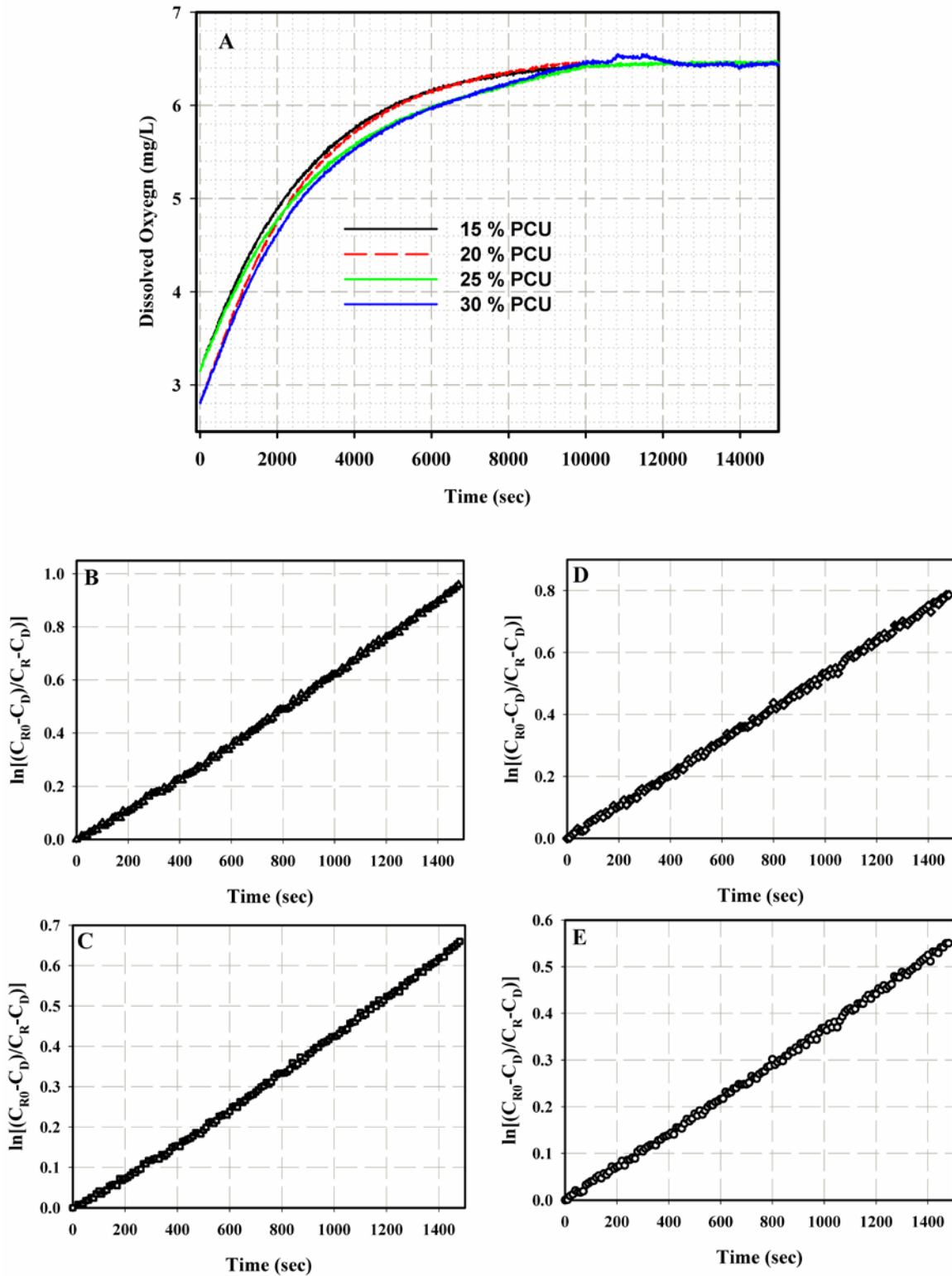


Figure 3.4: A) Oxygen concentration detected in the receiver chamber as a function of time. Data used to calculate the effective oxygen diffusivity, D_{eff} B) for 15% PCU, C) 20% PCU, D) 25% PCU and E) 30% PCU.

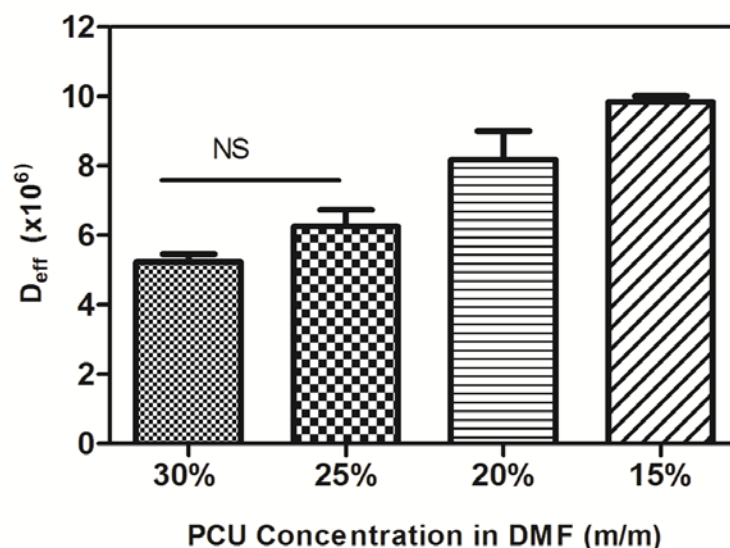


Figure 3.5: Effective oxygen diffusivity (cm^2/s) in 3D scaffolds fabricated from different PCU concentrations. Data are mean \pm SD for 3 independent experiments. NS means not significant.

3.3.3 Fluorescence staining and confocal microscopy

HCASMC-seeded disk-shaped scaffolds with 1mm thickness were cultured in a perfusion bioreactor where the culture media flows through the scaffold. After 4 days of culture, the cell-seeded scaffolds were imaged. A diffused red autofluorescence was observed due to the PCU scaffolds helped to demonstrate that HCASMCs were penetrating into the scaffold, but this did not affect the imaging process. HCASMCs were uniformly distributed on the scaffold as shown in Figure 3.6. Comparing with the static culture control, the cell density of the dynamic culture appeared to be similar. However, taking a series of confocal images with $10\ \mu\text{m}$ apart from the top of the scaffold to the point where there are no more HCASMCs encountered, penetration depth to the scaffolds in dynamic cultures was considerably higher than the static control cultures ($230\ \mu\text{m}$ vs. $120\ \mu\text{m}$) suggesting that dynamic cultures improve cell penetration depths to the scaffolds whereas

this is not totally unexpected it does underscore the role of dynamic cultures to enhance cell distribution and penetration depth.

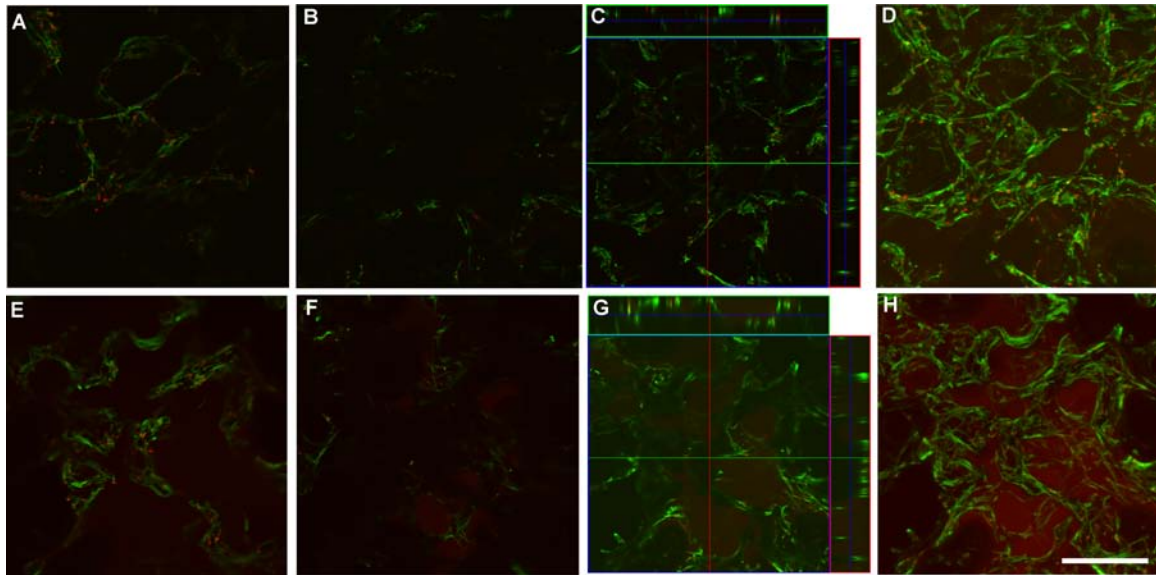


Figure 3.6: Confocal microscopy images of HCASMCs cultured on disk shape PCU scaffold in static (A-D) and dynamic (E-H) culture conditions. The top of the scaffolds are shown in A and E whereas the bottom side are B and F, and the orthogonal projections are C and G. Scale bar for all the images is 200 μ m.

In addition, HCASMCs seeded on tubular scaffolds were cultured for 4 days, 7 days, 14 days, and 28 days in a perfusion bioreactor where the culture medium flows through the lumen of the tubular scaffolds. Cells were seeded from the lumen direction and cultured in slowly rotating tubular glass for two days; this seeding approach with the high seeding density helped to uniformly distribute throughout the scaffold from the lumen direction. Figure 3.7 shows the confocal images of HCASMCs taken from different areas of the scaffold. The cytoskeleton of the cells cultured in dynamic environment in the confocal images are somewhat diffused in their quality. This is likely due to the topography effect since the static cultures were conducted using porous disks whereas the dynamic cultures were done using tubular scaffolds. In both cases, however, the high density of cells is evident.

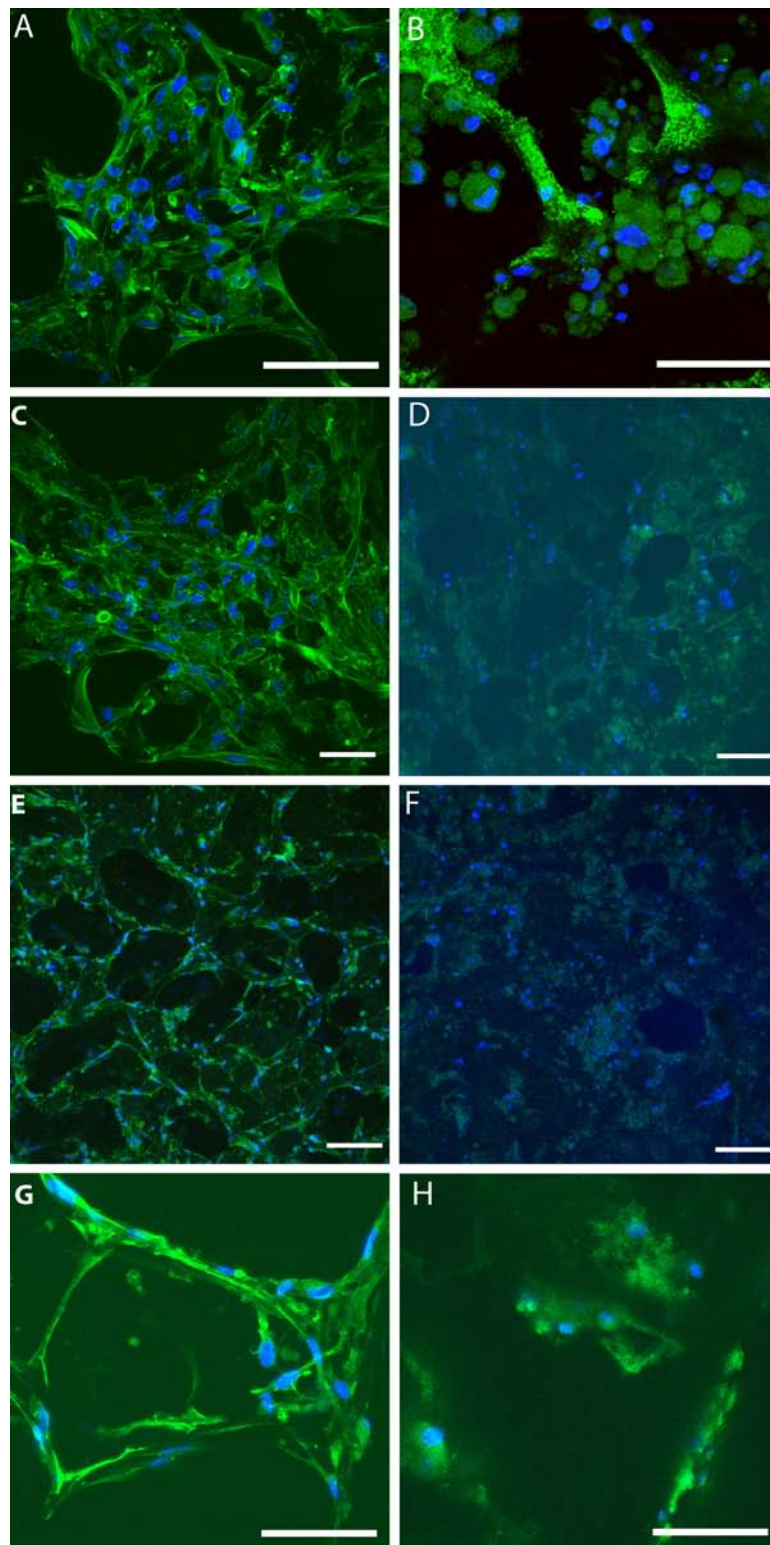


Figure 3.7: Confocal microscopy images of HCASMCs cultured on tubular PCU scaffolds in static (A, C, E and G) and dynamic (B, D, F and H) culture conditions for 4 days (A&B) 7days (C&D) 14 days (E& F) and 28 days (G&H). Scale bar for A,B,G and H is 200 μ m and for C,D,E and F is 100 μ m.

3.3.4 Cross-sectional histological staining

Homogeneous distribution of HCASMCs in the tubular PCU scaffolds was confirmed by means of histological staining with H & E as shown in Figure 3.8 which is consistent with confocal images of the fluorescent staining. The high magnification of the H & E staining shows a uniformly distributed of HCASMCs throughout the tubular PCU scaffold (B, D and E). A high HCASMCs staining with the number of culture days was an indication of cell proliferation.

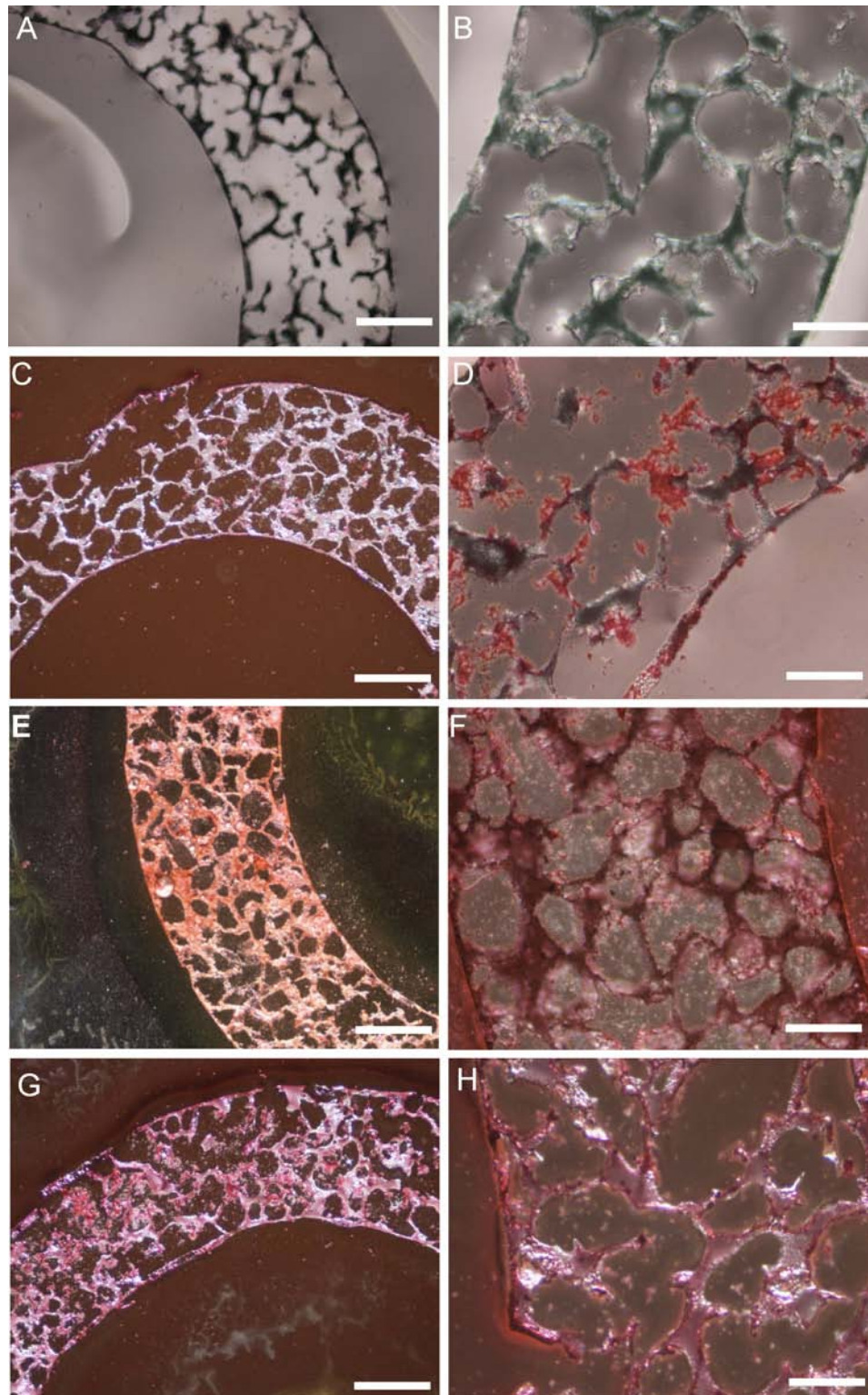


Figure 3.8: H&E staining of cross sections of HCASMCs seeded tubular PCU scaffolds cultured under dynamic condition for 7 days (B and C), 14 days (E and F) and 28 days (G and H). Bare scaffold was stained and imaged as a control (A and B). Scale bar for A, C, E and G is 0.2mm and for B, D, F and H is 0.1mm.

3.3.5 Western blot analysis

The total amount of protein from cell lysates cultured in dynamic and static conditions for 14 and 28 days was quantified using BSA protein assay. An equal amount of protein (50 μ g) in each lane of the PAGE was run and the gel was stained using coomassie blue, and subsequently imaged by Bio-RAD camera (Molecular imager Chemi Doc™). The intensity of the protein bands in each lane is indicative of the relative amounts of protein present. In the region of 50 kda to 100 kda, most proteins were upregulated in dynamic cultures than in static culture controls as shown in Figure 3.9A. Therefore, further staining for elastin (molecular weight ~66kda) and Smooth muscle α -actin (molecular weight ~42kda) showed an upregulation in dynamic cultures than in static cultures as shown in Figure 3.9 B. indicating a more synthetic phenotype of HCASMCs in dynamic than static cultures. However, a more controlled and detailed experiments need be done in order to get a better conclusive result.

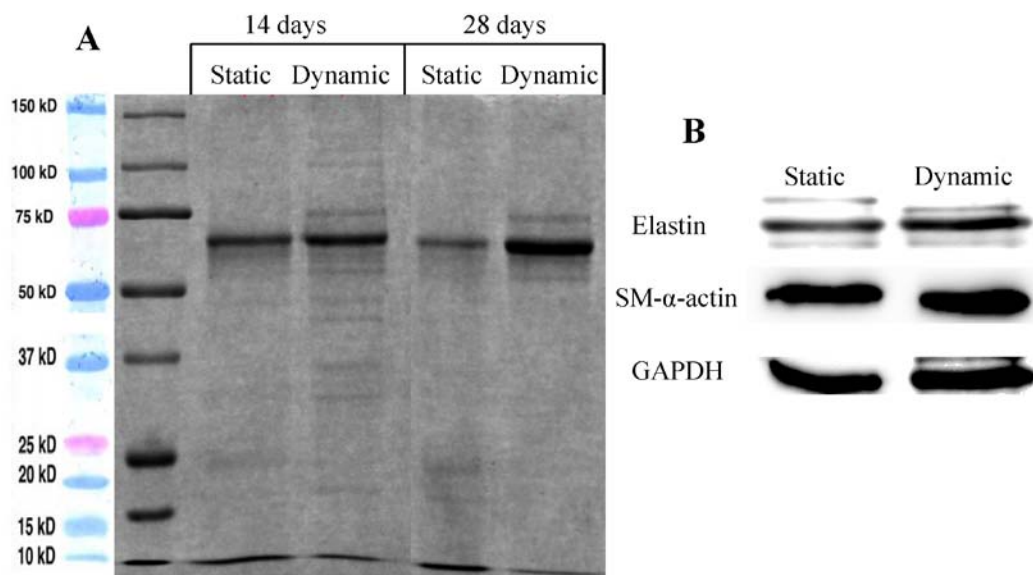


Figure 3.9: Western blots of 14 days and 28 day cultures in static and dynamic conditions coomassie blue staining and antibody staining of elastin, SM- α -actin and GAPDH for 14 days culture.

3.4 Discussion

The effective diffusivity measures the ability of a scaffold to allow the transport of oxygen through it. In this study it is shown that 15 wt% polymer concentration has a higher diffusion coefficient allowing higher amount of oxygen to be transported; these results in higher cell viability, penetration depth into the scaffolds, and proliferation. These findings suggest at least a partial dependence of oxygen transport on the polymer concentration, porosity, and/or tortuosity of the scaffold. The tortuosity of the scaffold were not directly measured in this study but instead incorporated into the effective diffusivity variable.¹⁹ The SEM results also suggested 15 wt% polymer concentration scaffolds resulted in higher pore interconnectivity. Whereas most studies on oxygen diffusion through tissue engineering scaffolds focused on numerical analysis approaches²⁰⁻²³, there are few studies related to the current work for experimentally determining oxygen diffusivity. For example, Valentin et al²⁴ measured oxygen diffusivity of small intestine submucosa, urinary bladder submucosa, and Dacron[®]. Not unexpectedly, their data indicated that each scaffold has unique oxygen diffusivity values ranging from 2.4×10^{-6} cm²/s to 6.6×10^{-6} cm²/s, and these values were dependent on the scaffold's ultrastructure. Dacron[®] had oxygen diffusivity which was one order magnitude higher than the ECM scaffolds presumably due to the woven nature of it. In another related study, Androjna et al²⁵ measured the oxygen diffusivity of intestine submucosa, human dermis (Alloderm[®]), and canine fascia lata and reported the effective diffusion coefficients of all 3 ECM-based scaffolds to be to be in the order of 7×10^{-6} cm²/s to 4×10^{-5} cm²/s with the intestine submucosa tended to have the lowest oxygen. The differences in the reported ranges are likely due to varying matrix structure porosity and tortuosity that

is inherent in these tissues. In view of these cited studies, the oxygen diffusivity in all PCU scaffolds (Figure 3.5) was comparable to natural ECM scaffolds. More importantly, the oxygen diffusivity for 15wt% was better than ECM scaffolds but lower than Dacron[®]. From this comparison it is possible to deduce that our scaffolds transports oxygen higher than biological scaffolds but lower than synthetic scaffold Dacron[®]. To the best of our knowledge, this study is the first to show oxygen diffusivity in PCU scaffolds as a function of polymer concentration during the fabrication process.

HCASMCs penetration depth increased in dynamic cultures than the static culture controls. This signifies higher cell population in the 3D scaffold, a finding that is also supported by prior studies as Chan and Chong showed that perfusion systems increased the oxygen profile in the scaffold, which in turn, increased the cell number with uniform cell density.²⁶ In addition, HCASMCs penetrated throughout the thickness of the tubular scaffold as shown by the H&E staining. These results are consistent with literature reports for other types of scaffolds. For instance, using H&E staining, Poot and coworkers showed that VSMCs seeded into porous, tubular, flexible, and elastic poly(trimethylene carbonate) scaffolds and cultured under perfusion had higher cell numbers. Interestingly cell number peaked at day 7 and then decreased at day 14.^{3, 27} The mechanical properties of the scaffolds also increased with culture time suggesting possible matrix deposition. Although direct comparison with the above cited work cannot be done as we have not specifically stained for ECM components in the histology study, reasonable inferences can be drawn from the Western blot data (Figure 3.9B) that HCASMCs started expressing elastin, one of the most important ECM component for vascular tissues. Previous studies

from our laboratory also demonstrated the biosynthesis of both elastin and collagen by HCASMC seeded to PCU scaffolds.^{28, 29}

Notwithstanding the above, however, endothelialisation of the luminal surface of the engineered vascular tissues is an additional requirement that must be satisfied from a practical standpoint. Previously, the co-culturing of human coronary artery endothelial cells and HCASMCs on scaffolds by using Matrigel coating was reported.² Matrigel-coated layer not only was a structural mimic for the basement membrane (internal elastic lamina), but also functioned to help chemically anchor other components, such as laminins, collagen IV, nidogens (entactin) and heparan sulfate proteoglycan (perlecan).³⁰ This approach could also be used for endothelialisation of the constructs described in the present work. Furthermore, co-culture of endothelial cells and HCASMCs play a role in the alignment of HCASMCs along the direction of flow.³¹ Moreover, co-culturing plays a significant role in the phenotype regulation of HCASMCs. Our group showed evidences that contact of HCASMCs and endothelial cells is required for the regulating smooth muscle cell differentiation.³² .

3.5 Conclusions

A new way of screening scaffolds with effective diffusivity led to an observation that 15 wt% PCU scaffold could be used to engineer vascular grafts with good structures and pore interconnectivity. Porous tubular and disk-shaped PCU scaffolds were seeded with HCASMCs and subsequently cultured up to 28 days under flow conditions in a bioreactor and static conditions. Both confocal and histological studies showed that dynamic culture conditions significantly improved HCASMC penetration and uniform distribution

throughout the scaffold as compared with static culture controls. The results of this study indicated that a potentially useful tissue engineered vascular grafts can be fabricated by dynamic culturing of human HCASMCs seeded in porous tubular PCU scaffolds.

3.6 References

1. Conte, M. S., The ideal small arterial substitute: a search for the Holy Grail? *FASEB J* **1998**, 12, (1), 43-45.
2. Zhang, X. H.; Wang, X. L.; Keshav, V.; Wang, X. Q.; Johanas, J. T.; Leisk, G. G.; Kaplan, D. L., Dynamic culture conditions to generate silk-based tissue-engineered vascular grafts. *Biomaterials* **2009**, 30, (19), 3213-3223.
3. Song, Y.; Wennink, J. W. H.; Kamphuis, M. M. J.; Sterk, L. M. T.; Vermes, I.; Poot, A. A.; Feijen, J.; Grijpma, D. W., Dynamic Culturing of Smooth Muscle Cells in Tubular Poly(Trimethylene Carbonate) Scaffolds for Vascular Tissue Engineering. *Tissue Eng Part A* **2011**, 17, (3-4), 381-387.
4. Engbers-Buijtenhuijs, P.; Buttafoco, L.; Poot, A. A.; Dijkstra, P. J.; de Vos, R. A. I.; Sterk, L. M. T.; Geelkerken, R. H.; Vermes, I.; Feijen, J., Biological characterisation of vascular grafts cultured in a bioreactor. *Biomaterials* **2006**, 27, (11), 2390-2397.
5. Hahn, M. S.; McHale, M. K.; Wang, E.; Schmedlen, R. H.; West, J. L., Physiologic pulsatile flow bioreactor conditioning of poly(ethylene glycol)-based tissue engineered vascular grafts. *Ann Bio Eng* **2007**, 35, (2), 190-200.
6. Jeong, S. I.; Kim, S. Y.; Cho, S. K.; Chong, M. S.; Kim, K. S.; Kim, H.; Lee, S. B.; Lee, Y. M., Tissue-engineered vascular grafts composed of marine collagen and PLGA fibers using pulsatile perfusion bioreactors. *Biomaterials* **2007**, 28, (6), 1115-1122.
7. Billaud, M.; Marthan, R.; Savineau, J. P.; Guibert, C., Vascular Smooth Muscle Modulates Endothelial Control of Vasoreactivity via Reactive Oxygen Species Production through Myoendothelial Communications. *Plos One* **2009**, 4, (7).
8. Cheng, G.; Markenscoff, P.; Zygorakis, K., A 3D Hybrid Model for Tissue Growth: The Interplay between Cell Population and Mass Transport Dynamics. *Biophys J* **2009**, 97, (2), 401-414.
9. Pittman, R. N., Oxygen transport and exchange in the microcirculation. *Microcirculation* **2005**, 12, (1), 59-70.
10. Soulls, J. V.; Farmakis, T. M.; Giannoglou, G. D.; Louridas, G. E., Wall shear stress in normal left coronary artery tree. *J Biomech* **2006**, 39, (4), 742-749.

11. Malda, J.; Klein, T. J.; Upton, Z., The roles of hypoxia in the In vitro engineering of tissues. *Tissue Eng* **2007**, 13, (9), 2153-2162.
12. Ho, Q. T.; Verlinden, B. E.; Verboven, P.; Vandewalle, S.; Nicolai, B. M., A permeation-diffusion-reaction model of gas transport in cellular tissue of plant materials. *J Exp Bot* **2006**, 57, (15), 4215-4224.
13. Valentin, J. E.; Freytes, D. O.; Grasman, J. M.; Pesyna, C.; Freund, J.; Gilbert, T. W.; Badylak, S. F., Oxygen diffusivity of biologic and synthetic scaffold materials for tissue engineering. *J Biomed Mater Res-A* **2009**, 91A, (4), 1010-1017.
14. Li, Q.; Hou, T. Y.; Zhao, J. N.; Xu, J. Z., Vascular Endothelial Growth Factor Release from Alginate Microspheres Under Simulated Physiological Compressive Loading and the Effect on Human Vascular Endothelial Cells. *Tissue Eng Part A* **2011**, 17, (13-14), 1777-1785.
15. Beamish, J. A.; He, P.; Kottke-Marchant, K.; Marchant, R. E., Molecular Regulation of Contractile Smooth Muscle Cell Phenotype: Implications for Vascular Tissue Engineering. *Tissue Eng Part B-Rev* **2010**, 16, (5), 467-491.
16. Williams, C.; Wick, T. M., Perfusion Bioreactor for small diameter tissue-engineered arteries. *Tissue Eng* **2004**, 10, (5-6), 930-941.
17. Williams, C.; Wick, T. M., Endothelial cell-smooth muscle cell co-culture in a perfusion bioreactor system. *Ann Biomed Eng* **2005**, 33, (7), 920-928.
18. Grenier, S.; Sandig, M.; Mequanint, K., Polyurethane biomaterials for fabricating 3D porous scaffolds and supporting vascular cells. *J Biomed Mater Res-A* **2007**, 82A, (4), 802-809.
19. Han, H. C., Blood vessel buckling within soft surrounding tissue generates tortuosity. *J Biomech* **2009**, 42, (16), 2797-2801.
20. Ahn, G.; Park, J. H.; Kang, T.; Lee, J. W.; Kang, H. W.; Cho, D. W., Effect of Pore Architecture on Oxygen Diffusion in 3D Scaffolds for Tissue Engineering. *J Biomech Eng-T Asme* **2010**, 132, (10).
21. Coletti, F.; Macchietto, S.; Elvassore, N., Mathematical modeling of three-dimensional cell cultures in perfusion bioreactors. *Ind Eng Chem Res* **2006**, 45, (24), 8158-8169.
22. Coletti, F.; Macchietto, S.; Elvassore, N., Mathematical modelling of three-dimensional cell cultures in perfusion bioreactors. Part II. *16th European Symposium on Computer Aided Process Engineering and 9th International Symposium on Process Systems Engineering* **2006**, 21, 1699-1704.
23. Croll, T. I.; Gentz, S.; Mueller, K.; Davidson, M.; O'Connor, A. J.; Stevens, G. W.; Cooper-White, J. J., Modelling oxygen diffusion and cell growth in a porous,

- vascularising scaffold for soft tissue engineering applications. *Chem Eng Sci* **2005**, 60, (17), 4924-4934.
24. Valentin, J. E.; Freytes, D. O.; Grasman, J. M.; Pesyna, C.; Freund, J.; Gilbert, T. W.; Badylak, S. F., Oxygen diffusivity of biologic and synthetic scaffold materials for tissue engineering. *J Biomed Mater Res A* **2009**, 91, (4), 1010-7.
 25. Androjna, C.; Gatica, J. E.; Belovich, J. M.; Derwin, K. A., Oxygen diffusion through natural extracellular matrices: implications for estimating "critical thickness" values in tendon tissue engineering. *Tissue Eng Part A* **2008**, 14, (4), 559-69.
 26. Chan, W. Y.; Chong, C. K., Perfusion Bioreactors Improve Oxygen Transport and Cell Distribution in Esophageal Smooth Muscle Construct. *13th International Conference on Biomedical Engineering, Vols 1-3* **2009**, 23, (1-3), 1523-1526.
 27. Song, Y.; Wennink, J. W. H.; Kamphuis, M. M. J.; Vermes, I.; Poot, A. A.; Feijen, J.; Grijpma, D. W., Effective seeding of smooth muscle cells into tubular poly(trimethylene carbonate) scaffolds for vascular tissue engineering. *J Biomed Mater Res-A* **2010**, 95A, (2), 440-446.
 28. Grenier, S.; Sandig, M.; Mequanint, K., Smooth muscle alpha-actin and calponin expression and extracellular matrix production of human coronary artery smooth muscle cells in 3D scaffolds. *Tissue Eng Part A* **2009**, 15, (10), 3001-11.
 29. Lin, S.; Sandig, M.; Mequanint, K., Three-dimensional topography of synthetic scaffolds induces elastin synthesis by human coronary artery smooth muscle cells. *Tissue Eng Part A* **2011**, 17, (11-12), 1561-71.
 30. Hallmann, R.; Horn, N.; Selg, M.; Wendler, O.; Pausch, F.; Sorokin, L. M., Expression and function of laminins in the embryonic and mature vasculature. *Physiol Rev* **2005**, 85, (3), 979-1000.
 31. Campbell, J. H.; Campbell, G. R., Endothelial-Cell Influences on Vascular Smooth-Muscle Phenotype. *Ann Rev Physiol* **1986**, 48, 295-306.
 32. Xia, Y.; Bhattacharyya, A.; Roszell, E. E.; Sandig, M.; Mequanint, K., The role of endothelial cell-bound Jagged1 in Notch3-induced human coronary artery smooth muscle cell differentiation. *Biomaterials* 33, (8), 2462-2472.

CHAPTER

4

4 EXPERIMENTAL AND MODELING STUDIES OF OXYGEN TENSION IN VASCULAR TISSUE ENGINEERING WITH AND WITHOUT AN OXYGEN CARRIER*

Overview: This chapter provides the use of perfluorodecalin (PFD) as oxygen carrier in vascular tissue engineering. In doing so the amount of oxygen dissolved in PFD emulsion was measured and the toxicity of PFD to vascular smooth muscle cells seeded on 3D scaffold were examined and finally a mathematical model was developed for oxygen profile in the lumen and 3D scaffold constructs.

Summary

The technology of vascular tissue engineering holds promise in the design of responsive living conduits with properties similar to those of the native tissue. This approach, however, constitutes an important engineering challenge because of the difficulty to grow cells in high density, due to mass transfer limitations (delivery of nutrients and removal of metabolic waste products). The major mass transfer challenge in tissue engineering arises from the inability to deliver sufficient oxygen because of its low solubility and diffusivity in culture media. In this work the utility of perfluorodecalin (PFD) as an oxygen carrier to enhance oxygen delivery for the growth of human coronary artery smooth muscle cells

* A version of this chapter is published: Seifu, D; Mequanint, K. (2011) Experimental and Modeling Studies of Oxygen Tension in Vascular Tissue Engineering. Journal of Biomaterials and Tissue Engineering 1, 49-59

(HCASMCs) seeded at high density on porous 3D polyurethane (PCU) scaffolds is described. Furthermore, the diffusive and convective lumen and ablumen oxygen distribution in engineered vascular tissue constructs is modeled. Both experimental and modeling data demonstrated that oxygen tension on 3D scaffolds was improved by using PFD as an oxygen carrier. Dissolved oxygen in the culture media with PFD was significantly higher than the other fluids tested ($p = 0.0017$). Furthermore, HCASMC number was significantly higher in the presence of PFD than in control scaffolds. Taken together, these data suggest that PFD could be used as oxygen delivery vehicle in vascular tissue engineering strategies.

Keywords

Vascular tissue engineering, oxygen transport, perfluorodecalin

4.1 Introduction

The strategy of in vitro vascular tissue fabrication is conceptually simple and appealing yet it has proven to be a challenging engineering endeavour. Despite rapid advances made in this field, success is still limited.¹ Compared with native tissues, one of the major unsolved challenges in engineering three-dimensional (3D) tissues is the lack of vascularization resulting in poor oxygen mass transfer. Oxygen can be supplied to vascular cells seeded into a tubular scaffold by radial diffusion from the lumen such that the oxygen concentration decreases from the lumen and the outer limit of the construct. Oxygen diffusion within the scaffold can be enhanced by increasing the overall diffusion coefficient, decreasing the diffusion distance, and increasing convective transport. Since tissue engineering is carried out in a bioreactor, hydrodynamic conditions can affect in

vitro tissue formation in at least two ways:² i) by direct effects of hydrodynamic forces on cell morphology and function, and ii) by indirect flow-induced changes in mass transfer of nutrients and metabolites. In static flask bioreactors, tissues are fixed in place and cultured without hydrodynamic shear at tissue surfaces while relying on diffusional oxygen transport for cell survival. In spinner flask bioreactors, tissues are fixed in place and exposed to the steady turbulent flow of medium, which enhances oxygen mass transfer but the level of mixing intensity required often surpasses the shear tolerance of the cells.³ In a rotating-wall bioreactor, tissues are dynamically suspended in a laminar, rotational flow field, and mass transfer is enhanced by laminar convection due to construct settling. However, cell-seeded scaffolds often undergo repeated wall collisions in rotating bioreactors, which disrupted tissue formation.⁴ Further, rotating-wall bioreactor provided oxygen transfer only to the outer 100 μ m thick layer.⁵ Due to a tubular scaffold requirement, none of the aforementioned bioreactor designs are suitable for fabricating vascular tissues.

In order to improve oxygen transfer, oxygen generating scaffolds and perfluorocarbon compounds as oxygen carriers has been proposed. For example, in cardiac and tracheal tissue engineering, perfluorocarbons have been shown to improve construct oxygenation without the above-mentioned adverse effects to the growing constructs.⁶⁻⁸ In this regard, a steady state model for oxygen distribution in cardiac tissue constructs with parallel channel array mimicking the in vivo capillary tissue bed and PFC compound oxygen carrier was developed by Vunjak-Novakovic and co-workers.⁶ Despite this interesting approach, the application of this model is limited to tissues such as cardiac and cartilage because of the impracticality to create channel arrays within the cross section of vascular

scaffolds. Further, at a wall-to-wall channel spacing of $\sim 370\mu\text{m}$, supply of sufficient oxygen to seeded cardiomyocytes was not achieved. In vascular tissue engineering, culture medium is pulsed and allowed to flow through the lumen which is anticipated to cause transmural oxygen diffusion through the construct wall. However, in previous studies the oxygen tension in the scaffold cross-section was neither predicted nor measured.^{9, 10} Another reported approach to fabricate vascular tissues is a radial flow culture system where oxygen dissolved in the culture medium entered into the lumen at one end and forced out through the scaffold wall as transmural flow (by sealing the other end of the lumen).¹¹ However, the oxygen distribution in this study was not reported. In fact, it can be argued that bioreactors for vascular tissue engineering have been studied primarily for mechanotransduction rather than for oxygen transport studies.^{12, 13} Recently, Bjork and Tranquillo¹⁴ reported a novel approach by combining both transmural and axial flows to enhance oxygen transfer to rat vascular smooth muscle cells seeded into 3D fibrin gel. Their data, however, suggest detrimental effects due to the luminal pressure needed to force transmural flow exceeding the burst pressure of the construct.

To overcome the aforementioned drawbacks while still at the same time delivering sufficient oxygen, we propose a combined approach whereby perfluorodecalin-supplemented culture medium flows from both the lumen and ablumen sides of the construct. In this manuscript we first present experimental evidences on the feasibility of perfluorodecalin as an oxygen carrier. This is followed by a mathematical model for the lumen and the tissue space oxygen distribution with perfluorodecalin as oxygen carrier in a tubular scaffold both in static and in convective transport modes.

4.2 Methods

4.2.1 Fabrication of 3D scaffolds

A medical grade poly(carbonate urethane) (PCU) (Bionate[®] 55D), kindly donated by the Polymer Technology Group (Berkeley, CA), was used to fabricate 3D scaffolds by a solvent casting and particulate leaching method as previously described.¹⁵ Briefly, ground and sieved NH₄Cl porogens (180-250 μm) were packed into a cylindrical infiltration chamber, the polymer solution (15 wt% PCU dissolved in N,N-dimethylformamide) was subsequently poured over the porogen bed and pressurized to infiltrate the porogen bed. Following this, the scaffolds were removed from the assembly and the solvent was allowed to evaporate in a fume hood. Finally, NH₄Cl porogens were leached out using de-ionized water to obtain porous vascular scaffolds (Figure 4. 1A).

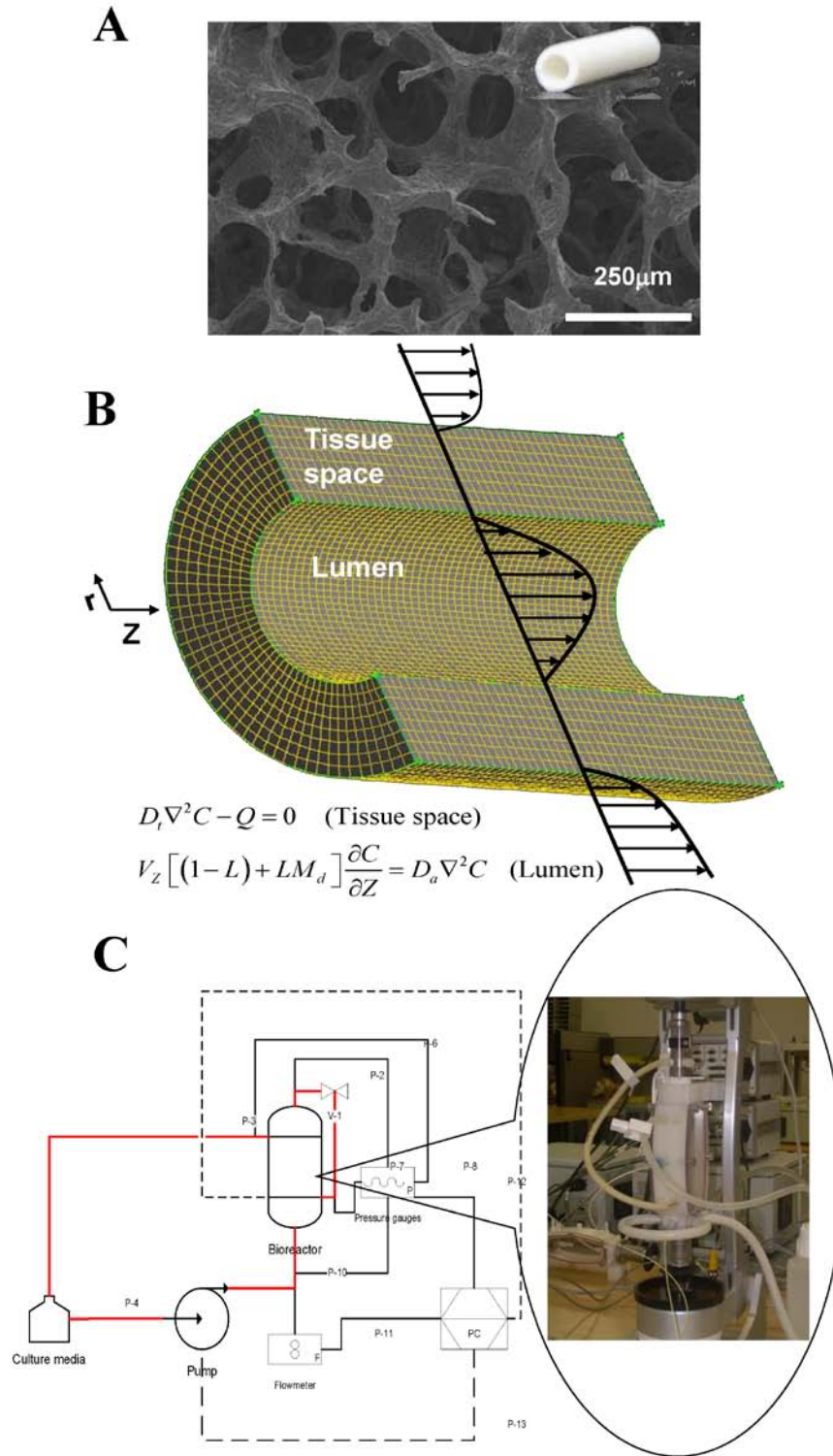


Figure 4.1: SEM and digital image of PCU scaffold (A), tubular construct of porous cell-seeded scaffold and mesh alignment of the model (B), perfusion bioreactor digital image and schematic flow diagram including the setup (C)

4.2.2 Dissolved oxygen measurements

Fibre optic oxygen probe model NeoFox (Ocean Optics, Dunedin, FL) equipped with NeoFox software was used to measure dissolved oxygen. 2% perfluorodecalin (PFD) (95% mixture of cis and trans; Sigma-Aldrich) was emulsified in the presence of smooth muscle culture medium and continuously stirred at 37°C while the assembly was left open to atmospheric air. A 300nm diameter oxygen probe was used to measure the dissolved oxygen and a two point calibration, where 20.9% of oxygen at standard temperature and pressure and 0% of oxygen in 100% nitrogen, was used.

4.2.3 Cell culture on 3D scaffolds

Primary human coronary artery smooth muscle cells (HCASMCs) and smooth muscle growth media (SmGM®-2 BulletKit) were purchased from Lonza Walkersville Inc (Walkersville, MD, USA). Cells were cultured according to supplier's instructions in smooth muscle growth media (SmGM®-2 BulletKit), supplemented with 100 units/mL penicillin G sodium, and 100 µg/mL streptomycin sulphate (Invitrogen, Burlington, ON, Canada). All cultures were maintained in a humidified chamber at 37°C containing 5% CO₂. HCASMCs were passaged every 7 days at a split ratio of 1:3 and used between passages 4 to 7. Scaffolds were sterilized with 70% ethanol for 30 min and allowed to dry under UV light in tissue culture hood for 30 min. After soaking the scaffolds in Hank's Buffered Salt Solution (HBSS, Invitrogen, Burlington, ON, Canada) all scaffolds were coated with fibronectin (10 µg/cm²; Santa Cruz, CA, USA). Cells were seeded onto fibronectin-coated PCU scaffolds at an initial cell density of $\sim 3 \times 10^5$ cells/scaffold. HCASMCs were cultured for 7 days, 14 days, and 21 days.

4.2.4 Cytotoxicity assay and cell number quantification

For colorimetric assays of the metabolic activity of viable cells, 3-(4,5-dimethylthiazol-2-yl)-2,5-diphenyltetrazolium bromide (MTT) (Invitrogen, Burlington, ON, Canada) was used to quantify cytotoxicity following 24 h culture. MTT salts are reduced to a water-insoluble formazan salt only by metabolically active cells allowing the assay to detect viable cells exclusively. After it was solubilized, the formazan formed was quantified by a plate reader at 570 nm (maximum absorbance). Negative control experiments were carried out by adding MTT to 3D scaffolds and culture medium without cells. For cell proliferation, cells were removed from the scaffolds according to our reported methodology¹⁶ following specified culture times and counted using a hemocytometer.

4.2.5 Fluorescence staining and laser scanning confocal microscopy

HCASMCs were fixed at room temperature for 1 h with 4% (w/v) paraformaldehyde (EMD Chemicals Inc.) and permeabilized for 10 min in cation free phosphate buffered saline (PBS) containing 0.1% (v/v) Triton X-100. Cells were incubated for 1 h at room temperature in 1% BSA/PBS containing Alexa Fluor 488-conjugated phalloidin (1:50 dilution), followed by 3 washes with PBS. DAPI (300nM in PBS; Invitrogen, Burlington, ON, Canada) was used to label nuclei. Samples were mounted on slides in SHUR/Mount™ (TBS[®], NC, USA) and analyzed with a Zeiss LSM 410 confocal microscope (Zeiss, Canada) equipped with an argon/neon as well as a UV laser.

4.2.6 Mathematical model for lumen oxygen profile

A cylindrical coordinate as shown in **Figure 4.1B** is used to model oxygen transfer in cell seeded vascular scaffolds. A steady state oxygen balance in the scaffold lumen can be described by the conservation equation:¹⁷

$$V_z [1 - L + LM_d] \frac{\partial C}{\partial Z} = \frac{D_{eff}}{r} \left[\frac{\partial}{\partial r} \left(r \frac{\partial C}{\partial r} \right) + \frac{\partial^2 C}{\partial Z^2} \right] \quad (1)$$

Where V_z is the culture medium velocity, L is the PFD volume fraction, M_d is the oxygen dissociation constant of PFD, Z is the axial direction, r is the radial direction, D_{eff} is the effective oxygen diffusion constant and C is the oxygen concentration. Equation (1) is subject to the following boundary and initial conditions:

$$\text{B.C1: } \left(\frac{\partial C(r, Z)}{\partial r} \right)_{r=0} = 0 \quad ; \quad \text{B.C2: } J = -D_{eff} \left(\frac{\partial C(r, z)}{\partial r} \right)_{r=R} \quad ; \quad \text{I.C: } C(r, 0) = C_o$$

The flow of the medium in the lumen is assumed to be fully developed and, the velocity profile is given by;

$$V_z = 2V_m \left(1 - \left(\frac{r}{R} \right)^2 \right) \quad (2)$$

Where V_m is the average fluid velocity.

In order to calculate the effective diffusion coefficient in equation (1), the following expression was used.¹⁸

$$D_e = D_a \left[1 + 3 \left(\frac{\gamma - 1}{\gamma + 2} \right) L \right] \quad (3)$$

Where $\gamma = \frac{C_p D_p}{C_a D_a}$; D_a is the aqueous phase diffusivity, C_a dissolved oxygen in aqueous phase, D_p is diffusivity of PFD, and C_p is dissolved oxygen in PFD.

4.2.7 Mathematical model for cell-seeded scaffold oxygen profile

A homogeneous cell-seeded scaffold, where culture medium flows both from the lumen and ablumen, was considered to model the oxygen profile in the tissue space. The flux of oxygen from the lumen and ablumen were calculated with a consumption rate and with the effective diffusivity. A steady state differential equation for cell-seeded scaffold will have both the diffusion term and a consumption term (as represented by Michaelis-Menten kinetics) in accordance with following equation:

$$\nabla(D_t \nabla(C)) = \frac{V_{\max} C}{K_m + C} \quad (4)$$

The boundary conditions for equation 4 are:

$$J_{\text{lumen}} = D_t \left(\frac{\partial C(r, Z)}{\partial r} \right)_{r=R_{in}} \quad \text{and} \quad J_{\text{ablumen}} = D_t \left(\frac{\partial C(r, Z)}{\partial r} \right)_{r=R_{out}}$$

D_t is the effective oxygen diffusivity in the tissue space and, the values were adopted from Riley et al ¹⁹ based on Monte-Carlo simulation. For cell volume fraction $0.04 < \phi < 0.95$ in the scaffold:

$$\frac{D_t}{D_o} = 1 - \left(1 - \frac{D_{\text{cell}}}{D_o} \right) (1.727\phi - 0.8177\phi^2 + 0.09075\phi^3) \quad (5)$$

Where D_{cell} is the diffusivity of oxygen in cells, D_o is the diffusivity of oxygen through the interstitial fluid space and φ is the volume fraction of cells.

4.2.8 Model parameters

The mathematical model equations presented above were implemented for the set of experimental conditions summarized in Table 4.1. In order to maintain the wall shear stress within the reported physiological values of normal coronary arteries²⁰ and to show the effect of flow rates, a flow rate of 15mL/min ($\tau_{wall} = 0.65$ dynes/cm²), 23 mL/min ($\tau_{wall} = 1$ dynes/cm²), and 40mL/min ($\tau_{wall} = 1.74$ dynes/cm²) were used. Average velocity was calculated based on cross-section area of the lumen. Maximum oxygen consumption (V_{max}) for vascular smooth muscle cells was taken from literature.²¹ The volume fraction of the circulating PFD molecules was 2%. In addition to the lumen oxygen profile, the model was used to predict oxygen concentration profiles for vascular tissue constructs of clinically relevant thickness (1mm), flow rates, and cell density ranging from 10^6 cell/mL to 5×10^6 cell/mL. The cells were assumed to be uniformly distributed throughout the pores of the 3D scaffold. The corresponding volumetric maximum oxygen consumption rate (V_{max} per unit volume) was calculated for the respective cell numbers. Culture medium at the inlet of the construct was assumed to be fully saturated with atmospheric oxygen with an oxygen partial pressure of 160 mmHg. The partial pressure of oxygen for culture medium supplemented with PFD was measured to be 220 mmHg using the reported value of oxygen solubility in PFD 37°C.²²

4.2.9 Numerical solutions

The solutions for the model equations were obtained using the PDE toolbox built in MatLab R2009a utilizing finite element model. In order to use the toolbox, the boundary conditions were modified as follows.

- $\vec{n}(D_e \nabla C) = J_{wall}$ (Neumann condition). Since the generalized Neumann condition in the PDE toolbox software is $\vec{n}(D_e \nabla C) + qC = g$, and C depends on r in this problem, this boundary condition was expressed as $\vec{n}(D_e \nabla C) = J_{wall}(\vec{r})$
- $C = 220$ mmHg at the left end of the cylinder (Dirichlet condition).
- The cylinder axis at $r = 0$ is not a boundary in the original problem but in 2D treatment, due to symmetry, $\vec{n}(D_e \nabla C) = 0$.

Solving equations (1) and (4) took up to 1933 successful steps, zero failed attempts, 4053 evaluated functions, 511 LU decomposition, 4053 solutions of linear systems with computation times ranging from 4 to 7 min.

4.2.10 Statistical analysis

The results for the dissolved oxygen study were analyzed by analysis of variance (ANOVA). Student's t-test was used to analyze the cytotoxicity of PCU scaffold and proliferation of HCASMC as a function of culture time. For all analyses, significance was assigned for $p < 0.05$.

4.3 Results and discussion

4.3.1 The effect of PFD on dissolved oxygen in HCASMCs culture medium, cell spreading and cell viability.

In this work the feasibility of PFD to enhance oxygen delivery to vascular smooth muscle cells seeded into 3D scaffolds was investigated. The rationale for choosing PFD was twofold. Firstly, while dissolving high level of oxygen (ca. 42.3 ml per 100 ml of O₂), it is reported that PFD has longer tissue retention time which holds promise for a clinical application compared with the most widely used perflubron²³. Secondly, unlike Oxygent™ whose primary content is perflubron, PFD is not investigated as oxygen carrier for tissue engineering applications. Because in vitro cell culture data using PFD is not reported, it was first investigated if this molecule could be a candidate to enhance oxygen delivery in vascular tissue engineering. Figure 4.2 shows the measured dissolved oxygen concentration in PFD-supplemented HCASMC culture medium and other fluids at 37°C and atmospheric pressure. There was no statistical significance between DI water, PBS and HCASMC culture medium. The oxygen solubility values in these fluids were comparable to the calculated value using Henry's law. However, in comparison to the variety of biological fluids tested, there was a highly significant difference when 2% PFD was added in HCASMC culture medium (p=0.0017). This data shows that by incorporating 2% PFD in culture media, there was a significant increase of dissolved oxygen at 37°C. Dissolved gases are transported by perfluorinated compounds due to increased solubility in accordance with Henry's Law. The increase is attributed due to the existence of loose, non-directional van der Waals interactions leading to low cohesive energy densities, which facilitates mutual solubilization of oxygen in the fluorine

compound that is bound to the surface of the emulsion.²⁴ To evaluate the possible cytotoxic effect of 2% PFD on cultured HCASMC, cells were cultured on coverslips with and without PFD for up to 7 days. The phase-contrast microscopy images (2D cultures) and confocal microscopy images (3D scaffolds) presented in Figure 4.3 demonstrated that the morphology and spreading of cells were not affected by the presence of PFD. The MTT assay data presented in Figure 4.4 also affirmed that 2% PFD was not cytotoxic to HCASMCs. Although data is not available for vascular smooth muscle cells, perfluorocarbon emulsions even at low concentrations are in general considered to be cytotoxic and inhibitor to proliferation in cultured human fibroblast cells^{25, 26}. Figure 4.4, on the other hand, demonstrates excellent cell viability which could be due to the differences in the type of perfluorocarbon used in our study and in the above-cited studies. Based on the feasibility data presented herein, a fixed 2% PFD was used to investigate cell growth in 3D scaffolds and to predict oxygen tension in our mathematical model.

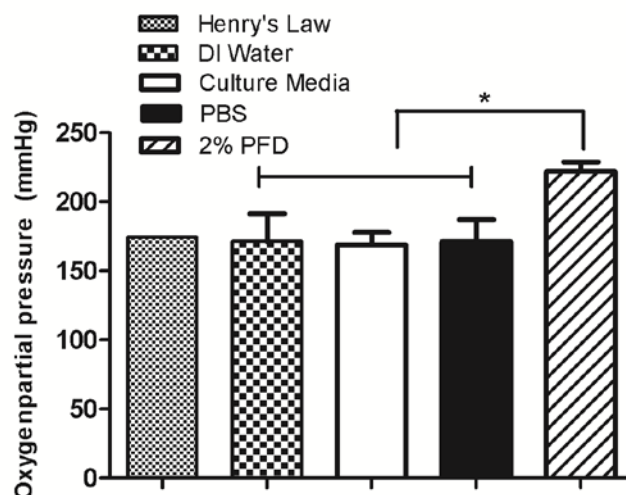


Figure 4.2: Dissolved oxygen partial pressure in different fluids measured at 37 °C. Oxygen concentration was measured using fibre optic probe. Data are mean \pm SD for experiments conducted in triplicate. * indicates statistical significance.

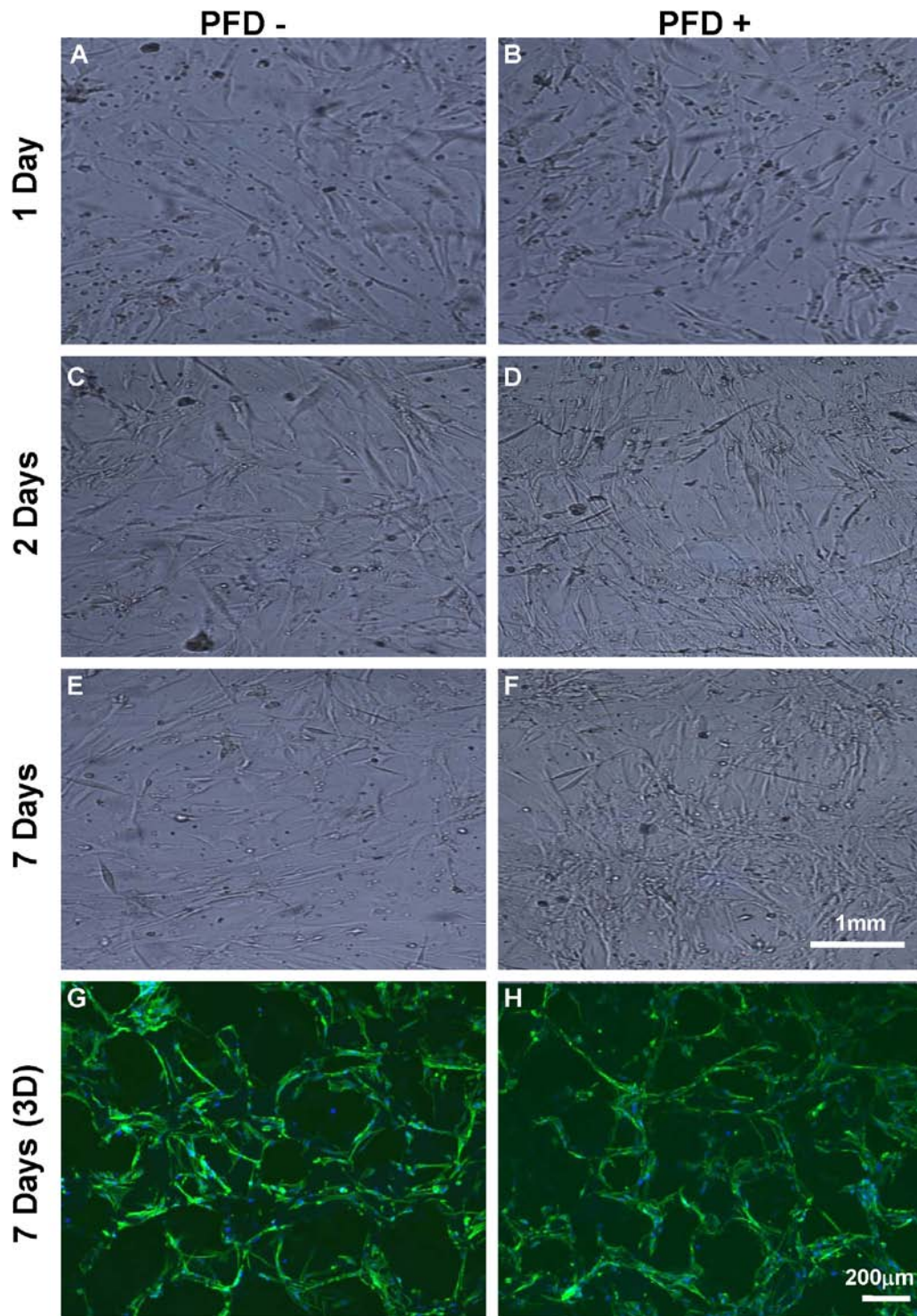


Figure 4.3: Phase contrast images of HCASMC, cultured without PFD supplemented medium (A, C and E) and with PFD (B, D and F) for 1 days, 2 days and 7 days. Confocal microscopy images of HCASMCs cultured on 3D scaffolds with PFD (H) and without PFD supplemented medium (G).

4.3.2 HCASMC proliferation when seeded to 3D scaffolds with 2% PFD-supplemented medium.

In order to rationalize the modeling approach and to examine the effect of 2% PFD in culture medium, HCASMC proliferation on 3D scaffolds was investigated. The results presented in Figure 4.5 demonstrated that cell number significantly increased following 7 days, 14 days and 21 days of culture with 2% PFD ($p < 0.05$). Since equal numbers of cells were seeded on all scaffolds and that both scaffolds and PFD were not cytotoxic, the significant increase in cell numbers as a function of time indicates that an environment conducive for cell growth was established by providing sufficient oxygen tension as will be shown in the mathematical model in the next section.

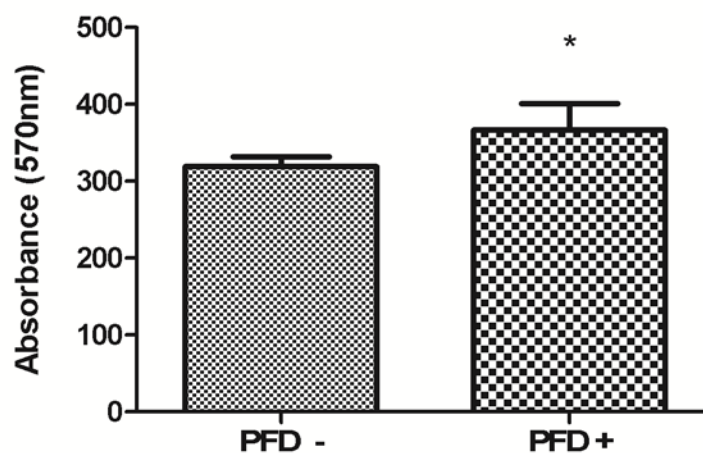


Figure 4.4: HCASMC viability using MTT assay on 3D PCU scaffold cultured with and without PFD supplemented medium. Data are mean \pm SD for experiments conducted in triplicate. * indicates statistical significance

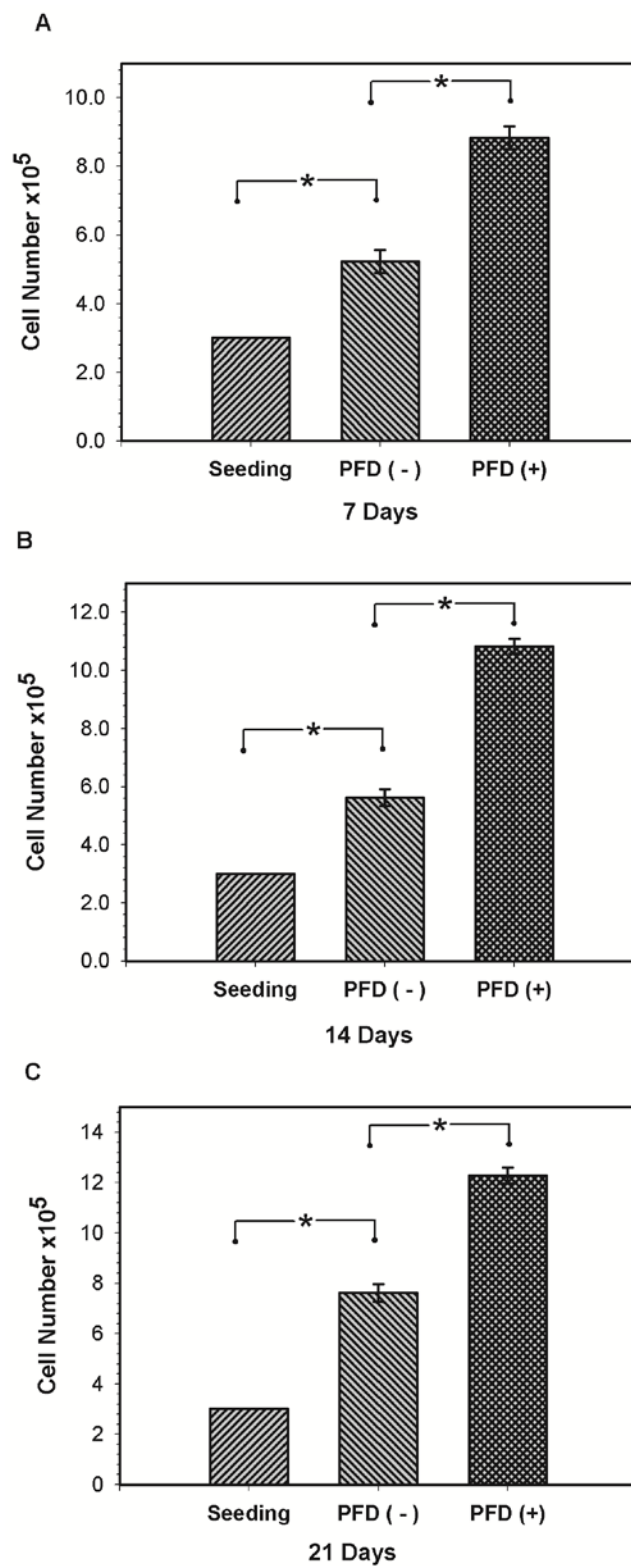


Figure 4.5: HCASMC proliferation on 3D scaffolds with and without PFD supplemented medium for 7 days (A) 14 days (B) and 21 Days (C). Data are mean \pm SD for experiments conducted in triplicate. * indicates statistical significance.

4.3.3 Numerical solution for oxygen profiles in static 3D cultures.

Diffusion and convection are the two main mass transfer mechanisms in cell seeded 3D scaffolds. To establish a baseline, the oxygen profile in both the lumen and tissue space was first simulated for static cultures where the lumen is filled by a stagnant culture medium. Since cells are seeded only to the scaffolds, there is no lumen oxygen consumption in the model equation so the lumen oxygen profile represents this fact. Therefore, it is expected that the oxygen distribution within the lumen is governed only by diffusion. Due to symmetry, only half of the lumen was modeled and, a representative lumen oxygen profile is shown in Figure 4.6A, from which it can be inferred that the oxygen partial pressure decreased rapidly as we move from the two ends of the scaffold lumen to the centre along the axis of the scaffold. The oxygen flux from the lumen by diffusion will be consumed by cells in the scaffold. At a cell density of 2.5×10^6 cells/mL which was used to obtain the data for Figure 4.6A, the oxygen profile at the midpoint of the scaffold luminal length ($Z = 0$) reached zero. Figure 4.6A also shows that at any cross section of the lumen the concentration of oxygen is minimum at the interface between the scaffold and culture media and maximum at the center which follows the flux as shown by the direction fields (indicated by a series of red arrows in the radial direction). To study the effect of cell density, the lumen-scaffold interface oxygen concentration was plotted (Figure 4.6B). The model indicates that from all cell densities shown, oxygen diffusion from the lumen was sufficient only for low cell seeding density. Above 1.5×10^6 cells/ml diffusion alone was not able to deliver oxygen for cell survival as indicated by the corresponding partial pressure that drops to zero. It is to be recognized that a minimum oxygen concentration above 20 mmHg must be maintained in the lumen

to avoid a necrotic environment in the tissue space.^{27, 28} In addition to the lumen oxygen profile, the tissue space oxygen profile with and without PFD supplement was modeled and, the results are presented in Figure 4.7. Without PFD, oxygen partial pressure dropped to below 20 mmHg at a scaffold depth of ≈ 0.15 mm (Figures 4.7 A &C). Despite the enhancement in the oxygen penetration depth into the tissue space to about 0.4mm, the presence of 2% PFD does not appear to be sufficient to supply enough oxygen to seeded HCASMCs as shown by the rapid depletion of oxygen with increased scaffold thickness (Figures 4.7 B &C).

Table 4.1: Model parameters used to predict oxygen concentration profiles in a vascular tissue constructs oxygenated with PFD supplemented culture medium.

Model parameters	Value	Source
R_{in} (lumen radius)	3mm	Measured
R_{out} (lumen + tissue radius)	4mm	Measured
L (construct length)	10mm	Measured
U (average velocity)	3.14 cm/s (15 mL/min) 5.35 cm/s (23 mL/min) 9.09 cm/s (40 mL/min)	Calculated
Oxygen consumption (V_{max})	2.6×10^{-15} mol/min/cell	Motterlini et al. ²¹
Michaelis-Menten constant (K_m)	7.75nmol/mL (7.75 μ M)	Bjork et al. ¹⁴
PFD in culture medium	2% v/v	Measured
Solubility of oxygen in PFD 37°C	42.3mg/mL	King et al ²²
D_a (oxygen diffusivity in the aqueous phase)	2.4×10^{-5} cm ² /s	Radisic et al. ⁶
D_t (oxygen diffusivity in the tissue space)	1.06×10^{-5} cm ² /s	Calculated
C_{in} (inlet oxygen concentration in aqueous phase)	297.23 μ M (220 mmHg for PFD)	Measured

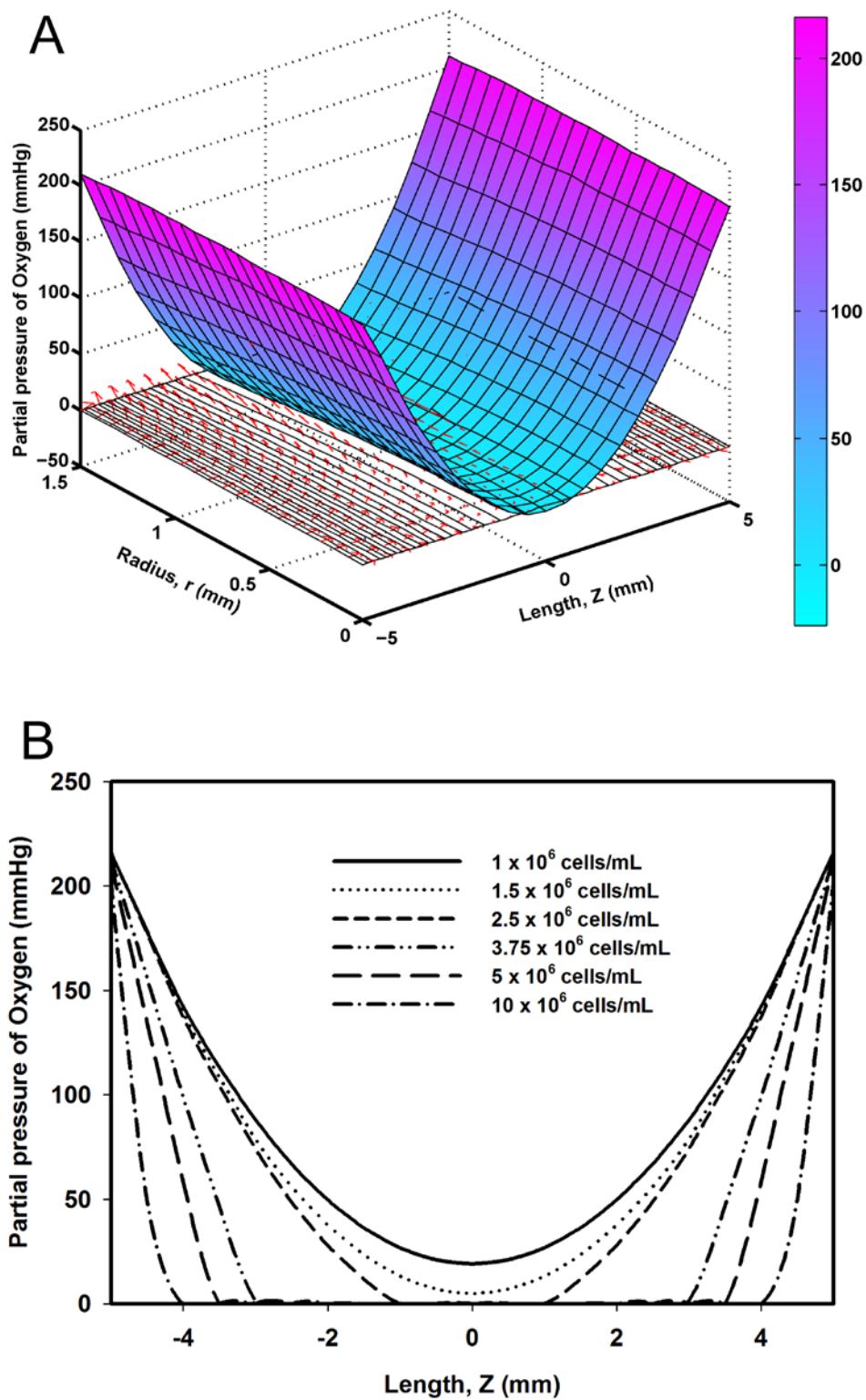


Figure 4.6: Model prediction of oxygen profile in the lumen at static culture condition in 3D plot (A) and a plot of lumen-scaffold interface oxygen partial pressure for different cell densities (B).

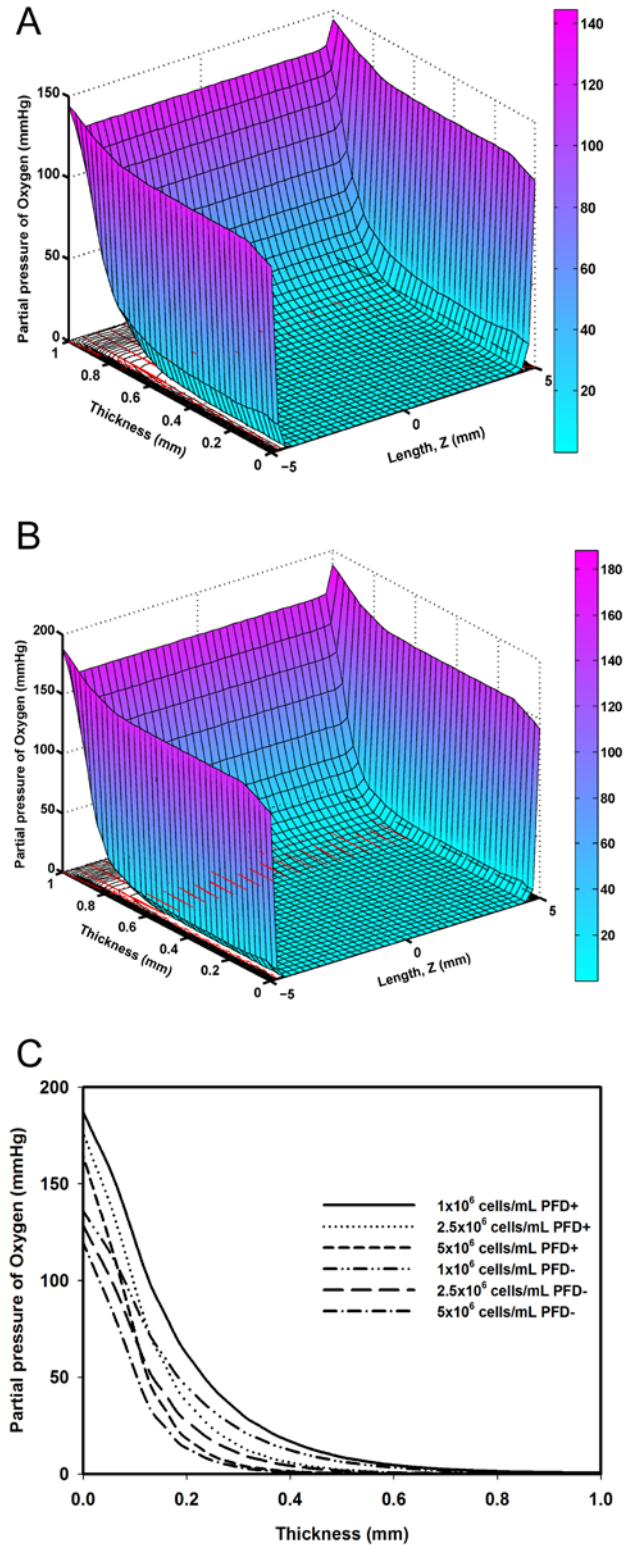


Figure 4.7: Oxygen profile in the scaffold (tissue space) at static condition in 3D plot with and without PFD supplemented medium (B, C) and a plot of cross sectional oxygen partial pressure for different cell densities (C).

4.3.4 Numerical solution for oxygen profiles in 3D cultures with convection

The second part of the modeling study was done to include convective mass transfer to the diffusion. We assumed that the medium flow to be fully developed laminar flow which is reasonable because many practical bioreactors including ours have long tubing often forming loops from the pulse generator to the tissue construct (Figure 4.1C). Due to symmetry, only half of the lumen was modeled and; the concentration of oxygen on the Z direction is maximum at the inlet and minimum at the exit (Figure 4. 8A&B). In addition to that, Figure 4.8B shows that at any cross section of the lumen, the concentration of oxygen is minimum at the interface between the scaffold and culture medium and maximum at the center in the direction of the flux. The model prediction shows that the best result for oxygen profile in the lumen with 2% PFD is obtained when the flow rate is 40 ml/min and HCASMCs are seeded at a density of 2.5×10^6 cells/ml. Although it is possible to increase the flow rate to enhance oxygen transfer either for higher cell density than the one assumed herein in the scaffolds or for longer scaffolds than the one utilized in this model, it should be pointed out that this can be done at the detriment due to excessive wall shear stress. At a lumen radius of 3mm, the wall shear stresses calculated in this model varied from 0.65 dynes/cm^2 (corresponding to 15 ml/min medium flow) to 1.74 dynes/cm^2 (corresponding to 40 ml/min medium flow) which are physiologically relevant.²⁰

To model the oxygen profile in the tissue space, a homogeneous cell-seeded scaffold where culture medium flows both from the lumen and ablumen was considered. The rationale for the ablumen flow was to mimic the vasa vasorum that supply oxygen to smooth muscle and fibroblast cells within the media and adventitia of arteries. The

bioreactor in our laboratory is also able to supply essential nutrient from the lumen and the ablumen.

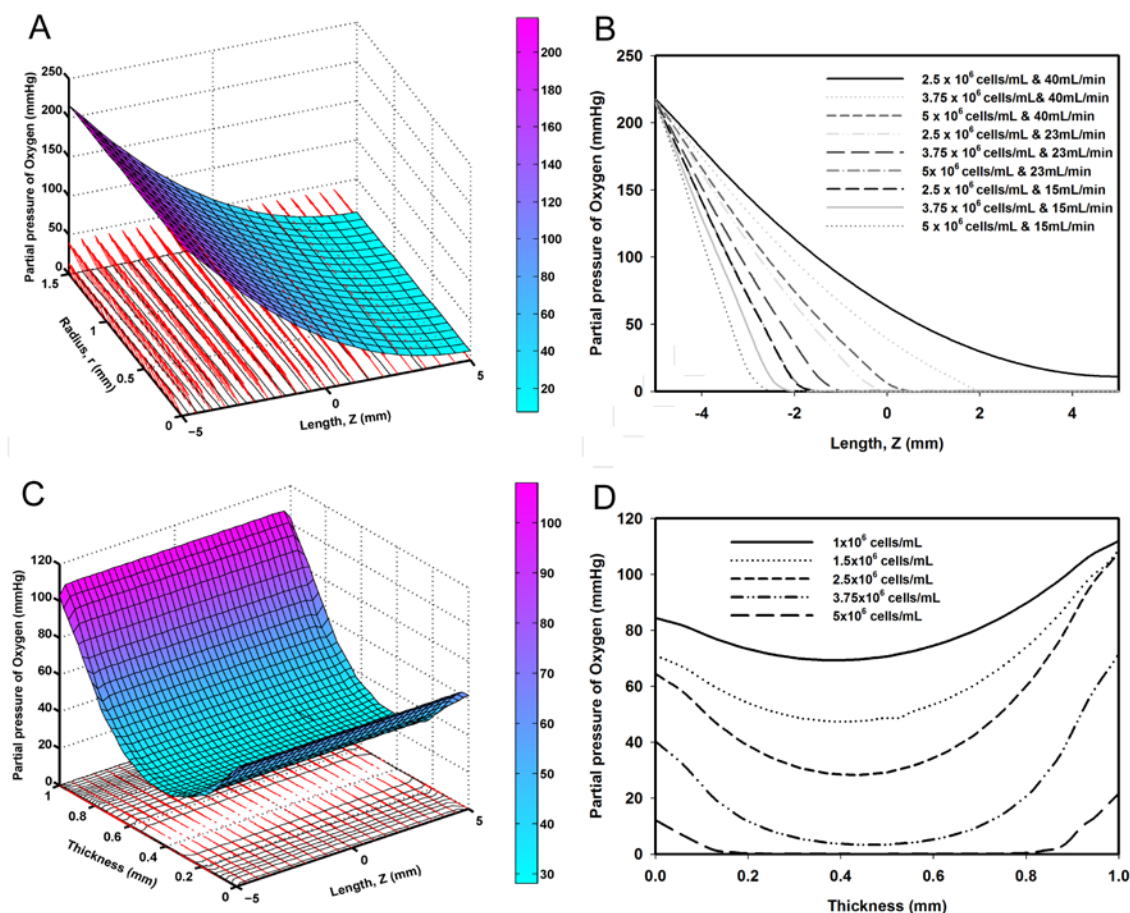


Figure 4.8: Oxygen profile in the lumen and in the scaffold at a flow condition. A 3D representation of the oxygen partial pressure in half of the lumen (A), a plot of lumen-scaffold interface oxygen partial pressure for different cell densities (B), a 3D plot of the oxygen partial pressure in scaffold (C) and a plot oxygen partial pressure across the cross section of the scaffold for different cell densities (D).

The flux of oxygen from the lumen and ablumen was calculated with a Michaelis-Menten consumption rate and with effective diffusivity and was subsequently used as a boundary condition to solve the oxygen profile in the tissue space. The numerical solution of the PDE given in equation 1 plotted in Figures 4.8 C&D showed that the concentration of oxygen is maximum at the scaffold-lumen interface and minimum at the centerline of the

scaffold wall thickness. At concurrent lumen and ablumen flow rate of 40 ml/min, culture medium supplemented with 2% PFD provided the necessary oxygen for up to, 3.75×10^6 cells/ml. Although the vascular smooth muscle cells density assumed in this study is relatively lower compared with the physiologic values,²⁹ it is deemed to be an acceptable density for vascular tissue engineering. The plots in Figure 4.8D showed that the oxygen partial pressure continuously decreased as one moves from the lumen-scaffold interface (thickness = 0) to the scaffold centreline (thickness = 0.5). This was followed by a continuous upward swing towards the outer scaffold space, reaching a maximum at thickness = 1mm. The oxygen partial pressure values at thickness = 0 and at thickness = 1mm are not the same because of the differences in the outer and inner radius of the tissue space used in the model. Since the total flux is fixed based on oxygen consumption, oxygen transfer from the ablumen is higher than the lumen due to increased radius (and hence surface area).

One key design element in tissue engineering is maintaining adequate mass transfer while at the same time providing local conducive environment to the differentiated state of seeded cells. The mechanism of oxygen transport and consumption in cells is an important problem which has received considerable attention in recent years³⁰⁻³². Hoare and coworkers³³ reported a window of operation to engineer vascular constructs with sufficient oxygen delivery based on convection and diffusion from the lumen. Whereas their approach captured the practical aspect of cell density in the construct space and the wall shear stress (calculated based on the given critical flow rates), the model underestimates both the wall thickness (0.2mm used in the model vs. 0.5mm-1mm for typical coronary arteries) and the oxygen consumption of vascular smooth muscle cells.

Specifically, the oxygen consumption data used in their model is an order magnitude lower than the oxygen demand of vascular smooth muscle cells.^{14, 21} Due to these underestimations, we believe that their prediction will fall short of the physiologic relevance in both the wall thickness of the vascular constructs and the oxygen consumption of vascular smooth muscle cells. Although the oxygen consumption rate data in the work of Bjork and Tranquillo¹⁴ is realistic for vascular smooth muscle cells, the pressure required to deliver oxygen via transmural flow was detrimental to the growing tissue constructs thus limiting their efforts. In addition, the 0.2 mm wall thickness used is lower than typical coronary arteries. By combining a practical wall thickness (1 mm), experimentally determined oxygen consumption rate of vascular smooth muscle cells, and physiologic wall shear stress, the present study suggests that without oxygen carrier molecules, fabrication of tissue engineered vascular constructs may be limited by oxygen mass transfer. This, in turn, could limit the initial mechanical functionality and subsequent in vivo function of grafts of clinically relevant size.

Because of the poor solubility of oxygen in culture media at physiologic temperature, its delivery represents one of the most critical issues in engineering clinically relevant functional 3D tissues.³¹ While cells consume approximately six mole of soluble oxygen per mole of glucose, the solubility of oxygen in typical culture media is an order magnitude lower than the available glucose. As a result, engineered tissues that are more than approximately 100- μm -thick and supplied with nutrients solely by diffusion may have insufficient oxygen transport to the cells. It has been widely acknowledged that the supply of oxygen becomes critically limiting for the in vitro culture of 3D tissues.³⁴ This is demonstrated by early studies showing that cellular spheroids larger than 1 mm in

diameter generally contain a hypoxic and necrotic center, surrounded by a rim of viable cells.³⁵ Similar observations beyond depths of 0.25 mm were reported for hepatocytes, osteoblasts and cardiomyocytes cultured on 3D scaffolds under static conditions.³⁶⁻³⁸ As a result, tissue engineered constructs frequently have an inhomogeneous structure consisting of a dense layer of cells and extracellular matrix concentrated along the periphery, and a necrotic interior region.³⁹ Because engineered blood vessels should be at least 0.5 mm in wall thickness, oxygen mass transfer limitations represent a critical design issue to be addressed for tissue functionality.

The metabolic oxygen consumption rate is generally a function of concentration. The most common oxygen consumption rate expression (per unit volume per unit time) is the Michaelis-Menten equation:

$$\text{Oxygen consumption rate} = \frac{V_{\max} C}{K_m + C}$$

The above equation reduces to zero-order consumption when the available oxygen concentration is high (i.e. $C \gg K_m$) and to first-order kinetics for low oxygen concentrations (i.e. $C \ll K_m$). The zero-order limit is often considered as a reasonable approach because the condition $C \gg K_m$ is easily met physiologically. However, in tissue engineering, available oxygen quickly depletes and it is equally likely that the condition $C \ll K_m$ to be satisfied. In this study the model is tested with all these possibilities (Figure 4.9). It is evident that zero-order consumption led to the local oxygen concentration to drop to unacceptably low levels, even with 2% PFD. In many instances

oxygen delivery to cells is bounded by zero-order and first-order consumption rates in accordance with the Michaelis-Menten equation.

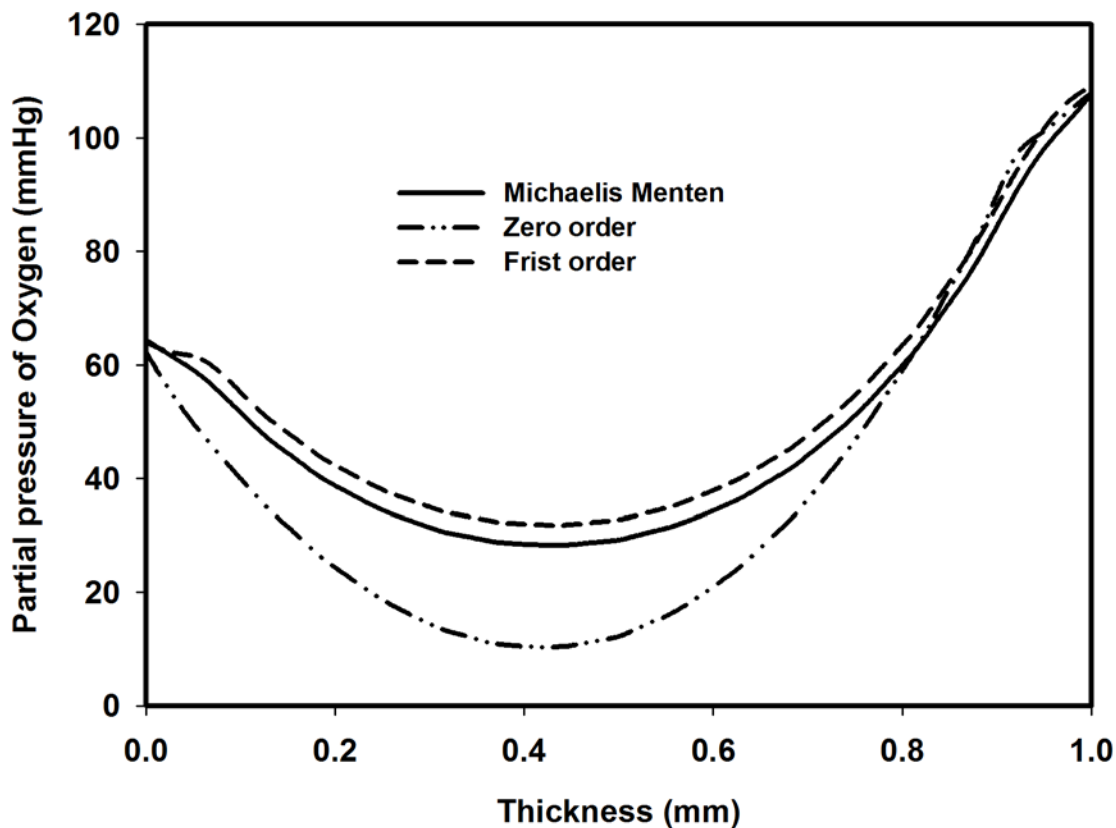


Figure 4.9: A plot oxygen partial pressure across the cross section of the scaffold for 2.5×10^6 cell/ml density for zero order, Michaelis-Menten and first order kinetics. medium flow rate was 40 ml/min.

Despite oxygen delivery challenges, tissue engineering of vascular constructs have been achieved using different bioreactors.^{10, 14, 29} In many of these instances, the wall shear stress due to increased flow rates inadvertently compromised the integrity of the tissue by altering cellular responses. In the present work the use of 2% PFD as oxygen carrier allow us to deliver oxygen to tissue constructs at physiologic shear forces and flow rates. Further we made use of realistic vascular tissue diameter and wall thickness to model the oxygen profile concentration within the engineered tissue. This is expected to improve

design optimization in order to ensure long-term viability and functional property maintenances for human implantation.

4.4 Conclusions

One unsolved problem in tissue engineering is overcoming hypoxia in thick, three-dimensional engineered tissues, which is caused by the diffusional limitations of oxygen in the centre of the scaffold and lack of internal vasculature to facilitate mass transfer. In order to combat this obstacle, a steady state mathematical model was developed to simulate transport of oxygen in both the lumen and the tissue space. In this study, a mathematical model was developed using PFD as oxygen carrier in 3D tissue engineered scaffold. Dissolved oxygen concentration significantly increased in the presence of PFD in a culture media. Vascular smooth muscle cell viability was not affected by the presence of the PFD and; cell proliferation with PFD was significantly higher than those without PFD. Our data suggest that PFD emulsion increase the oxygen tension in 3D tissue engineered scaffolds and enhanced oxygen delivery to cells.

Acknowledgment

This work was funded by the Heart and Stroke Foundation of Ontario (HSFO) grant # NA6345.

4.6 References:

1. Naito, Y.; Shinoka, T.; Duncan, D.; Hibino, N.; Solomon, D.; Cleary, M.; Rathore, A.; Fein, C.; Church, S.; Breuer, C., Vascular tissue engineering: Towards the next generation vascular grafts. *Adv Drug Deliv Rev* **2011**.
2. Vunjak-Novakovic, G.; Freed, L. E.; Biron, R. J.; Langer, R., Effects of mixing on the composition and morphology of tissue-engineered cartilage. *AIChE Journal* **1996**, 42, (3), 850-60.
3. Vunjak-Novakovic, G.; Obradovic, B.; Martin, I.; Freed, L. E., Bioreactor studies of native and tissue engineered cartilage. *Biorheology* **2002**, 39, (1-2), 259-68.
4. Yu, X.; Botchwey, E. A.; Levine, E. M.; Pollack, S. R.; Laurencin, C. T., Bioreactor based bone tissue engineering: Influence of wall collision on osteoblast cultured on polymeric Microcarrier scaffolds in rotating bioreactors. *Mater Res Soc Symp P* **2005**, 845, (Nanoscale Materials Science in Biology and Medicine), 333-338.
5. Carrier, R. L.; Papadaki, M.; Rupnick, M.; Schoen, F. J.; Bursac, N.; Langer, R.; Freed, L. E.; Vunjak-Novakovic, G., Cardiac tissue engineering: cell seeding, cultivation parameters, and tissue construct characterization. *Biotechnol Bioeng* **1999**, 64, (5), 580-9.
6. Radisic, M.; Deen, W.; Langer, R.; Vunjak-Novakovic, G., Mathematical model of oxygen distribution in engineered cardiac tissue with parallel channel array perfused with culture medium containing oxygen carriers. *Am J Physiol Heart Circ Physiol* **2005**, 288, (3), H1278-89.
7. Radisic, M.; Park, H.; Chen, F.; Salazar-Lazzaro, J. E.; Wang, Y.; Dennis, R.; Langer, R.; Freed, L. E.; Vunjak-Novakovic, G., Biomimetic approach to cardiac tissue engineering: oxygen carriers and channeled scaffolds. *Tissue Eng* **2006**, 12, (8), 2077-91.
8. Tan, Q.; El-Badry, A. M.; Contaldo, C.; Steiner, R.; Hillinger, S.; Welti, M.; Hilbe, M.; Spahn, D. R.; Jaussi, R.; Higuera, G.; van Blitterswijk, C. A.; Luo, Q.; Weder, W., The effect of perfluorocarbon-based artificial oxygen carriers on tissue-engineered trachea. *Tissue Eng Part A* **2009**, 15, (9), 2471-80.
9. Iwasaki, K.; Kojima, K.; Kodama, S.; Paz, A. C.; Chambers, M.; Umezu, M.; Vacanti, C. A., Bioengineered three-layered robust and elastic artery using hemodynamically-equivalent pulsatile bioreactor. *Circulation* **2008**, 118, (14 Suppl), S52-7.

10. Williams, C.; Wick, T. M., Perfusion bioreactor for small diameter tissue-engineered arteries. *Tissue Eng* **2004**, 10, (5-6), 930-41.
11. Kitagawa, T.; Yamaoka, T.; Iwase, R.; Murakami, A., Three-dimensional cell seeding and growth in radial-flow perfusion bioreactor for in vitro tissue reconstruction. *Biotechnol Bioeng* **2006**, 93, (5), 947-54.
12. Shi, Z. D.; Tarbell, J. M., Fluid Flow Mechanotransduction in Vascular Smooth Muscle Cells and Fibroblasts. *Ann Biomed Eng* **2011**.
13. Lesman, A.; Blinder, Y.; Levenberg, S., Modeling of flow-induced shear stress applied on 3D cellular scaffolds: Implications for vascular tissue engineering. *Biotechnol Bioeng* **2010**, 105, (3), 645-54.
14. Bjork, J. W.; Tranquillo, R. T., Transmural flow bioreactor for vascular tissue engineering. *Biotechnol Bioeng* **2009**, 104, (6), 1197-206.
15. Grenier, S.; Sandig, M.; Mequanint, K., Polyurethane biomaterials for fabricating 3D porous scaffolds and supporting vascular cells. *J Biomed Mater Res A* **2007**, 82, (4), 802-9.
16. Grenier, S.; Sandig, M.; Mequanint, K., Smooth muscle alpha-actin and calponin expression and extracellular matrix production of human coronary artery smooth muscle cells in 3D scaffolds. *Tissue Eng Part A* **2009**, 15, (10), 3001-11.
17. Patel, S.; Mehra, A., Modeling of oxygen transport in blood-perfluorocarbon emulsion mixtures - Part II: Tissue oxygenation. *Asaio J* **1998**, 44, (3), 157-165.
18. Deen, W. M., *Analysis of transport Phenomena*. 1998; p 316.
19. Riley, M. R.; Muzzio, F. J.; Buettner, H. M.; Reyes, S. C., A simple correlation for predicting effective diffusivities in immobilized cell systems. *Biotechnol Bioeng* **1996**, 49, (2), 223-7.
20. Soulis, J. V.; Farmakis, T. M.; Giannoglou, G. D.; Louridas, G. E., Wall shear stress in normal left coronary artery tree. *J Biomech* **2006**, 39, (4), 742-9.
21. Motterlini, R.; Kerger, H.; Green, C. J.; Winslow, R. M.; Intaglietta, M., Depression of endothelial and smooth muscle cell oxygen consumption by endotoxin. *Am J Physiol* **1998**, 275, (3 Pt 2), H776-82.
22. King, A. T.; Mulligan, B. J.; Lowe, K. C., Perfluorochemicals and Cell-Culture. *Bio-Technol* **1989**, 7, (10), 1037-1042.
23. Lowe, K. C., Fluorinated blood substitutes and oxygen carriers. *J Fluorine Chem* **2001**, 109, (1), 59-65.

24. Riess, J. G., Understanding the fundamentals of perfluorocarbons and perfluorocarbon emulsions relevant to in vivo oxygen delivery. *Artif Cells Blood Substit Immobil Biotechnol* **2005**, 33, (1), 47-63.
25. Wake, E. J.; Studzinski, G. P.; Bhandal, A., Changes in human cultured cells exposed to a perfluorocarbon emulsion. *Transfusion* **1985**, 25, (1), 73-7.
26. Centis, V.; Doillon, C. J.; Vermette, P., Perfluorocarbon emulsions cytotoxic effects on human fibroblasts and effect of aging on particle size distribution. *Artif Organs* **2007**, 31, (8), 649-53.
27. Patel, S.; Mehra, A., Modeling of oxygen transport in blood-perfluorocarbon emulsion mixtures - Part 1: Oxygen uptake in tubular vessels. *ASAIO J* **1998**, 44, (3), 144-156.
28. Dvir, T.; Benishti, N.; Shachar, M.; Cohen, S., A novel perfusion bioreactor providing a homogenous milieu for tissue regeneration. *Tissue Eng* **2006**, 12, (10), 2843-2852.
29. Dahl, S. L.; Rhim, C.; Song, Y. C.; Niklason, L. E., Mechanical properties and compositions of tissue engineered and native arteries. *Ann Biomed Eng* **2007**, 35, (3), 348-55.
30. Rouwkema, J.; Koopman, B.; Blitterswijk, C.; Dhert, W.; Malda, J., Supply of nutrients to cells in engineered tissues. *Biotechnol Genet Eng Rev* **2010**, 26, 163-78.
31. Martin, Y.; Vermette, P., Bioreactors for tissue mass culture: design, characterization, and recent advances. *Biomaterials* **2005**, 26, (35), 7481-503.
32. Curcio, E.; Macchiarini, P.; De Bartolo, L., Oxygen mass transfer in a human tissue-engineered trachea. *Biomaterials* **2010**, 31, (19), 5131-6.
33. Gerontas, S.; Farid, S. S.; Hoare, M., Windows of operation for bioreactor design for the controlled formation of tissue-engineered arteries. *Biotechnol Prog* **2009**, 25, (3), 842-53.
34. Martin, I.; Wendt, D.; Heberer, M., The role of bioreactors in tissue engineering. *Trends Biotechnol* **2004**, 22, (2), 80-6.
35. Sutherland, R. M.; Sordat, B.; Bamat, J.; Gabbert, H.; Bourrat, B.; Mueller-Klieser, W., Oxygenation and differentiation in multicellular spheroids of human colon carcinoma. *Cancer Res* **1986**, 46, (10), 5320-9.
36. McClelland, R. E.; Coger, R. N., Use of micropathways to improve oxygen transport in a hepatic system. *J Biomech Eng* **2000**, 122, (3), 268-73.

37. Ishaug, S. L.; Crane, G. M.; Miller, M. J.; Yasko, A. W.; Yaszemski, M. J.; Mikos, A. G., Bone formation by three-dimensional stromal osteoblast culture in biodegradable polymer scaffolds. *J Biomed Mater Res* **1997**, 36, (1), 17-28.
38. Radisic, M.; Malda, J.; Epping, E.; Geng, W.; Langer, R.; Vunjak-Novakovic, G., Oxygen gradients correlate with cell density and cell viability in engineered cardiac tissue. *Biotechnol Bioeng* **2006**, 93, (2), 332-43.
39. Wendt, D.; Stroebel, S.; Jakob, M.; John, G. T.; Martin, I., Uniform tissues engineered by seeding and culturing cells in 3D scaffolds under perfusion at defined oxygen tensions. *Biorheology* **2006**, 43, (3-4), 481-8.

CHAPTER

5

5 TISSUE ENGINEERING SCAFFOLDS CONTAINING EMBEDDED FLUORINATED-ZEOLITE OXYGEN VECTORS*

Overview: This chapter provides the use of fluorinated Zeolite particles as oxygen delivery vector. Fluorinated Zeolite particles were prepared and examined for their ability to dissolve oxygen in aqueous media. The toxicity of these particles was examined and embedded into 3D PCU scaffolds. Finally their effect as an oxygen vector was investigated by culturing vascular smooth muscle cells on fluorinated Zeolite embedded 3D PCU scaffolds.

Summary

Efficient oxygen supply is a continued challenge for the fabrication of successful tissue engineered constructs with clinical relevance. In an effort to enhance oxygen delivery, the feasibility of fluorinated-zeolite particles that are embedded into 3D polyurethane scaffolds as novel oxygen vectors is reported herein. First, 1H, 1H, 2H, 2H-perfluorodecyltriethoxysilane was successfully coupled to zeolite framework particles to examine the dose-dependent dissolved oxygen concentration. Following this, the fluorinated-zeolite (FZ) particles were embedded into 3D tissue engineering polyurethane scaffolds. The data demonstrated an even distribution of FZ particles into 3D scaffolds

* A version of this chapter is published: Seifu, D.G; Isimjan, T.T; Mequanint, K. (2011) Tissue engineering scaffolds containing embedded fluorinated-zeolite oxygen vectors. Acta Biomaterialia 7: 3670–3678

without affecting the scaffold porosity and pore sizes. Human coronary artery smooth muscle cells (HCASMCs) proliferation on FZ-containing polyurethane (PCU-FZ) scaffolds was significantly higher than the control scaffolds ($p = 0.05$). Remarkably, cell infiltration depths on PCU-FZ scaffolds was doubled compared with PCU control scaffolds. Taken together, these data suggest the potential of PCU-FZ scaffolds for tissue engineering with enhanced oxygen delivery to cells.

Keywords: Oxygen delivery, 3D scaffolds, zeolite nanoparticles, tissue engineering

5.1 Introduction

The biomedical applications of nanomaterials such as drug delivery systems, diagnostic imaging agents, and microfluidics are drawing attentions due to the unique features they present.¹⁻³ Tissue engineering strategies benefited from advances made in nanomaterials specifically on the utility of carbon nanotube scaffolds.⁴⁻⁷ Although progress has been made to fabricate engineered tissues in vitro using both conventional and nanomaterials, the inability to deliver sufficient oxygen to the growing constructs (due to its poor solubility in culture media) remained to be a formidable task.^{8, 9} This is exemplified by early studies showing that cellular spheroids generally contain a hypoxic and necrotic center surrounded by a rim of viable cells.^{10, 11} Similar observations were reported for osteoblasts, hepatocytes, and cardiomyocytes cultured in 3D scaffolds under static conditions.¹²⁻¹⁴

Previous attempts to overcome oxygen transfer limitations in tissue engineering relied on perfusion bioreactors where oxygen dissolved in the culture medium diffuses to the scaffold's interior. However, the high flow rate required to maintain adequate oxygen

concentration for cell viability often surpasses the shear stress tolerance of the cells.^{15, 16} In an alternative, the use of perfluorocarbon (PFC) emulsions as an oxygen carrier in tissue engineering has been investigated where the oxygen unloading of PFC emulsion was facilitated by the increased surface area provided by the emulsion droplet size.¹⁷ In spite of the reported encouraging data, the high density of the PFC emulsion meant that the droplets could easily settle either in the culture well or in the medium reservoir.¹⁸ This, in turn, implies that PFC emulsions may not be effective oxygen carriers. In view of the above, it would be advantageous if the oxygen carrier molecules could be bound to the scaffold. In this regard, Harrison and coworkers reported calcium peroxide-based oxygen generating particles incorporated into the scaffold to provide a sustained oxygen release over an extended period of time.¹⁹ The reaction products, namely Ca(OH)_2 and H_2O_2 are, however, strong base and strong oxidizing agents respectively, in which the drawback could outweigh the benefit. This drawback is exemplified by a recent study which demonstrated significant reduction of fibroblast viability when calcium peroxide was incorporated to polycaprolactone fibrous scaffolds.²⁰ In addition, the calcium peroxide loaded to the scaffold will eventually be depleted making this approach limited to short term cultures.

In this study, a novel approach of enhanced oxygen delivery to cells seeded in 3D scaffolds by incorporating fluorinated porous zeolite particles as an integral part of the scaffolds is reported.

5.2 Materials and Methods

5.2.1 Preparation of fluorinated-zeolite (FZ)

Analytical grade chemicals and reagents used for the preparation of FZ were purchased from Sigma–Aldrich (Milwaukee, WI) unless otherwise stated and, were used as received. Zeolite Y powder was crystallized from a synthetic gel with a molar composition of: 4 Na₂O : 1 Al₂O₃ : 6 SiO₂ : 200 H₂O : 5 (TMA)₂O , where (TMA)₂O designates tetramethylammonium hydroxide (25%, Merck KGaA, Darmstadt, Germany) used as a organic template or structural directing agent. The synthetic gel was prepared by dissolving appropriate amounts of sodium aluminates (NaAlO₂) as Al source and sodium hydroxide (NaOH) to a mixture of water and (TMA)₂O under vigorous stirring until a homogenous solution was obtained. Silica gel (as Si source) was then added to the resulting solution in a 30 ml Teflon reactor and mixed for 10 min. The resulting synthetic gel was aged for 48 h under static condition. The zeolite Y product was allowed to crystallize from the aged gel at 100°C in an oven for 48 h. When the reaction was completed, the pure crystalline zeolite powders were recovered from the suspension by centrifugation at 10,000 rpm. The solid particles were re-dispersed in deionized water and centrifuged again. The washing and centrifugation process were repeated three times. The solid products were dried at 50°C for 24 h, followed by calcinations at 500°C for 5 h in a programmable furnace with the heating and cooling rate of 1°C/min to activate the zeolite by removing the organic residues and water. The resulting zeolite-Y was then fluorinated with 1 wt % methanol solution of 1H, 1H, 2H, 2H-perfluorodecyltriethoxysilane (PTES) for 1 h, filtered and then heated at 140°C for an additional 1 h. The particle sizes of the zeolite were in the range of 850 nm-1000 nm.

5.2.2 Fabrication of PCU-FZ scaffolds

A medical grade poly(carbonate urethane) (PCU) (Bionate[®] 55D) was kindly donated by the Polymer Technology Group (Berkeley, CA). 3D scaffolds were fabricated by a solvent casting and particulate leaching method as previously described²¹ with some modifications. Ground and sieved NH₄Cl porogens (180-250 μm) were packed into a 6 mm diameter cylindrical infiltration chamber together with 2 wt% FZ nanoparticles and, the polymer solution (15 wt% PCU dissolved in N,N-dimethylformamide) was subsequently poured over the porogen bed and pressurized to infiltrate the porogen bed. Following this, the scaffolds were removed from the assembly and the solvent was allowed to evaporate in a fume hood. Finally, NH₄Cl porogens were leached out using deionized water and, the scaffolds were sectioned into 1.5 mm height disks using a microtome. This height (or thickness) of the scaffolds was chosen to mimic the thicknesses of many soft tissues such as cartilages,²² skin,²³ cardiac,²⁴ and blood vessels²⁵ that are the subject of tissue engineering . Two different control scaffolds, namely PCU scaffolds without FZ particles and, scaffolds that contained non-fluorinated zeolite particles, were fabricates in a similar way.

5.2.3 Dissolved oxygen measurement

Fibre optic oxygen sensor model NeoFox (Ocean Optics, Dunedin, FL) equipped with NeoFox software was used to measure dissolved oxygen. The sensor uses ruthenium (II) complexes suspended in a support matrix and attached at the tip of the fiber optic cable. When excited by a light emitting diode at 475 nm, the ruthenium complex fluoresces and emission occurs at 620 nm. When the excited ruthenium complex encounters an oxygen

molecule, the emission is quenched allowing the intensity of the fluorescence to be related to the oxygen concentration. Accordingly, the more oxygen that is present, the lower the emission intensity and vice-versa. In the absence of oxygen, the maximum fluorescent intensity of emitted light is observed. FZ nanoparticles at concentrations of 0.5%, 1%, and 2% were suspended in deionized water and continuously stirred at 37°C while the assembly was left open to atmospheric air. Deionized water and non-fluorinated Zeolite particles (non-FZ) suspended in deionized water (at 2% concentration) were used as controls. A 300 nm diameter oxygen probe was used to measure the dissolved oxygen following a two point calibration with 20.9% of oxygen at standard temperature and pressure and 0% oxygen in 100% nitrogen.

5.2.4 Chemical composition and morphological studies of FZ and PCU-FZ scaffolds

The crystallinity of the zeolite particles was measured by powder X-ray diffractometer (XRD), (Rigaku RINT 2500, Tokyo, Japan) with Cu K radiation ($\lambda = 1.54$ Å) at 40 kV and 50 mA with a scan rate of 0.02 degrees per second over a 2θ ranges of 2° to 40°. The zeolite particle pore size and surface area were determined by a BET (Brunauer, Emmett and Teller) method using nitrogen adsorption–desorption isotherms by means of an ASAP2010 instrument (Micromeritics Instrument Corporation, Norcross, GA). The zeolite pore size was also calculated by the advanced Barrett–Joyner–Halenda (BJH) method using the adsorption-desorption branches of the isotherms. Prior to these measurements, the samples were degassed at 170°C for 24 h in vacuum. To investigate the surface and cross-section morphology of scaffolds, high-resolution scanning electron microscope (SEM) images were captured using model FIB/SEM LEO 1540XB microscope (Carl Zeiss, Oberkochen, Germany) operating at electron beam voltage of 1

kV. Scaffolds were affixed on a carbon sample holder and were coated with 4 nm osmium vapor before imaging. In addition, energy dispersive X-ray spectroscopy (EDX) was used to map the elemental composition and distribution within the scaffolds. Elemental compositions of the fluorinated zeolite particles and the scaffolds were determined by X-ray photoelectron spectroscopy (XPS, Perkin Elmer, Waltham, MA) and EDX. The XPS analyses were carried out with a Kratos Axis Ultraspectrometer using a monochromatic Al K α source (15 mA, 14 kV).

5.2.5 Scaffold porosity measurements

Mercury porosimetry measurements were made using an Autopore IV porosimetry (Micromeritics, Norcross, GA). Samples of PCU and PCU-FZ scaffolds were cut into cylindrical disks with 1.5 mm height and 6 mm in diameter, before placing in the penetrometer. Care was taken to place adequate sample in the penetrometer to achieve significantly measurable intrusion volumes while maintaining unimpeded access by the mercury to the entire surface of the samples. Prior to mercury intrusion, the penetrometer was degassed to approximately 4kPa to remove air from the system. Mercury filling of the penetrometer was performed at 3.5kPa. Logarithmically spaced data points were taken at pressures ranging from 0.35kPa to 410kPa. An equilibrium intrusion rate threshold was set at 0.003 mL/g/s. For purposes of data analysis, the surface tension of mercury and the intrinsic contact angle with the scaffolds were taken to be $\gamma_{\text{Hg}} = 480 \text{ N/m}$ and $\theta = 140^\circ$ respectively. Average pore areas were corrected for deformation of the scaffold under elevated pressure, as described elsewhere²⁶.

5.2.6 Cell culture on PCU and PCU-FZ scaffolds

Primary human coronary artery smooth muscle cells (HCASMCs) and smooth muscle growth media (SmGM[®]-2 BulletKit) were purchased from Lonza Walkersville Inc. (Walkersville, MD, USA). Cells were cultured according to supplier's instructions in smooth muscle growth media (SmGM[®]-2 BulletKit), supplemented with 100 units/ml penicillin G sodium, and 100 µg/ml streptomycin sulphate (Invitrogen, Burlington, ON, Canada). All cultures were maintained in a humidified incubator at 37°C containing 5% CO₂. HCASMCs were passaged every 7 days at a split ratio of 1:3 and used between passages 4 to 7. Cylindrical scaffolds were affixed to glass coverslips using silicone grease, sterilized with 70% ethanol for 30 min and allowed to dry under germicidal UV light in tissue culture hood for 30 min. After soaking the scaffolds in Hank's Buffered Salt Solution (HBSS, Invitrogen, Burlington, ON, Canada), all scaffolds were coated with fibronectin (10 µg/cm²; Santa Cruz, CA, USA). Cells were seeded into the interstices fibronectin-coated PCU and PCU-FZ scaffolds at an initial cell density of $\sim 3 \times 10^4$ cells/scaffold. This relatively low seeding density was chosen such that we can verify cell infiltration depths into the scaffold interstices without cells outgrowing from the scaffold surface as is the case in high-density seeding. HCASMCs were cultured for 4 days, 7 days, and 14 days and the culture medium was exchanged every other day.

5.2.7 Cytotoxicity assay

For colorimetric assays of the metabolic activity of viable cells, 3-(4,5-dimethylthiazol-2-yl)-2,5-diphenyltetrazolium bromide (MTT) (Invitrogen, Burlington, ON, Canada) was used to quantify cytotoxicity and cell proliferation. MTT salts are reduced to a water-

insoluble formazan salt only by metabolically active cells allowing the assay to detect viable cells exclusively. After it was solubilized, the formazan formed was quantified in a conventional plate reader at 570 nm (maximum absorbance). PCU-FZ and PCU scaffolds were affixed in 96-well culture plates using silicone grease and sterilized with 70% ethanol for 30 min. After drying for 30 min, the scaffolds were soaked in HBSS and $\sim 3 \times 10^4$ HCASMCs were seeded and cultured for 24 h in a humidified chamber at 37°C containing 5% CO₂. After changing the culture media, 10 μL of MTT was added to each well and incubated for 4 h. Then 100 μL of sodium dodecyl sulphate (Invitrogen, Burlington, ON, Canada) was added and mixed thoroughly and finally incubated for an additional 4 h before reading its absorbance at 570 nm using a multiplate reader. Two different negative control experiments were carried out: (i) by adding MTT to the culture medium only and, (ii) by adding MTT to the scaffolds only to rule out the possibility that trapped reagents in the scaffold may contribute to background reading.

5.2.8 Immunofluorescence staining and laser scanning confocal microscopy

HCASMCs were fixed at room temperature for 1 h with 4% (w/v) paraformaldehyde (EMD Chemicals Inc.) and permeabilized for 10 min in cation free phosphate buffered saline (PBS) containing 0.1% (v/v) Triton X-100. Cells were incubated for 1 h at room temperature in 1% BSA/PBS containing AlexaTM Fluor 488-conjugated phalloidin (1:50 dilution), followed by three washes with PBS. DAPI (300 nM in PBS; Invitrogen, Burlington, ON, Canada) was used to label nuclei. Samples were mounted on slides in SHUR/MountTM (TBS[®], NC, USA) and analyzed with a Zeiss LSM 410 confocal microscope (Zeiss, Canada) equipped with an argon/neon as well as a UV laser.

5.2.9 Statistical analysis.

The results for the dissolved oxygen study were analyzed by analysis of variance (ANOVA). Student's *t*-test was used to analyze the cytotoxicity of PCU-FZ scaffold and proliferation of HCASMC as a function of culture time. For all analyses, significance was assigned for $p < 0.05$.

5.3 Results and Discussion

5.3.1 Characterization of fluorinated zeolite (FZ)

In the biomedical field, the use of particles as contrasting agents in imaging and as drug delivery vehicles is an emerging area.¹⁻³ In order to expand their potential application for tissue engineering scaffolds with oxygen binding capability, porous fluorinated zeolite particles with a pore size of ~ 7.4 Å and surface area of 750 m²/g were prepared. The schematic framework structure of zeolite (Y-type) is shown in Figure. 1A. This zeolite was fluorinated with a methanol solution of hydrolyzed 1 wt% 1H, 1H, 2H, 2H-perfluorodecyltriethoxysilane (PTES) (Figure 5.1B). When PTES is attached on the surface of zeolite particles, it forms a monolayer at a temperature of 140°C . The XRD patterns of the current particles are presented in Figure 5.1C and, are consistent with literature data.²⁷ Furthermore, the fluorination step did not affect the crystalline peaks of the zeolite particles.

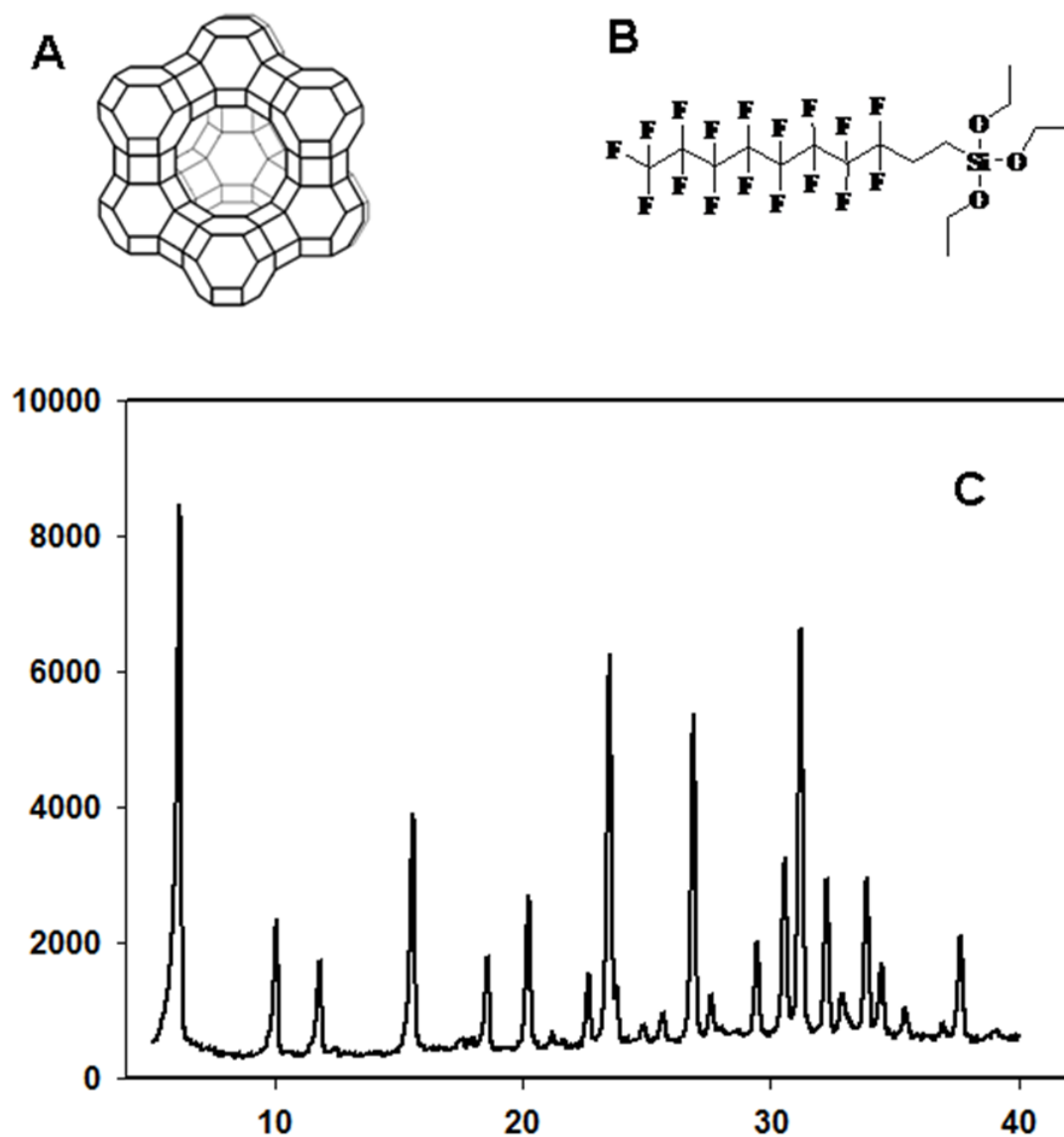


Figure 5.1: (A) Framework structure of Zeolite Y, (B) chemical structure of PTES, and (C) XRD pattern of the prepared fluorinated Zeolite Y.

5.3.2 Dissolved oxygen concentration in FZ particles

Measurements of dissolved oxygen concentration in the presence of different weight percentage of FZ particles were conducted in deionized water at 37°C and atmospheric pressure using a fiber optic oxygen sensor (Figure 5.2). There was no statistical significance between the control (0% FZ) and 0.5% FZ. Similarly, there was no statistical

significance in the amounts of oxygen dissolved between 1% and 2% FZ ($p < 0.05$). However there was a significant difference between the other groups of FZ contents ($p < 0.05$). These data show that by incorporating 2% FZ in deionized water, there was a significant increase of dissolved oxygen at 37°C. It seems that there is a minimum threshold of 1% FZ that is needed to increase the dissolved oxygen concentration in a significant way. On the other hand, when non-fluorinated zeolite particles were suspended in deionized water, there was no difference in the amount of dissolved oxygen compared with deionized water alone. As will be shown shortly in Table 5.2, 73% of the fluorinated molecules that are responsible for dissolving oxygen were located at the surface of the zeolite particles which, in turn, were exposed to the bulk liquid. This is contrary to conventional fluorinated emulsions where the oxygen is trapped in the core of the particle. Consequently, the probe measures total dissolved oxygen concentrations present both in water and in the fluorinated particles. Thus the increased oxygen concentration is attributed to the presence of 1H, 1H, 2H, 2H-perfluorodecyltriethoxysilane at the surface of the zeolite particles. Gases are transported by perfluorinated compounds due to increased solubility in accordance with Henry's law. The increase is attributed due to the existence of loose, non-directional van der Waals interactions leading to low cohesive energy densities,²⁸ which facilitates mutual solubilization of oxygen in the fluorine compound that is bound to the surface of the particles that are embedded in the scaffold. Oxygen solubility also reflects the very low intermolecular interactions (fluorine's low polarizability translates into low van der Waals forces) within a FZ monolayer. Unlike a chemical binding situation known in hemoglobin, solubilized oxygen can be rapidly and extensively extracted from the perfluorinated molecules when needed. Although FZ above 2-wt% could have been

theoretically incorporated in our experiments, inclusion of more than 2% particles into the scaffolds was not possible because the fabricated scaffolds lacked mechanical integrity.

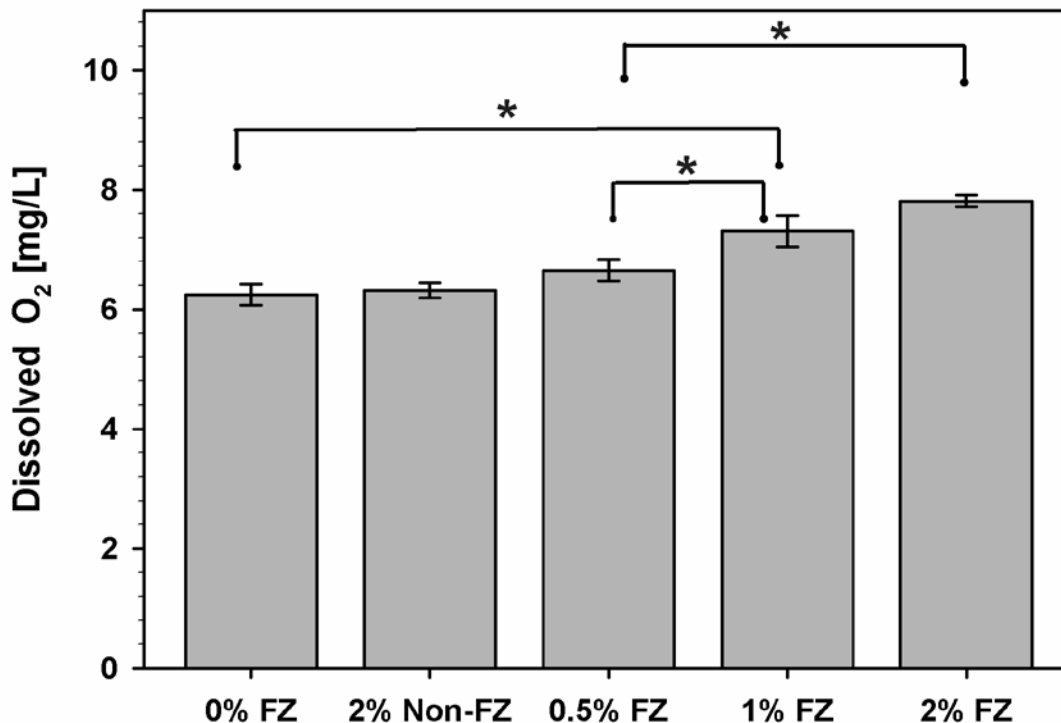


Figure 5.2: Dissolved oxygen concentrations in de-ionized water at 37°C, in the presence of non-fluorinated Zeolite particles, and in the presence of different weight percentages of fluorinated Zeolite particles. Oxygen concentrations were measured using a fiber optics probe. Data are means ± SD for experiments conducted in triplicate. * indicates statistical significance at $p < 0.05$.

5.3.3 FZ modified scaffolds characterization

Tissue engineering scaffolds are required to have high porosity and pore interconnectivity, and high surface area to volume ratio for cellular infiltration, matrix remodelling, and nutrient transport to take place. Using MicroCT imaging, our group have previously reported PCU scaffolds having a porosity of 84%.²⁹ Therefore the effect of FZ incorporation on the porosity of PCU scaffolds was examined. Mercury porosimeter analysis of both control scaffolds and those incorporating FZ particles

showed porosities of 90% (Table 5.1). These results indicate that the pore area and porosity of the scaffolds was not affected by FZ incorporation.

Table 5.1: Mercury porosimetry analysis data for PCU and PCU-FZ scaffolds.

Attributes	PCU scaffolds	PCU/FZ scaffolds
Total Intrusion Volume	5.56 mL/g	5.924 mL/g
Total Pore Area	15.15 m ² /g	14.90 m ² /g
Sample Weight	0.0108 g	0.0101 g
Porosity	89.67%	90.05%

The pore-size distribution obtained from the mercury porosimetry is shown in Figure 5.3. It is clearly shown that the addition of the FZ particles did not affect the pore size distribution. It also shows that the differential intrusion volume, which is an indicator of the scaffold porosity, was the same for both PCU and PCU-FZ scaffolds. The porosity data presented in Table 5.1 affirms this observation. The intrusion and subsequent extrusion cycles during the mercury porosimetry experiments resulted in negligible hysteresis indicating that scaffold compression at the operating pressures was minimal.

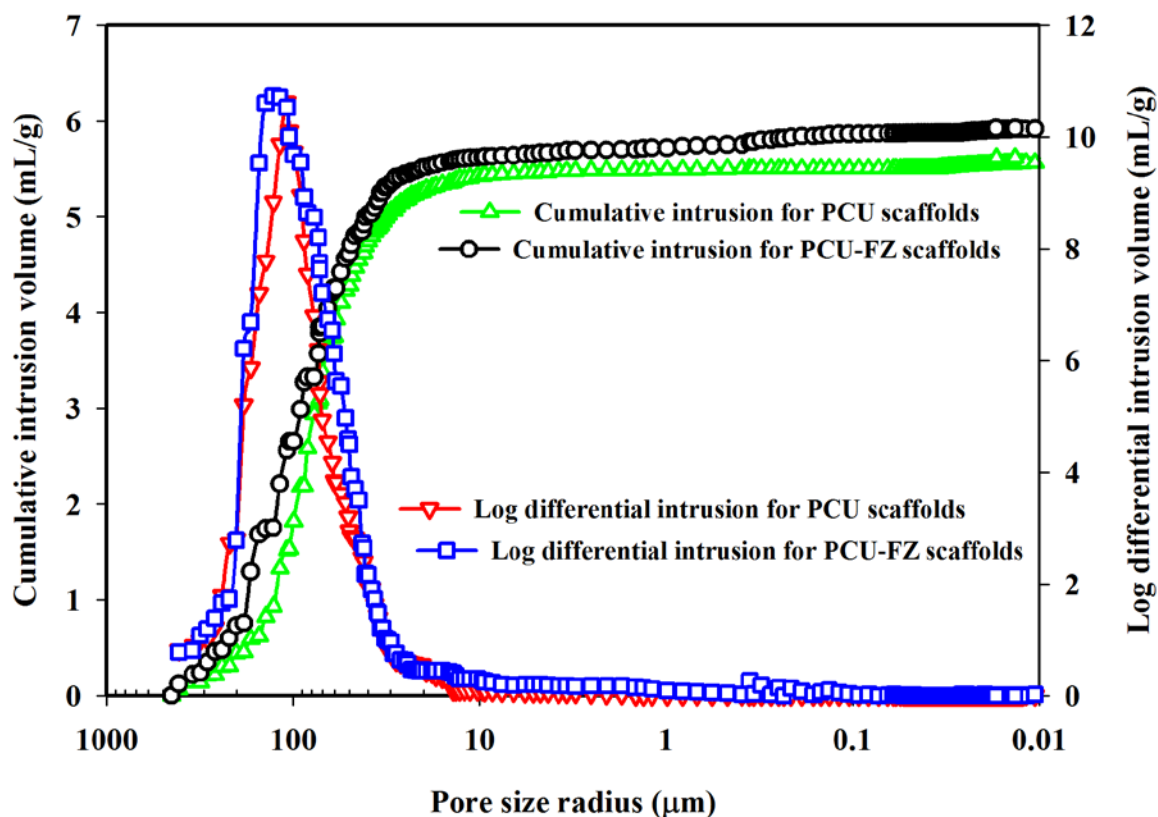


Figure 5.3: Scaffold pore size distribution obtained by mercury porosimetry for PCU and PCU-FZ scaffolds plotted as a function of differential and cumulative intrusion volumes

The SEM images of scaffolds presented in Figure 5.4A-D shows that the pores were open, interconnected, and well-defined. This is needed for cell infiltration and unrestricted cell-cell communications. All scaffolds had similar pore sizes, ranging from 50-200 μm which are ideal for many tissue engineering applications. At high magnification, the embedded FZ particles ($\approx 1\mu\text{m}$ size) in the FZ -containing scaffolds are evident (see insert in Figure. C) indicating that the salt leaching process did not affect the particles whereas, at the same magnification, control PCU scaffolds showed smooth scaffold struts and walls. Furthermore, these images show that the FZ particles were

uniformly distributed along the struts and walls of the scaffolds without affecting the macroporosity of the scaffolds.

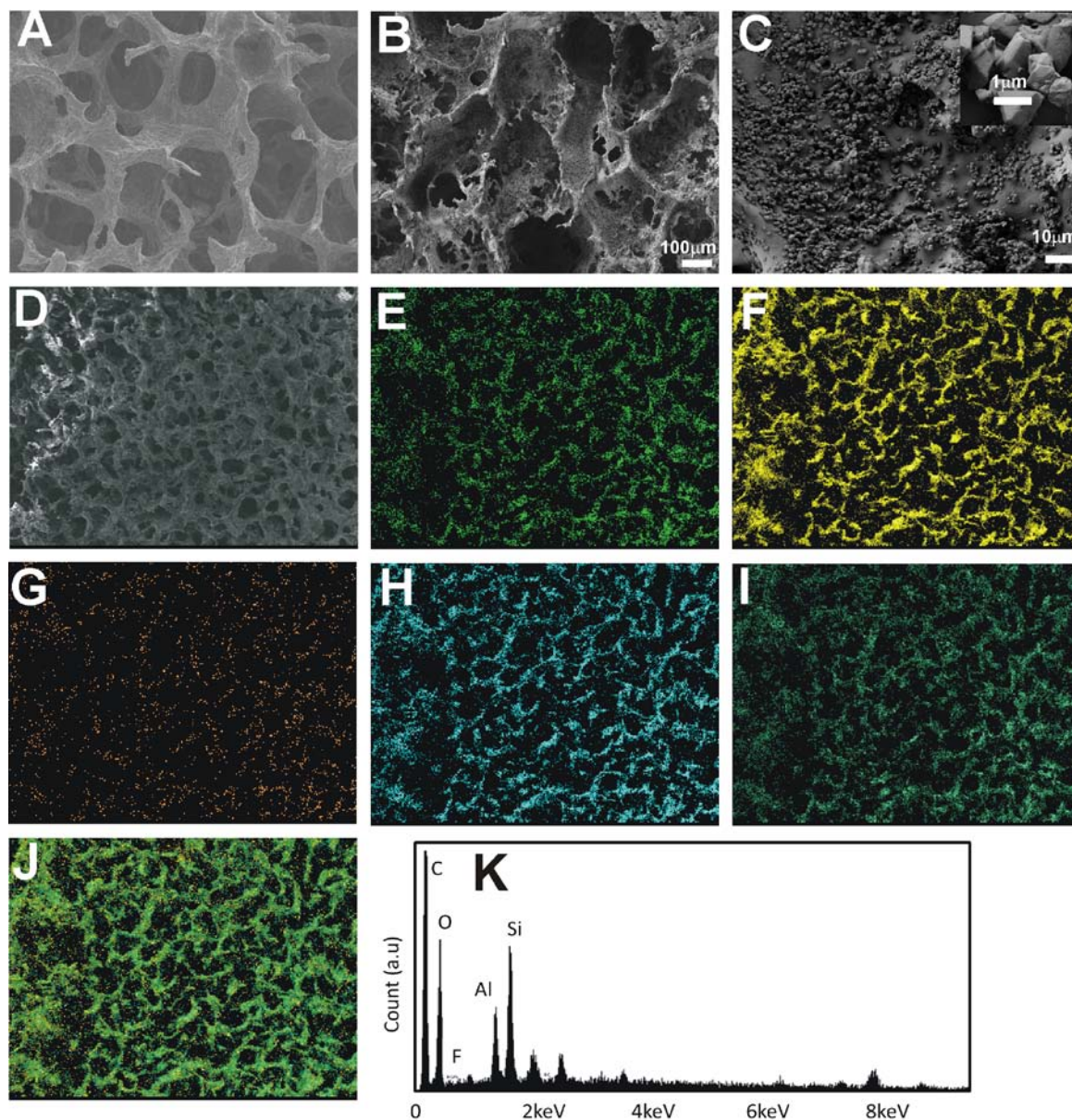


Figure 5.4: SEM and EDX analyses of fluorinated Zeolite-modified PCU scaffolds. (A) Control PCU scaffolds; (B) FZ-modified PCU scaffolds; (C) high magnification images of the struts in FZ-modified PCU scaffolds (inset: high magnification image showing the FZ particles); (D) SEM image of the area where EDX mapping was undertaken; (E–J) EDX elemental mapping for (E) Al, (F) C, (G) F, (H) O, (I) Si and (J) a combination of all elements; (K) EDX spectrum for FZ-modified PCU scaffolds. Images were captured using a Zeiss LEO 1530 SEM microscope at working voltages of 1 keV for high magnifications and 5 keV for low magnifications.

Given that we have used a solvent casting and particulate leaching method to fabricate these scaffolds, it is remarkable that the FZ particles were not affected during the NH_4Cl leaching step in water. This is very likely to be the result of better interfacial adhesion between the polymer and the FZ particles facilitating improved entrapment of the FZ particles. Strong adhesive forces between a zeolite coating layer and bone biomaterials have been recently suggested to their enhanced in vitro performance.³⁰ Additional evidences for the successful incorporation and uniform distribution of the fluorinated particles into 3D scaffolds came from elemental mapping using EDX (Figure 5.4 E-K). The qualitative distribution of Al, Si, and F, which are only expected from the FZ-modified 3D scaffolds demonstrate this even distribution (Figure 5.4 E-J).

The elemental compositions of the FZ particles and the scaffolds were further studied using XPS. The position of the fluorine 1s peaks at 686.8 eV in the XPS spectrum is indicative of fluorine substitution in the SP^3 carbon framework. As can be seen in Table 2, the FZ particles had 40% fluorine and 23% carbon. Because the FZ particles are largely inorganic in their composition, the carbon atom is relatively low. The PCU scaffold which is used as a control had no fluorine peak at 686 eV and, a carbon atom of 81% is considerably high. This is not unexpected since the constituents of PCU control scaffolds are only carbon, oxygen, and nitrogen (as hydrogen cannot be detected using XPS). However, PCU scaffolds fabricated by incorporating fluorinated zeolite particles had very strong fluorine 1s peak with atomic percentage of 29% which was 73% of the fluorine found in the fluorinated zeolite particles. XPS results not only indicate the incorporation the fluorinated zeolite particles in the PCU scaffolds, but also revealed that most of the

fluorinated zeolite were on the surface of the scaffolds which is crucial for oxygen supply to seeded cell.

Table 5.2: XPS analysis of the fluorine content in FZ particles, PCU scaffolds and PCU-FZ scaffolds. The numbers in brackets indicate the corresponding binding energies.

Element	FZ particles	PCU Scaffolds	PCU-EZ Scaffolds
F1s	39.7% (686.8 eV)	–	28.8% (686.2 eV)
C1s	23.4% (290.0 eV)	80.9% (281.5 eV)	47.3% (282.2 eV)

5.3.4 HCASMC growth on PCU and PCU-FZ scaffolds

In a previous publication from our laboratory,³¹ it was shown that PCU scaffolds were not cytotoxic to HCASMC and, that cells proliferated without any phenotype modulation.³²

In view of this, the current study used PCU scaffolds as controls to evaluate HCASMC viability on PCU-FZ scaffolds using MTT assay. Figure 5.5A showed that PCU scaffolds incorporating fluorinated zeolite particles had no cytotoxic effect to seeded HCASMC.

This cytotoxicity data is consistent with literature reports suggesting the biological activity of silicate and aluminosilicate zeolites having no cytotoxic effects to cells.^{30, 33, 34}

The use of zeolite framework as a biocompatible and anticorrosive coating for titanium alloy biomaterials demonstrated pluripotent mouse embryonic stem cells having higher adhesion and proliferation on the 3D zeolite microstructure surface compared with a 2D glass surface, indicating that the zeolite coatings were highly cytocompatible.³⁰ Zeolites have also been demonstrated to be a safe oral contrast agent for clinical magnetic resonance imaging without significant adverse effects.³⁵ Moreover, zeolites are good adjuvant in anticancer therapy,³⁶ improve skin-whitening by inhibiting melanin

production in a dose-dependent manner,³⁴ and demonstrated to decrease TiO₂-photosensitized reactive oxygen species in cultured fibroblasts.³³

To examine the effect of fluorinated zeolite incorporation to 3D scaffolds, HCASMC proliferation on PCU-FZ scaffolds was investigated. The results presented in Figure 5.5B demonstrated that cell number significantly increased for 4 days and 7 days of culture for PCU-FZ scaffolds ($p < 0.05$). As an additional control experiment, cells were also seeded into scaffolds with embedded non-fluorinated zeolite particles to rule out the effect of surface topography due to the embedded particles. No difference compared with PCU scaffolds was observed. Given that we have seeded equal number of cells on both scaffolds and that both scaffolds were not cytotoxic, the significant increase in cell numbers on PCU-FZ indicates that these scaffolds provided an environment conducive for cell growth by providing sufficient oxygen. The apparent decrease in cell number at day 4 culture is explained as follows. The data at day 1 reflects the initial seeding density. The slight decrease in cell number at day 4 is likely attributed due to cell retention. Then, the retained cells started to proliferate which is clearly demonstrated at day 7. Although this study suggested an increase cell number for PCU-FZ scaffolds for up to 7 days culture, it is not known at this stage if the amount of dissolved oxygen will be sufficient to support longer culture times or higher cell seeding density that we have used. Further studies will be required to address these possibilities.

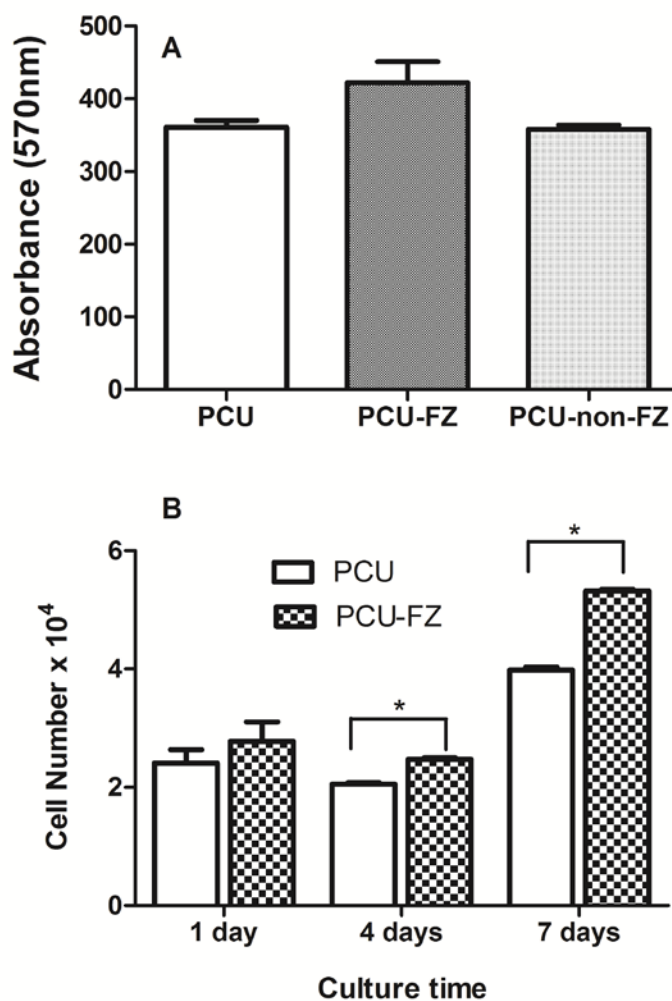


Figure 5.5: HCASMC (A) viability and (B) growth on PCU, PCU-FZ, and PCU-non-FZ 3-D scaffolds. Data are means \pm SD for experiments conducted in triplicate. *Indicates statistical significance.

5.3.5 HCASMC morphology and depth of infiltration on PCU-FZ scaffolds

In addition to the cytotoxicity and cell growth studies, information on the morphology and infiltration depths of HCASMCs on 3D PCU-FZ scaffolds is essential. Labeling for F-actin and DNA were used to examine cellular morphology following 4, 7 and 14 days of culture. Figure 5.6 shows that HCASMCs attached and spread on both scaffolds

regardless zeolite incorporation. At higher magnifications, cells making larger contacts on both scaffold surfaces are evident.

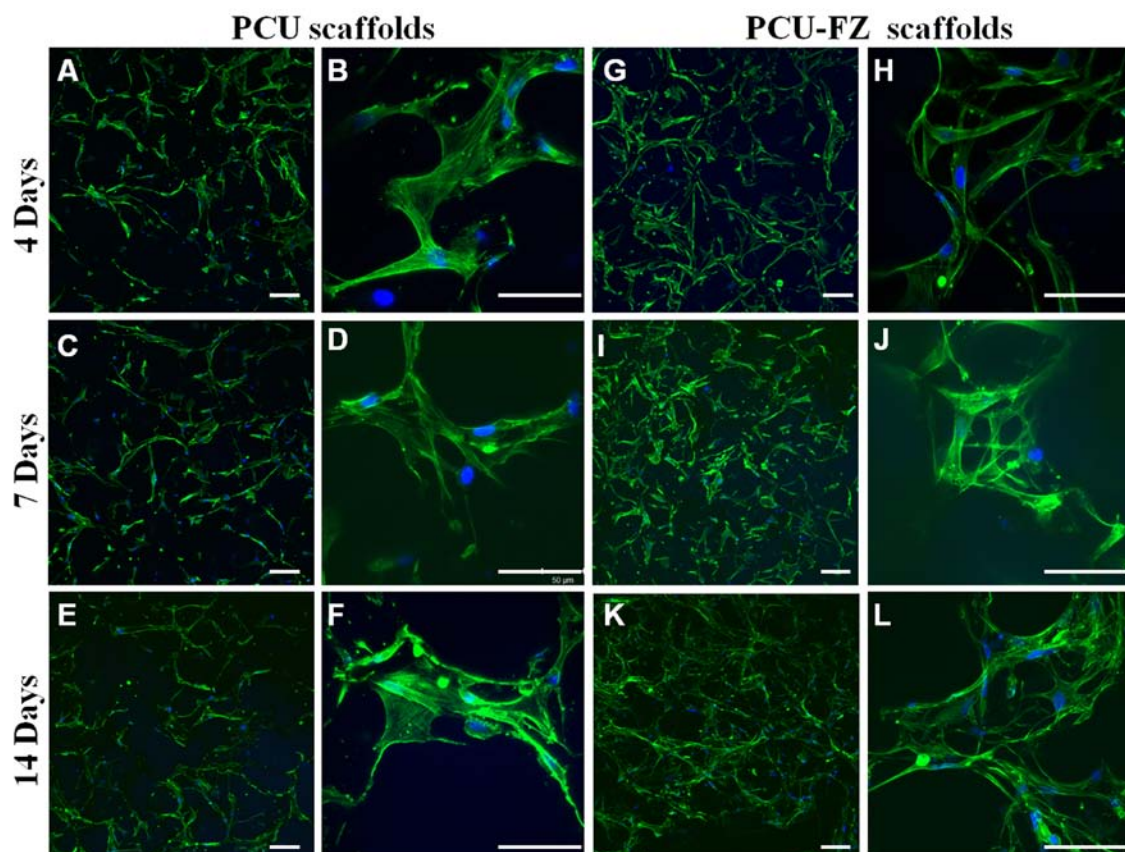


Figure 5.6: Confocal microscopy images of HCASM cultured on PCU and PCU-FZ scaffolds for 4 days (A, B, G, H), 7 days (C, D, I, J) and 14 days (E, F, K, L). HCASM cultured on both PCU and PCU-FZ scaffolds had similar morphologies but the cell density appeared to be higher on the PCU-FZ scaffolds. Scale bars: (A), (C), (E), (G), (I), (K), 200 μm ; (B), (D), (F), (H), (J), (L), 100 μm .

Given that these images are taken at a single plane (cell seeded side), insight into which cells infiltrated to the scaffolds is limited. To visualize cell distribution into the center of the scaffold, confocal stacks of images were taken such that each image is separated by 10 μm from the next. The procedure continued to deeper sections of the scaffolds until no more cells were detected. The images collected were then binned into 4 depth ranges namely, 0-50 μm ; 50-100 μm ; 100-150 μm ; 150-200 μm and, the results are presented in

Figure 5.7. Interestingly, cells on PCU scaffolds infiltrated only to about 100 μm whereas on PCU-FZ scaffolds, infiltration depths doubled to 200 μm during 7 days of culture. Since HCASMCs were seeded only on one side of the scaffolds; the observed infiltration depths are unlikely to be due to seeding techniques. Furthermore, both scaffolds had similar pore sizes and porosity as measured by mercury porosimetry (Table 5.2). Therefore, it is believed that enhanced HCASMCs infiltration and uniform distribution on PCU-FZ scaffolds is due to the available oxygen at deeper sections of the scaffolds. Since cell growth data (Figure 5.5) showed PCU-FZ scaffolds promoted HCASMCs proliferation, infiltration appeared to be driven primarily by localized proliferation rather than coordinated cellular migration.

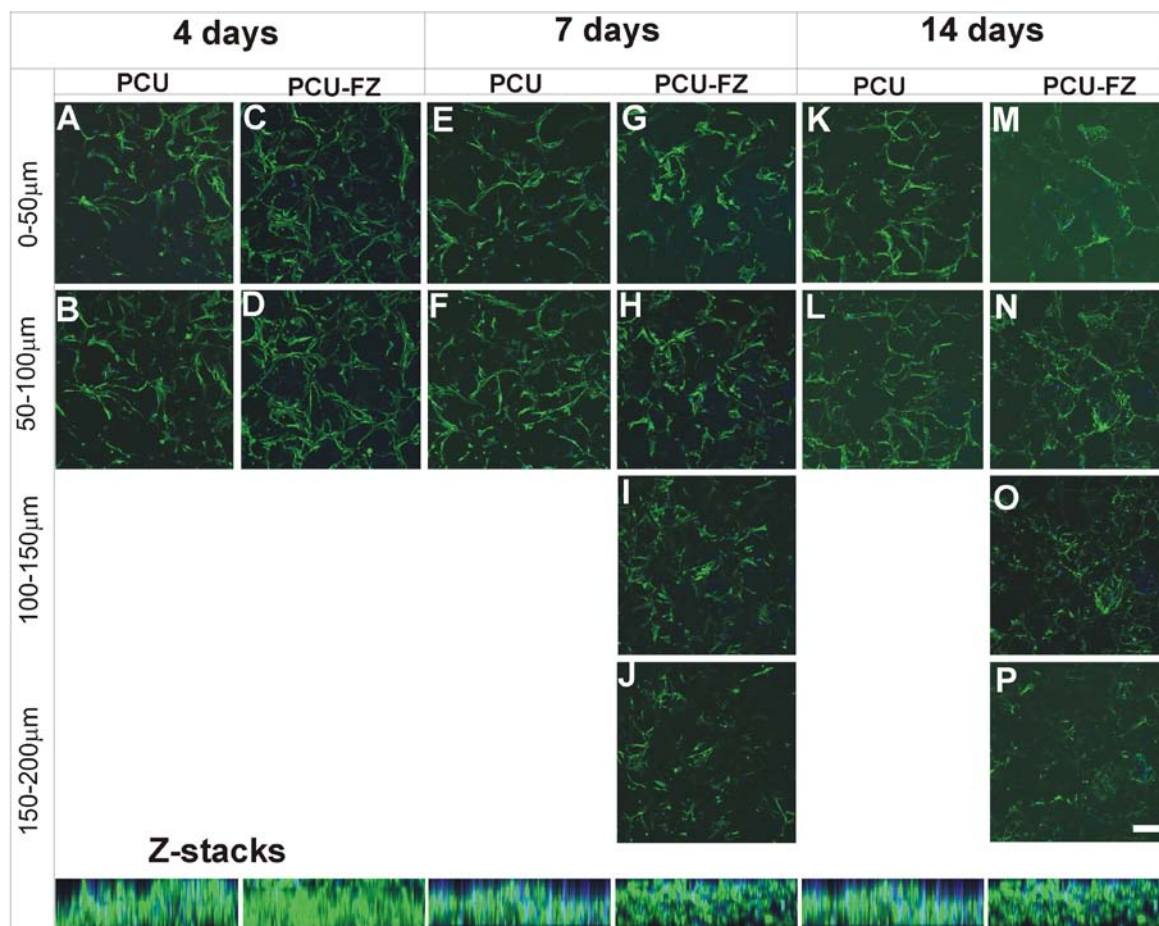


Figure 5.7: The effect of FZ incorporation on HCASMC spreading and infiltration after 4, 7 and 14 days of culture. (A, B, E, F, K, L) PCU scaffolds; (C, D, G–J, M–P) PCU-FZ scaffolds. Orthogonal views of the confocal images are shown at the bottom. Scale bar: 200 μm .

Tissue engineering has been motivated by the need to develop novel treatment options for the functional restoration of diseased tissues. Despite this, overcoming the diffusion barrier that limits the delivery of essential nutrients is a primary obstacle in the development of engineered tissues with clinical relevance. As a result, engineered tissues that are more than 100 μm -thick and supplied with nutrients solely by diffusion may have insufficient transport to and from the cells³⁷ since the cell microenvironment is dependent on both nutrient and oxygen availability within the scaffold and the surrounding medium. Because of the poor solubility of oxygen in culture media, its delivery represents the most

challenge in engineering functional 3D tissues. While cells consume approximately the same molar amount of soluble oxygen as glucose, the solubility of oxygen in typical culture media is an order magnitude lower than the available glucose. Conversely, an excess of oxygen in the medium surrounding the cells without an appropriate carrier such as hemoglobin, achieved by using pure oxygen instead of air or by increasing gas pressure induces the presence of free radicals, which are cytotoxic.³⁸ Oxygen delivery strategies such as perfusion bioreactors have been the most widely investigated where flow-induced hydrodynamic conditions were anticipated to increase the mass transport of oxygen without cell and tissue damage.³⁹ However, as stated earlier, the high flow rate required to maintain an adequate oxygen concentration for cell viability often surpasses the shear tolerance of the cells.^{15, 16} As an alternative, perfluorocarbon emulsions have been studied as a means to deliver oxygen to seeded cells.^{18, 40} In these studies, the perfluorocarbon compound was emulsified and added to cell culture medium. However their high density (~1.5 to 2 times that of water) make the emulsified particles to easily settle thus limiting their full potential. Further, the surfactant used to emulsify is considered to be undesirable.⁴¹

Despite the above-stated research efforts, oxygen transport remains one of the main limitations in maintaining cell viability and functionality, thus requiring novel approaches to deliver sufficient oxygen. The utility of zeolites for biomedical applications is not new,^{27, 30, 33-36} but the idea that fluorinated zeolites could be used as oxygen vector in tissue engineering is a novel concept. In this study, the fabrication of 3D porous PCU scaffolds with uniformly embedded fluorinated zeolite particles with oxygen delivery potential to cells is demonstrated. Furthermore, it is shown that the dissolved oxygen

increased with increased fluorinated zeolite particles in water indicating that the oxygen dissolving property of 1H, 1H, 2H, 2H-perfluorodecyltriethoxysilane was not affected by chemically immobilizing to the zeolite framework. To enhance oxygen transport to encapsulated cells, Roberts and coworkers suspended perfluorooctyl bromide and perfluorotributylamine to alginate hydrogels as an oxygen vector.^{42, 43} Although direct comparison with the current study is not possible, their results suggest the perfluoro compounds within hydrogel membrane improves effective oxygen diffusivity, ensuring cell viability and functionality for the encapsulated spheres over extended culture times.

5.4 Conclusions

In this study, zeolite particles were successfully fluorinated as an oxygen vector using 1H, 1H, 2H, 2H-perfluorodecyltriethoxysilane for tissue engineering application. Dissolved oxygen concentration significantly increased in the presence of fluorinated zeolite particles. The fluorinated particles were then uniformly embedded into 3D polyurethane scaffolds during the fabrication process. Vascular smooth muscle cell viability was not affected by the presence of the fluorinated zeolite particles and; cell proliferation on PCU-FZ scaffolds was significantly higher than the control PCU scaffolds. Cell infiltration depths on PCU-FZ scaffolds was doubled compared with PCU scaffolds. Taken together, these data suggest the potential of PCU-FZ scaffolds for tissue engineering with enhanced oxygen delivery to cells.

Acknowledgment

This work was funded by the Heart and Stroke Foundation of Ontario (HSFO) grant # NA6345.

5.5 References

1. Burtea, C.; Laurent, S.; Mahieu, I.; Larbanoix, L.; Roch, A.; Port, M.; Rousseaux, O.; Ballet, S.; Murariu, O.; Toubreau, G.; Corot, C.; Vander Elst, L.; Muller, R. N., In vitro biomedical applications of functionalized iron oxide nanoparticles, including those not related to magnetic properties. *Contrast Media Mol Imaging* **2011**, 6,(4), 236-50.
2. Corchero, J. L.; Villaverde, A., Biomedical applications of distally controlled magnetic nanoparticles. *Trends Biotechnol* **2009**, 27, (8), 468-76.
3. Rawat, M.; Singh, D.; Saraf, S., Nanocarriers: promising vehicle for bioactive drugs. *Biol Pharm Bull* **2006**, 29, (9), 1790-8.
4. Bhattacharya, M.; Wutticharoenmongkol-Thitiwongsawet, P.; Hamamoto, D. T.; Lee, D.; Cui, T.; Prasad, H. S.; Ahmad, M., Bone formation on carbon nanotube composite. *J Biomed Mater Res A* **2011**, 96, (1), 75-82.
5. Jang, M. J.; Namgung, S.; Hong, S.; Nam, Y., Directional neurite growth using carbon nanotube patterned substrates as a biomimetic cue. *Nanotechnology* **2010**, 21, (23), 235102.
6. Tutak, W.; Chhowalla, M.; Sesti, F., The chemical and physical characteristics of single-walled carbon nanotube film impact on osteoblastic cell response. *Nanotechnology* **2010**, 21, (31), 315102.
7. Zhang, Y.; Bai, Y.; Yan, B., Functionalized carbon nanotubes for potential medicinal applications. *Drug Discov Today* **2010**, 15, (11-12), 428-35.
8. Rappaport, C., Review-progress in concept and practice of growing anchorage-dependent mammalian cells in three dimension. *In Vitro Cell Dev Biol Anim* **2003**, 39, (5-6), 187-92.
9. Martin, Y.; Vermette, P., Bioreactors for tissue mass culture: design, characterization, and recent advances. *Biomaterials* **2005**, 26, (35), 7481-503.
10. Sutherland, R. M.; Sordat, B.; Bamat, J.; Gabbert, H.; Bourrat, B.; Mueller-Klieser, W., Oxygenation and differentiation in multicellular spheroids of human colon carcinoma. *Cancer Res* **1986**, 46, (10), 5320-9.
11. Wendt, D.; Stroebel, S.; Jakob, M.; John, G. T.; Martin, I., Uniform tissues engineered by seeding and culturing cells in 3D scaffolds under perfusion at defined oxygen tensions. *Biorheology* **2006**, 43, (3-4), 481-8.
12. Ishaug, S. L.; Crane, G. M.; Miller, M. J.; Yasko, A. W.; Yaszemski, M. J.; Mikos, A. G., Bone formation by three-dimensional stromal osteoblast culture in biodegradable polymer scaffolds. *J Biomed Mater Res* **1997**, 36, (1), 17-28.

13. McClelland, R. E.; Coger, R. N., Use of micropathways to improve oxygen transport in a hepatic system. *J Biomech Eng* **2000**, 122, (3), 268-73.
14. Radisic, M.; Malda, J.; Epping, E.; Geng, W.; Langer, R.; Vunjak-Novakovic, G., Oxygen gradients correlate with cell density and cell viability in engineered cardiac tissue. *Biotechnol Bioeng* **2006**, 93, (2), 332-43.
15. Vunjak-Novakovic, G.; Obradovic, B.; Martin, I.; Freed, L. E., Bioreactor studies of native and tissue engineered cartilage. *Biorheology* **2002**, 39, (1-2), 259-68.
16. Yu, X.; Botchwey, E. A.; Levine, E. M.; Pollack, S. R.; Laurencin, C. T., Bioreactor-based bone tissue engineering: The influence of dynamic flow on osteoblast phenotypic expression and matrix mineralization. *Proc Natl Acad Sci USA* **2004**, 101, (31), 11203-11208.
17. Radisic, M.; Deen, W.; Langer, R.; Vunjak-Novakovic, G., Mathematical model of oxygen distribution in engineered cardiac tissue with parallel channel array perfused with culture medium containing oxygen carriers. *Am J Physiol* **2005**, 288, (3, Pt. 2), H1278-H1289.
18. Radisic, M.; Park, H.; Chen, F.; Salazar-Lazzaro, J. E.; Wang, Y.; Dennis, R.; Langer, R.; Freed, L. E.; Vunjak-Novakovic, G., Biomimetic approach to cardiac tissue engineering: oxygen carriers and channeled scaffolds. *Tissue Eng* **2006**, 12, (8), 2077-91.
19. Oh, S. H.; Ward, C. L.; Atala, A.; Yoo, J. J.; Harrison, B. S., Oxygen generating scaffolds for enhancing engineered tissue survival. *Biomaterials* **2009**, 30, (5), 757-62.
20. Wang, J.; Zhu, Y.; Bawa, H. K.; Ng, G.; Wu, Y.; Libera, M.; van der Mei, H. C.; Busscher, H. J.; Yu, X., Oxygen-Generating Nanofiber Cell Scaffolds with Antimicrobial Properties. *ACS Appl Mater Interfaces* **2011**, 3, (1), 67-73.
21. Grenier, S.; Sandig, M.; Mequanint, K., Polyurethane biomaterials for fabricating 3D porous scaffolds and supporting vascular cells. *J Biomed Mater Res A* **2007**, 82A, (4), 802-809.
22. Shepherd, D. E.; Seedhom, B. B., Thickness of human articular cartilage in joints of the lower limb. *Ann Rheum Dis* **1999**, 58, (1), 27-34.
23. Laurent, A.; Mistretta, F.; Bottiglioli, D.; Dahel, K.; Goujon, C.; Nicolas, J. F.; Hennino, A.; Laurent, P. E., Echographic measurement of skin thickness in adults by high frequency ultrasound to assess the appropriate microneedle length for intradermal delivery of vaccines. *Vaccine* **2007**, 25, (34), 6423-30.
24. Zimmermann, W. H.; Melnychenko, I.; Wasmeier, G.; Didie, M.; Naito, H.; Nixdorff, U.; Hess, A.; Budinsky, L.; Brune, K.; Michaelis, B.; Dhein, S.; Schwoerer, A.; Ehmke, H.; Eschenhagen, T., Engineered heart tissue grafts

- improve systolic and diastolic function in infarcted rat hearts. *Nat Med* **2006**, 12, (4), 452-8.
25. Koch, S.; Flanagan, T. C.; Sachweh, J. S.; Tanios, F.; Schnoering, H.; Deichmann, T.; Ella, V.; Kellomaki, M.; Gronloh, N.; Gries, T.; Tolba, R.; Schmitz-Rode, T.; Jockenhoevel, S., Fibrin-poly lactide-based tissue-engineered vascular graft in the arterial circulation. *Biomaterials* **2010**, 31, (17), 4731-9.
 26. Lowery, J. L.; Datta, N.; Rutledge, G. C., Effect of fiber diameter, pore size and seeding method on growth of human dermal fibroblasts in electrospun poly(epsilon-caprolactone) fibrous mats. *Biomaterials* **2010**, 31, (3), 491-504.
 27. Holmberg, B. A.; Wang, H. T.; Norbeck, J. M.; Yan, Y. S., Controlling size and yield of zeolite Y nanocrystals using tetramethylammonium bromide. *Micropor Mesopor Mat* **2003**, 59, (1), 13-28.
 28. Riess, J. G., Understanding the fundamentals of perfluorocarbons and perfluorocarbon emulsions relevant to in vivo oxygen delivery. *Artif Cells Blood Substit Immobil Biotechnol* **2005**, 33, (1), 47-63.
 29. Grenier, S.; Sandig, M.; Holdsworth, D. W.; Mequanint, K., Interactions of coronary artery smooth muscle cells with 3D porous polyurethane scaffolds. *J Biomed Mater Res A* **2009**, 89, (2), 293-303.
 30. Bedi, R. S.; Beving, D. E.; Zanello, L. P.; Yan, Y., Biocompatibility of corrosion-resistant zeolite coatings for titanium alloy biomedical implants. *Acta Biomater* **2009**, 5, (8), 3265-71.
 31. Dubey, G.; Mequanint, K., Conjugation of fibronectin onto three-dimensional porous scaffolds for vascular tissue engineering applications. *Acta Biomater* **2011**, 7, (3), 1114-1125.
 32. Grenier, S.; Sandig, M.; Mequanint, K., Smooth Muscle alpha-Actin and Calponin Expression and Extracellular Matrix Production of Human Coronary Artery Smooth Muscle Cells in 3D Scaffolds. *Tissue Eng Part A* **2009**, 15, (10), 3001-3011.
 33. Shen, B.; Scaiano, J. C.; English, A. M., Zeolite encapsulation decreases TiO₂-photosensitized ROS generation in cultured human skin fibroblasts. *Photochem Photobiol* **2006**, 82, (1), 5-12.
 34. Shin, Y. J.; Han, C. S.; Lee, C. S.; Kim, H. S.; Ko, S. H.; Hwang, S. K.; Ko, S. G.; Shin, J. W.; Ye, S. K.; Chung, M. H., Zeolite 4A, a synthetic silicate, suppresses melanogenesis through the degradation of microphthalmia-associated transcription factor by extracellular signal-regulated kinase activation in B16F10 melanoma cells. *Biol Pharm Bull* **2010**, 33, (1), 72-6.

35. Young, S. W.; Qing, F.; Rubin, D.; Balkus, K. J., Jr.; Engel, J. S.; Lang, J.; Dow, W. C.; Mutch, J. D.; Miller, R. A., Gadolinium zeolite as an oral contrast agent for magnetic resonance imaging. *J Magn Reson Imaging* **1995**, 5, (5), 499-508.
36. Pavelic, K.; Hadzija, M.; Bedrica, L.; Pavelic, J.; Dikic, I.; Katic, M.; Kralj, M.; Bosnar, M. H.; Kapitanovic, S.; Poljak-Blazi, M.; Krizanac, S.; Stojkovic, R.; Jurin, M.; Subotic, B.; Colic, M., Natural zeolite clinoptilolite: new adjuvant in anticancer therapy. *J Mol Med* **2001**, 78, (12), 708-20.
37. Carrier, R. L.; Rupnick, M.; Langer, R.; Schoen, F. J.; Freed, L. E.; Vunjak-Novakovic, G., Perfusion improves tissue architecture of engineered cardiac muscle. *Tissue Eng* **2002**, 8, (2), 175-88.
38. Freshney, R. I., *Culture of Animal Cells*. 3rd ed.; Wiley-Liss: 1994, 358-359.
39. Bancroft, G. N.; Sikavitsas, V. I.; Mikos, A. G., Design of a flow perfusion bioreactor system for bone tissue-engineering applications. *Tissue Eng* **2003**, 9, (3), 549-54.
40. Spiess, B. D., Perfluorocarbon emulsions as a promising technology: a review of tissue and vascular gas dynamics. *J Appl Physiol* **2009**, 106, (4), 1444-52.
41. Castro, C. I.; Briceno, J. C., Perfluorocarbon-based oxygen carriers: review of products and trials. *Artif Organs* **2010**, 34, (8), 622-34.
42. Khattak, S. F.; Chin, K. S.; Bhatia, S. R.; Roberts, S. C., Enhancing oxygen tension and cellular function in alginate cell encapsulation devices through the use of perfluorocarbons. *Biotechnol Bioeng* **2007**, 96, (1), 156-66.
43. Chin, K.; Khattak, S. F.; Bhatia, S. R.; Roberts, S. C., Hydrogel-perfluorocarbon composite scaffold promotes oxygen transport to immobilized cells. *Biotechnol Prog* **2008**, 24, (2), 358-66.

CHAPTER

6

6 GENERAL DISCUSSION AND CONCLUSIONS

Overview: This chapter provides a general summary of the overall work of this thesis with specific objectives as mentioned in chapter 2. The strengths and limitations of the work are also briefly summarized with few future work directions. Finally a brief summary of the overall significance of vascular tissue engineering is included.

6.1 Summary

The main goal of this study was to increase the supply of oxygen to vascular smooth muscle cell seeded on 3D PCU scaffolds. The initial step consisted of fabricating 3D porous PCU scaffolds using a pressure differential/particulate leaching technique. NH_4Cl was used as a porogen and different concentration of polymer dissolved in DMF was used to fabricate disk and tubular shaped scaffolds. SEM micrographs were used to characterize the structures and a diffusion apparatus was designed to measure the effective diffusivity using of NeoFox oxygen sensor. The measured effective oxygen diffusion coefficient and morphology of the scaffold was used to screen the best scaffold for the work in this thesis. This helped for assessing scaffolds fabricated from different concentrations of PCU for vascular tissue engineering applications. To improve the adhesion of HCASMC on PCU scaffolds, scaffolds were modified by adsorbing fibronectin on the surface of scaffold. HCASMC seeded scaffolds were cultured in both static and flow conditions. Higher cell infiltration and proliferation were resulted in flow

conditions than the static culture controls. This is likely due to an improved oxygen supply by convective mass transfer in the cell-seed 3D PCU scaffolds.

PFD was used as an oxygen carrier because of its high oxygen solubility. Significant increase in the dissolved oxygen was measured when 2% PFD was emulsified in the culture media. Furthermore, PFD was found to have no toxicity and have no morphological effect on HCASMCs. This led us to use PFD as an oxygen carrier molecule in the culture medium to improve the supply of oxygen to cell-seeded 3D PCU scaffolds. Moreover, a better understanding could be obtained by modeling the oxygen profile in the cell-seeded scaffold and in the lumen both at static and flow conditions with and without oxygen carrier. Thus, a mathematical model was developed to simulate the oxygen in the cell seeded 3D scaffolds.

Another novel approach to improve the supply of oxygen to cell seeded 3D scaffold was developed by embedding oxygen carrier particles into the scaffold. Micro size Zeolite-Y particles were fluorinated using 1H, 1H, 2H, 2H-perfluorodecyltriethoxysilane (PFES) and characterized. The surface characterization showed higher fluorine on the surface of the particles. The surface modified particles significantly increased the dissolved oxygen in the water at 37°C and had no toxicity to HCASMCs. The fluorinated particles were successfully embedded into the skeleton of 3D PCU scaffold without any modification to the morphology of the scaffold. Mercury porosimetry results confirmed that the porosity and pore distribution of the scaffolds were not affected. A higher cell proliferation and penetration depth were observed when HCASMC cultured on scaffolds with embedded fluorinated Zeolite particle than HCASMC cultured on PCU control

scaffolds. Thus an improvement on the supply of oxygen to cells seeded on 3D PCU scaffolds was successfully achieved by embedding fluorinated particles as an oxygen vector.

6.2 Strengths and limitations

In this study, three significant and equally important strategies of improving the supply of oxygen to the cell seeded 3D scaffolds were demonstrated.^{1,2} Previous studies to improve the supply of oxygen mainly focused on scaffold materials and architecture. For example, the use of polymeric hydrogels has been studied and shown to have an improved supply of oxygen but weak mechanical properties of hydrogels may preclude practical applications.³⁻⁵ The use of polyurethane vascular grafts may overcome the mechanical properties limitation. Moreover, the porous polyurethane scaffold constructs, if fabricated from a non-degradable polyurethane, provide additional mechanical support, therefore reducing the in vitro maturation time and avoiding problems associated with polymer degradation.^{6,7} Microfabrication and microfluidics approaches of fabrication 3D scaffold showed improvements in the supply of oxygen but the fabrication methods were limited to simple structures and, when it comes to tubular and cylindrical structures, fabricating scaffolds with microfabrication approach becomes a complicated matter.⁸⁻¹⁰ Although, oxygen carriers and channeled scaffolds are reported to improve the supply of oxygen,¹¹⁻¹³ the practicality of channeling scaffolds with micro size spacing could reduce the mechanical property. Furthermore, to supply sufficient oxygen, the spacing should be very small which made it challenging to fabricate. The other strength of the study documented in this thesis is the use of adult human coronary artery smooth muscle cells which addresses the limitations related to species differences and unreliable data

extrapolation from animal cell sources to humans. Given that smooth muscle cell behavior is highly dependent on patient age and that elderly patients are in most need for CABG, the use of adult cells best matches the clinical reality.

Amongst the significant contributions of this work is the use of diffusion chamber to determine the effective diffusivity of scaffolds and use this parameter to screen the best scaffold for vascular tissue engineering. Further significant contributions of this study are the use of PFD as an oxygen carrier and the modeling of oxygen transfer with or without oxygen carrier compounds. Lastly, for the first time, inert Zeolite particles were fluorinated and embedded into 3D scaffolds as an oxygen vector for tissue engineering. In summation, this work improves the supply of oxygen to cell-seeded scaffolds using three different strategies namely:

- Convective mass transfer using a perfusion bioreactor,
- Oxygen carrier molecule in the culture media and,
- An oxygen vector embedded in the 3D scaffold

The main limitation of this study is that detailed histological studies and Western blot analyses for dynamic and static cultures were not done. Due to time constraints some studies of the dynamic cultures are also missing. Long-term maturation of the engineered vascular graft will lead for successful fabrication of vascular constructs. Overall this study attempted to solve one of limitation of tissue engineering which the supply of oxygen to 3D constructs and added significant knowledge to the field.

6.3 Future direction

This study sets the ground work for maturing vascular grafts in new and automatically controlled perfusion bioreactors with improved oxygen supply. In addition to flow conditions these bioreactors have to ability to simulate the physiological environment by inducing mechanical stimulation and different kinds of pulsatile flows. The load cells help to measure the applied forces like tensile, pulsatile and compression. The use of a bioreactor will facilitate long-term culture to mature grafts, while promoting cell distribution, cell proliferation, ECM synthesis and deposition, and tissue architecture. Future work to fully explore the extent of proliferation of smooth muscle cells seeded onto 3D polyurethane scaffolds, and the ability to switch phenotype in response to growth factors and mechanical stimulation is strongly recommended. Future work should also include the co-culture of endothelial cells and smooth muscle cells with different growth factors and the effect of co-culture in cell differentiation, matrix deposition and behaviour of smooth muscle cells at physiological conditions.

6.4 Significance

This study paves the way for the use of polyurethane scaffolds for fabricating tissue-engineered vascular substitutes with improved oxygen supply. The fact that this work was focused on vascular tissue engineering does not preclude the approach to be equally applicable to other engineer tissue. In general, the strategies of improving the supply of oxygen as documented in this thesis is anticipated to alleviate inhomogeneous cell distribution and matrix deposition in 3D cultures and help maturing vascular grafts. Matured tissue-engineered grafts have the potential to grow, self repair and self remodel and these make them very attractive for the treatment of congenital anomalies in pediatric

patients and atherosclerosis lesions in adults without immune-rejection. In addition to the obvious clinical use, vascular tissue-engineered constructs can also be used as pharmacological models to develop new drug candidates and test their toxicity and efficacy.

6.5 References

1. Seifu, D. G.; Isimjan, T. T.; Mequanint, K., Tissue engineering scaffolds containing embedded fluorinated-zeolite oxygen vectors. *Acta Biomater* **2011**, 7, (10), 3670-3678.
2. Seifu, D. G.; Mequanint, K., Experimental and Modeling Studies of Oxygen Tension in Vascular Tissue Engineering With and Without an Oxygen Carrier. *J Biomater Tissue Eng* 1, (1), 49-59.
3. Drury, J. L.; Mooney, D. J., Hydrogels for tissue engineering: scaffold design variables and applications. *Biomaterials* **2003**, 24, (24), 4337-4351.
4. Mann, B. K.; Gobin, A. S.; Tsai, A. T.; Schmedlen, R. H.; West, J. L., Smooth muscle cell growth in photopolymerized hydrogels with cell adhesive and proteolytically degradable domains: synthetic ECM analogs for tissue engineering. *Biomaterials* **2001**, 22, (22), 3045-3051.
5. Thebaud, N. B.; Pierron, D.; Bareille, R.; Le Visage, C.; Letourneur, D.; Bordenave, L., Human endothelial progenitor cell attachment to polysaccharide-based hydrogels: A pre-requisite for vascular tissue engineering. *J Mater Sci-Mater Med* **2007**, 18, (2), 339-345.
6. Bergmeister, H.; Grasl, C.; Walter, I.; Plasenzotti, R.; Stoiber, M.; Schreiber, C.; Losert, U.; Weigel, G.; Schima, H., Electrospun Small-Diameter Polyurethane Vascular Grafts: Ingrowth and Differentiation of Vascular-Specific Host Cells. *Artif Organs* **2011**, 36, (1), 54-61.
7. Xu, W. L.; Zhou, F.; Ouyang, C. X.; Ye, W. X.; Yao, M.; Xu, B. G., Mechanical properties of small-diameter polyurethane vascular grafts reinforced by weft-knitted tubular fabric. *J Biomed Mater Res A* **2010**, 92A, (1), 1-8.
8. Andersson, H.; van den Berg, A., Microfabrication and microfluidics for tissue engineering: state of the art and future opportunities. *Lab Chip* **2004**, 4, (2), 98-103.
9. Bettinger, C. J.; Weinberg, E. J.; Kulig, K. M.; Vacanti, J. P.; Wang, Y. D.; Borenstein, J. T.; Langer, R., Three-dimensional microfluidic tissue-engineering

scaffolds using a flexible biodegradable polymer. *Adv Mater* **2006**, 18, (2), 165-169.

10. Borenstein, J. T.; Terai, H.; King, K. R.; Weinberg, E. J.; Kaazempur-Mofrad, M. R.; Vacanti, J. P., Microfabrication technology for vascularized tissue engineering. *Biomed Microdevices* **2002**, 4, (3), 167-175.
11. Radisic, M.; Deen, W.; Langer, R.; Vunjak-Novakovic, G., Mathematical model of oxygen distribution in engineered cardiac tissue with parallel channel array perfused with culture medium containing oxygen carriers. *Am J Physiol-Heart C* **2005**, 288, (3), H1278-H1289.
12. Radisic, M.; Malda, J.; Epping, E.; Geng, W. L.; Langer, R.; Vunjak-Novakovic, G., Oxygen gradients correlate with cell density and cell viability in engineered cardiac tissue. *Biotech and Bioeng* **2006**, 93, (2), 332-343.
13. Radisic, M.; Park, H.; Chen, F.; Salazar-Lazzaro, J. E.; Wang, Y. D.; Dennis, R.; Langer, R.; Freed, L. E.; Vunjak-Novakovic, G., Biomimetic approach to cardiac tissue engineering: Oxygen carriers and channeled scaffolds. *Tissue Eng* **2006**, 12, (8), 2077-2091.

APPENDIX**Letters of copyright permission for published manuscripts**

**ELSEVIER LICENSE
TERMS AND CONDITIONS**

Apr 16, 2012

This is a License Agreement between Dawit G. Seifu ("You") and Elsevier ("Elsevier") provided by Copyright Clearance Center ("CCC"). The license consists of your order details, the terms and conditions provided by Elsevier, and the payment terms and conditions.

All payments must be made in full to CCC. For payment instructions, please see information listed at the bottom of this form.

Supplier	Elsevier Limited The Boulevard, Langford Lane Kidlington, Oxford, OX5 1GB, UK
Registered Company Number	1982084
Customer name	Dawit G. Seifu
Customer address	1151 Richmond Street London, ON N5A 5B9
License number	2887201280685
License date	Apr 13, 2012
Licensed content publisher	Elsevier
Licensed content publication	Acta Biomaterialia
Licensed content title	Tissue engineering scaffolds containing embedded fluorinated-zeolite oxygen vectors
Licensed content author	Dawit G. Seifu, Tayirjan T. Isimjan, Kibret Mequanint
Licensed content date	October 2011
Licensed content volume number	7
Licensed content issue number	10

Number of pages	9
Start Page	3670
End Page	3678
Type of Use	reuse in a thesis/dissertation
Portion	full article
Format	both print and electronic
Are you the author of this Elsevier article?	Yes
Will you be translating?	No
Order reference number	
Title of your thesis/dissertation	OXYGEN DELIVERY STRATEGIES IN TISSUE-ENGINEERED CONSTRUCTS
Expected completion date	Apr 2012
Estimated size (number of pages)	170
Elsevier VAT number	GB 494 6272 12
Permissions price	0.00 USD
VAT/Local Sales Tax	0.0 USD / 0.0 GBP
Total	0.00 USD
Terms and Conditions	

INTRODUCTION

1. The publisher for this copyrighted material is Elsevier. By clicking "accept" in connection with completing this licensing transaction, you agree that the following terms and conditions apply to this transaction (along with the Billing and Payment terms and conditions established by Copyright Clearance Center, Inc. ("CCC"), at the time that you opened your Rightslink account and that are available at any time at <http://myaccount.copyright.com>).

GENERAL TERMS

2. Elsevier hereby grants you permission to reproduce the aforementioned material subject to the terms and conditions indicated.

3. Acknowledgement: If any part of the material to be used (for example, figures) has appeared in our publication with credit or acknowledgement to another source, permission must also be sought from that source. If such permission is not obtained then that material may not be included in your publication/copies. Suitable acknowledgement to the source must be made, either as a footnote or in a reference list at the end of your publication, as follows:

“Reprinted from Publication title, Vol /edition number, Author(s), Title of article / title of chapter, Pages No., Copyright (Year), with permission from Elsevier [OR APPLICABLE SOCIETY COPYRIGHT OWNER].” Also Lancet special credit - “Reprinted from The Lancet, Vol. number, Author(s), Title of article, Pages No., Copyright (Year), with permission from Elsevier.”

4. Reproduction of this material is confined to the purpose and/or media for which permission is hereby given.

5. Altering/Modifying Material: Not Permitted. However figures and illustrations may be altered/adapted minimally to serve your work. Any other abbreviations, additions, deletions and/or any other alterations shall be made only with prior written authorization of Elsevier Ltd. (Please contact Elsevier at permissions@elsevier.com)

6. If the permission fee for the requested use of our material is waived in this instance, please be advised that your future requests for Elsevier materials may attract a fee.

7. Reservation of Rights: Publisher reserves all rights not specifically granted in the combination of (i) the license details provided by you and accepted in the course of this licensing transaction, (ii) these terms and conditions and (iii) CCC's Billing and Payment terms and conditions.

8. License Contingent Upon Payment: While you may exercise the rights licensed immediately upon issuance of the license at the end of the licensing process for the transaction, provided that you have disclosed complete and accurate details of your proposed use, no license is finally effective unless and until full payment is received from you (either by publisher or by CCC) as provided in CCC's Billing and Payment terms and conditions. If full payment is not received on a timely basis, then any license preliminarily granted shall be deemed automatically revoked and shall be void as if never granted. Further, in the event that you breach any of these terms and conditions or any of CCC's Billing and Payment terms and conditions, the license is automatically revoked and shall be void as if never granted. Use of materials as described in a revoked license, as well as any use of the materials beyond the scope of an unrevoked license, may constitute copyright infringement and publisher reserves the right to take any and all action to protect its copyright in the materials.

9. **Warranties:** Publisher makes no representations or warranties with respect to the licensed material.
10. **Indemnity:** You hereby indemnify and agree to hold harmless publisher and CCC, and their respective officers, directors, employees and agents, from and against any and all claims arising out of your use of the licensed material other than as specifically authorized pursuant to this license.
11. **No Transfer of License:** This license is personal to you and may not be sublicensed, assigned, or transferred by you to any other person without publisher's written permission.
12. **No Amendment Except in Writing:** This license may not be amended except in a writing signed by both parties (or, in the case of publisher, by CCC on publisher's behalf).
13. **Objection to Contrary Terms:** Publisher hereby objects to any terms contained in any purchase order, acknowledgment, check endorsement or other writing prepared by you, which terms are inconsistent with these terms and conditions or CCC's Billing and Payment terms and conditions. These terms and conditions, together with CCC's Billing and Payment terms and conditions (which are incorporated herein), comprise the entire agreement between you and publisher (and CCC) concerning this licensing transaction. In the event of any conflict between your obligations established by these terms and conditions and those established by CCC's Billing and Payment terms and conditions, these terms and conditions shall control.
14. **Revocation:** Elsevier or Copyright Clearance Center may deny the permissions described in this License at their sole discretion, for any reason or no reason, with a full refund payable to you. Notice of such denial will be made using the contact information provided by you. Failure to receive such notice will not alter or invalidate the denial. In no event will Elsevier or Copyright Clearance Center be responsible or liable for any costs, expenses or damage incurred by you as a result of a denial of your permission request, other than a refund of the amount(s) paid by you to Elsevier and/or Copyright Clearance Center for denied permissions.

LIMITED LICENSE

The following terms and conditions apply only to specific license types:

15. **Translation:** This permission is granted for non-exclusive world **English** rights only unless your license was granted for translation rights. If you licensed translation rights you may only translate this content into the languages you requested. A professional translator must perform all translations and reproduce the content word for word preserving the integrity of the article. If this license is to re-use 1 or 2 figures then permission is granted for non-exclusive world rights in all languages.
16. **Website:** The following terms and conditions apply to electronic reserve and author websites:

Electronic reserve: If licensed material is to be posted to website, the web site is to be password-protected and made available only to bona fide students registered on a relevant course if:

This license was made in connection with a course,

This permission is granted for 1 year only. You may obtain a license for future website posting,

All content posted to the web site must maintain the copyright information line on the bottom of each image,

A hyper-text must be included to the Homepage of the journal from which you are licensing at <http://www.sciencedirect.com/science/journal/xxxxx> or the Elsevier homepage for books at <http://www.elsevier.com> , and

Central Storage: This license does not include permission for a scanned version of the material to be stored in a central repository such as that provided by Heron/XanEdu.

17. **Author website** for journals with the following additional clauses:

All content posted to the web site must maintain the copyright information line on the bottom of each image, and

the permission granted is limited to the personal version of your paper. You are not allowed to download and post the published electronic version of your article (whether PDF or HTML, proof or final version), nor may you scan the printed edition to create an electronic version,

A hyper-text must be included to the Homepage of the journal from which you are licensing at <http://www.sciencedirect.com/science/journal/xxxxx> , As part of our normal production process, you will receive an e-mail notice when your article appears on Elsevier's online service ScienceDirect (www.sciencedirect.com). That e-mail will include the article's Digital Object Identifier (DOI). This number provides the electronic link to the published article and should be included in the posting of your personal version. We ask that you wait until you receive this e-mail and have the DOI to do any posting.

Central Storage: This license does not include permission for a scanned version of the material to be stored in a central repository such as that provided by Heron/XanEdu.

18. **Author website** for books with the following additional clauses:

Authors are permitted to place a brief summary of their work online only.

A hyper-text must be included to the Elsevier homepage at <http://www.elsevier.com>

All content posted to the web site must maintain the copyright information line on the bottom of each image

You are not allowed to download and post the published electronic version of your chapter, nor may you scan the printed edition to create an electronic version.

Central Storage: This license does not include permission for a scanned version of the material to be stored in a central repository such as that provided by Heron/XanEdu.

19. **Website** (regular and for author): A hyper-text must be included to the Homepage of the journal from which you are licensing at <http://www.sciencedirect.com/science/journal/xxxxx>. or for books to the Elsevier homepage at <http://www.elsevier.com>

20. **Thesis/Dissertation**: If your license is for use in a thesis/dissertation your thesis may be submitted to your institution in either print or electronic form. Should your thesis be published commercially, please reapply for permission. These requirements include permission for the Library and Archives of Canada to supply single copies, on demand, of the complete thesis and include permission for UMI to supply single copies, on demand, of the complete thesis. Should your thesis be published commercially, please reapply for permission.

21. **Other Conditions**:

v1.6

If you would like to pay for this license now, please remit this license along with your payment made payable to "COPYRIGHT CLEARANCE CENTER" otherwise you will be invoiced within 48 hours of the license date. Payment should be in the form of a check or money order referencing your account number and this invoice number RLNK500760168.

Once you receive your invoice for this order, you may pay your invoice by credit card. Please follow instructions provided at that time.

**Make Payment To:
Copyright Clearance Center**

Gratis licenses (referencing \$0 in the Total field) are free. Please retain this printable license for your reference. No payment is required.

AMERICAN SCIENTIFIC PUBLISHERS

Dear Mr. Seifu:

American Scientific Publishers grants permission to use your published paper in *Journal of Biomaterials and Tissue Engineering* titled "Experimental and Modeling Studies of Oxygen Tension in Vascular Tissue Engineering With and Without an Oxygen Carrier. 2011, 1, (1), 49-59." for your PhD thesis at the University of Western Ontario.

H. S. Nalwa, PhD

AMERICAN SCIENTIFIC PUBLISHERS

Dear Publisher:

My name is Dawit G Seifu. I am a PhD student at the University of Western Ontario, Canada. Part of my PhD work was published in *Journal of Biomaterials and Tissue Engineering* titled "Experimental and Modeling Studies of Oxygen Tension in Vascular Tissue Engineering With and Without an Oxygen Carrier. 2011, 1, (1), 49-59." I am writing my thesis for partial fulfillment of my PhD and I would like to have a copyright permission allowing the data to be included in my PhD thesis.

Thank you in advance.

Sincerely,

Dawit Gezahegn Seifu, Ph.D. Candidate,
Department of Chemical and Biochemical Engineering,
The University of Western Ontario,

CURRICULUM VITAE

Dawit Gezahegn Seifu

EDUCATION

- 2006 – 2012 PhD. Chemical and Biochemical Engineering
 The University of Western Ontario, London ON, Canada
- 2001 – 2005 BSc. Chemical Engineering
 Addis Ababa University, Addis Ababa, Ethiopia

TEACHING EXPERIENCE

Graduate Teaching Assistant

- 2006 – 2011 CBE 2214a: Engineering Thermodynamics
 CBE 2224b: Chemical Engineering Thermodynamics
 CBE 9150: Advance Chemical Engineering Thermodynamics
 CBE 3323a: Staged Operations
 CBE 4423a: Tissue Engineering

PUBLICATIONS IN JOURNALS

1. **Seifu, Dawit G**; Mequanint, K., Tissue Engineering scaffold fabrication, effective diffusion coefficient and dynamic cell culture. **2012**, (Under Review).
2. **Seifu, Dawit G**; Isimjan, T. T.; Mequanint, K., Tissue engineering scaffolds containing embedded fluorinated-zeolite oxygen vectors. *Acta Biomaterialia* **2011**, 7, (10), 3670-3678.
2. **Seifu, Dawit G**; Mequanint, K., Experimental and Modeling Studies of Oxygen Tension in Vascular Tissue Engineering With and Without an Oxygen Carrier. *Journal of Biomaterials and Tissue Engineering* **2011**, 1, (1), 49-59.
3. **Seifu, Dawit G**; Torras. C, Pitol-Filho. L, Garcia-Valls. R. Novel polymeric membrane structures: microcapsules. *Desalination* 200 (**2006**) 12–14

CONFERENCE PRESENTATIONS

Seifu, Dawit G; Mequanint K., Oxygen Delivery Strategies in 3D Cell Seeded Tissue-engineered Scaffolds. 61st CScHE Conference, London ON, October 23-26, 2011, *Oral presentation.*

Seifu, Dawit G; Mequanint K., Bioreactor Cultured Vascular Tissue Constructs with Improved Oxygen Supply. 28th CBS Conference, Kingston ON, June 2-4, 2010, *Oral presentation.*

Seifu, Dawit G; Mequanint K., Bioreactor Matured Vascular Tissue Substitutes. Research Bridges at the Sarnia Research Park, Sarnia ON, May 6, 2010, *Oral presentation.*

Seifu, Dawit G; Mequanint K., Bioreactor Oxygen Profile in Cell Seeded Vascular Tissue Constructs. 27th CBS Conference, Quebec City QC, May 20-23, 2009, *Oral presentation.*

Seifu, Dawit G; Mequanint K., Oxygen Delivery Strategy for Tissue Engineered Vascular Constructs. 2nd Annual Symposium Particle Technology Research Centre (PTRC), London ON, July 13, 2008, *Oral presentation.*

HONOURS AND AWARDS

2006 – 2012	Western Graduate Research Scholarship
2003 – 2005	First Prize Scholastic Awards from the Ethiopian Society of Chemical Engineering
2004 – 2005	Ethiopian Association of Japan Scholarship Award for Ethiopian University Students
2005	Faculty Engineering Gold Medal, Addis Ababa University, Ethiopia